Mendel University in Brno
Faculty of AgriSciences
Department of Agrosystems and Bioclimatology

Comparison of evapotranspiration measurement methods in agricultural landscape

„Srovnání metod měření evapotranspirace v zemědělské krajině“

Ph.D. Thesis

Supervisor:
prof. Mgr. Ing. Miroslav Trnka, Ph.D.

Author:
Ing. Gabriela Pozníková

Brno 2016

Acknowledgements

I would like to acknowledge my supervisor prof. Mgr. Ing. Miroslav Trnka, Ph.D. and also my supervisor specialist Ing. Milan Fischer, Ph.D. for leadership, help, creative ideas and expertise. I would also like to thank prof. Ing. Zdeněk Žalud, Ph.D., the head of Department of Agrosystems and Bioclimatology, for support and providing interesting working and research conditions. Special thanks go to prof. Dipl. Ing. Josef Eitzinger, Ph.D. (BOKU University in Venna) and Mag. Dr. Andreas Schaumberger, MSc (ECRG, Irdning) for their willing cooperation and patience while choosing and negotiating experimental localities in Austria. They were both always very helpfull and supporting. Furthermore, I am very grateful to Dr. Frank Beyrich (DWD Lindenberg, Germany) and Dr. Bram van Kesteren (Scintec, Germany) for help with scintillometer data processing and analysis. Moreover, I was pleased to visit Observatory in Lindenberg and this study stay motivated me and gave me great impulse for further work. Above this, both gentlemen agreed to visit the Czech Republic in return, they gave lecture at CzechGlobe institute and on the top of all, they helped me with installation of the scintillometer in Polkovice. I would also like to thank Ing. Petr Hlavinka, Ph.D. for help with negotiating experimental site in Polkovice, and management and employees of the farm for indulgent cooperation during the field campaign. I am grateful to Ing. Vojtěch Lukas, Ph.D. for cooperation during project COST CZ No. LD14121 program of the Ministry of Education, Youth and Sports (MEYS) CR "The possibilities of using remote sensing to determine actual evapotranspiration of selected field crops". He was in charge of remote sensing data collection and processing and these results are presented within this thesis in section Variability of the field. Last but not least, I would like to express my gratitude to all opponents for their time, useful comments, and valuable suggestions.

This thesis was financially supported by the specific university research fund through project IGA AF „Analysis of temperature profiles in the boundary layer of the atmosphere and the link to the gradient measurements of evapotranspiration No. IP 10/2013 and No. TP 10/2013 "Study of some factors affecting Implementation of the biological potential of agricultural crops". This work was also supported by the Global Change Research Institute by the MEYS CR within the National Sustainability Program I (NPU I), grant No. LO1415 CzechGlobe 2020.

Čestné prohlášení

Prohlašuji, že jsem práci: „Srovnání metod měření evapotranspirace v zemědělské krajině" (Comparison of evapotranspiration measurement methods in agricultural landscape) vypracovala samostatně a veškeré použité prameny a informace uvádím v seznamu použité literatury. Souhlasím, aby moje práce byla zveřejněna v souladu s § 47b zákona č. 111/1998 Sb., o vysokých školách ve znění pozdějších předpisů a v souladu s platnou *Směrnicí o zveřejňování vysokoškolských závěrečných prací.*

Jsem si vědoma, že se na moji práci vztahuje zákon č. 121/2000 Sb., autorský zákon, a že Mendelova univerzita v Brně má právo na uzavření licenční smlouvy a užití této práce jako školního díla podle § 60 odst. 1 autorského zákona.

Dále se zavazuji, že před sepsáním licenční smlouvy o využití díla jinou osobou (subjektem) si vyžádám písemné stanovisko univerzity, že předmětná licenční smlouva není v rozporu s oprávněnými zájmy univerzity, a zavazuji se uhradit případný příspěvek na úhradu nákladů spojených se vznikem díla, a to až do jejich skutečné výše.

V Brně dne:……..

……..

Podpis

TABLE OF CONTENTS

SÚHRN

Evapotranspirácia (ET) je významnou súčasťou vodnej aj energetickej bilancie. Predstavuje hlavnú stratovú zložku vodnej bilancie v agrosystémoch. Skladá sa z evaporácie – výpar z pôdy, povrchu rastlín (intercepcia) a z transpirácie – voda vychádzajúca z rastlinných prieduchmi. Táto zložka sa významne podieľa na tvorbe výnosov. Presná informácia o množstve vody „stratenej“ vyparovaním sa využíva pri plánovaní závlah ale má významnú úlohu aj v ďalších oboroch ako sú klimatické, hydrologické či meteorologické modelovanie. Modely sú osožným nástrojom, no každý model je nutné kalibrovať a validovať pomocou pozemných meraní.

Existuje mnoho prístupov ako určiť aktuálnu ET. V predkladanej práci budú základné metódy zhrnuté a popísane s dôrazom na štyri metódy, ktoré sú v experimentálnej časti práce porovnávané. Ide o metódy: „eddy covariance“ (EC), metóda Bowenovho pomeru a energetickej bilancie (BREB), a metóda „surface renewal“ (SR), ktoré sú príkladmi bodového merania. Poslednou metódou je scintilometria. Jej hlavnou výhodou oproti bodovým meraniam je schodnosť vypočítať energetické toky ako priemer s väčšej plochy. Túto vlastnosť možno využiť pri validácii modelov, ktoré sú spravidla založené na použití satelitných snímok s rozlíšením jedného gridu s veľkosťou min 500x500 m.

Naším počiatočným cieľom bolo nainštalovať a prevádzkovať súčasne meranie štyrmi metódami nad homogénnym povrchom a v ďalšej fáze rozšíriť našu sieť pozemných meraní aj o heterogénne povrchy. Testovanie homogenity experimentálnej lokality v Polkoviciach (Česká republika) sa uskutočnilo porovnaním satelitných snímok (NDVI, povrchová teplota) a snímok získaných pri prelete lietadla nad lokalitou s pozemným meraním pôdnej vlhkosti a indexu listovej plochy. Z výsledkov môžeme súdiť, že naša lokalita spĺňa predpoklady rozsiahleho, homogénneho a vyrovnaného povrchu ideálneho na mikrometeorologické merania, a tak môžeme súdiť, že zdrojové územie (footprint) je pre všetky metódy je dostatočne homogénne.

Ďalším cieľom predkladanej práce bolo ohodnotiť porovnávané metódy z hľadiska ich optimálnosti pre používateľa a navrhnúť zlepšenie našej monitorovacej siete. Metóda BREB sa ukázala byť spoľahlivou a ponúka dobrú zhodu s EC, avšak je veľmi citlivá na presnosť použitých kombinovaných senzorov teploty vzduchu a relatívnej vlhkosti (RH) vzhľadom k tomu, že pri výpočte sa používa ich gradient. Metóda EC bola v teréne veľmi spoľahlivá a nenáročná na údržbu. Nevýhodou je vyššia cena prístroja a komplikované následné spracovanie dát, ktoré vyžaduje mnoho korekcií, a teda zaškolený personál. Otázkou je tiež typické podhodnocovanie tokov a neuzatváranie energetickej bilancie. Scintilometre mali tendenciu nadhodnocovať tok turbulentného (tzv. cíteného) tepla. Pri výpočte výparu (ET) je táto metóda do značnej miery závislá na presnosti merania ostatných zložiek energetickej bilancie, podobne ako metóda SR. Navyše „veľký“ scintilometer (BLS) vyžaduje postavenie infraštruktúry (4 m vysoké stožiare) a má vyššie energetické nároky pri rovnakom výsledku ako „malý“ scintilometer (SLS) pri prevádzke nad homogénnym povrchom. Avšak BLS má potenciál pri meraní omnoho väčších plôch nad heterogénnym územím. Metóda SR má potenciál byť vhodnou alternatívou k BREB,

keďže ukázala sľubné výsledky a je najmenej finančne náročná spomedzi všetkých testovaných metód. Výzvou však ostáva vyriešenie problému korektného určenia variability signálu spojeného s prenosom energie.

Zohľadňujúc všetky spomínané výhody aj nevýhody porovnaných metód odporúčame ďalej používať EC metódu na kľúčových lokalitách monitorovacej siete. Potenciál scintilometrie vidíme v rozšírení nad heterogénne územia – meranie s väčším footprintom. Metóda BREB je spoľahlivou metódou a po prehodnotení a výmene senzorov na meranie RH profilu odporúčame túto metódu naďalej používať na vzdialenejších extenzívne udržiavaných lokalitách. Zo všetkých testovaných metód navrhujem pre ďalší výskum metódu SR, ktorá má vzhľadom k cene a výsledkom značný výskumný potenciál.

1 INTRODUCTION

"If there is magic on this planet, it is contained in water." Loren Corey Eiseley

It is a cliché to start with but water is truly the essence of life. United Nations emphasized in their Resolution adopted by the General Assembly in 2003 that “water is critical for sustainable development, including environmental integrity and the alleviation of poverty and hunger, and is indispensable for human health and well-being”. It plays an inevitable role in all ecosystems and life as a whole. Not only it allows organisms to live (it comprises great part of their bodies and enables chemical processes in metabolism) but also it helps to create comfortable climate on Earth. It is involved in greenhouse effect which enables the agreeable Earth´s temperature. Moreover, the energy involved in changing water states (liquid, ice, vapour) drives energy transfer in the plant-soil-atmosphere system. By evaporating one litter of water 2.45 MJ of energy coming from the sun are consumed (at 20 °C). Thus the evaporation has a great cooling effect in terrestrial environments. Evapotranspiration (evaporation from the soil and transpiration through plants) creates a link between water and energy cycles of our planet.

Water demands are expected to rise with increasing human population and ongoing climate change. Consumption of fresh water for humans and agriculture is becoming increasingly scarce (Smith, 2000). Sustainable food production requires judicious water use since future food demands and competition for clean water will grow. There are few options to increase water use efficiency such as: the rainfall conservation, irrigation water losses reduction or cultural practices leading to increased production per unit of water (Smith, 2000).

To reduce irrigation water losses proper quantification of ET is essential. The ET is a complicated invisible process and its calculation involves numerous fields of science, such as soil hydrology, plant physiology, and meteorology (Novák, 2012). There are different attitudes towards its estimation from modelling to point measurements. Nowadays, the fluxes of heat, and water vapour on the local scale and over a homogeneous surface are usually measured by eddy covariance. It is a method using fast response wind, temperature, and humidity sensors. However, for many applications, such as agriculture, water management, validation of weather prediction or climate models, larger area-averaged fluxes representative for areas ~0.1–10 km^2 are of our interest. For such purposes scintillometers are being used increasingly in the recent past. In presented study scintillometry was used for the first time in the Czech Republic to measure actual evapotranspiration in the agricultural field and the results were compared to eddy covariance and other traditional methods. Although, the measured data were not related to remote sensing images, this issue will be addressed further as an objective of future research.

The presented thesis is organized in following order. First of all, theoretical background of the measurement techniques and review on their comparison is presented in section 2 Literature review. It is followed by chapter 3 Objectives of the thesis, and 4 Materials and methods describing experimental site, set-up, and data processing. This section is followed by the sections 5 Results and 6 Discussion where the results of the comparison and auxiliary

measurements are presented and discussed in the context of feasibility for agricultural monitoring. The main findings are summarized in section 7 Conclusions. In Appendices section after the list of symbols and abbreviations, list of tables and figures two case studies can be found. In Appendix D – dual crop coefficient case study, and Appendix E – detailed temperature profile measurements. These were included because they are closely related to ET study and there was no space to add them as original chapters into the thesis.

2 LITERATURE REVIEW

2.1 Energy and water cycles

The turbulent fluxes of heat, and water vapour play an essential role in the natural water and energy cycles representing important exchange processes between the atmosphere and the underlying surface. The process of evapotranspiration (ET) is important part of the water cycle and significant consumer of energy. That is why, ET plays crucial role in both energy balance of the Earth and also in the soil-plant-atmosphere system. Fig 1 (ESA, 2004) shows an illustration of different terrestrial and atmospheric components of energy and water cycles. The main part of water balance which leads the water away from agrosystems is ET. Up to 90 % of precipitation is turned into ET in dry regions, and on average 60 % of annual rainfall reaching ecosystems is evaporated (Novák, 2012).

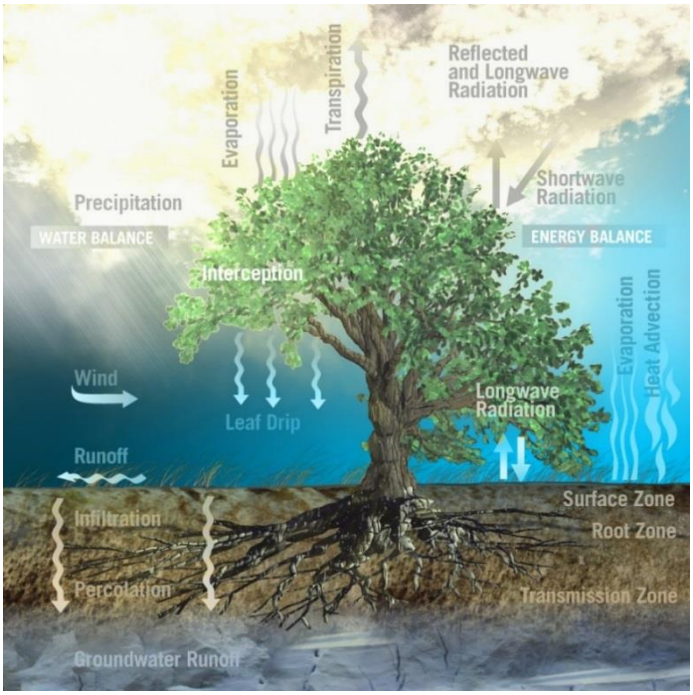

Fig 1 The energy and water balance of the physical climate system including terrestrial and atmospheric components of the water cycle (ESA, 2004).

On the global scale, energy is distributed between the sun, atmosphere and the Earth´s surface according to Earth's annual and global mean energy balance (Fig 2). The global energy balance considers the energy flows within the climate system and their exchanges with outer space. About half of the incoming solar radiation is absorbed by the Earth's surface. This energy is transferred to the atmosphere by warming the air in contact with the surface (sensible heat), by evapotranspiration (latent heat) and by long wave radiation that is absorbed by clouds and greenhouse gases (Kiehl and Trenberth, 1997). The atmosphere in turn radiates long wave energy back to Earth as well as out to space. Compared to the top of the atmosphere, the estimation of surface energy fluxes is associated with larger uncertainties (Liou et al., 2014).

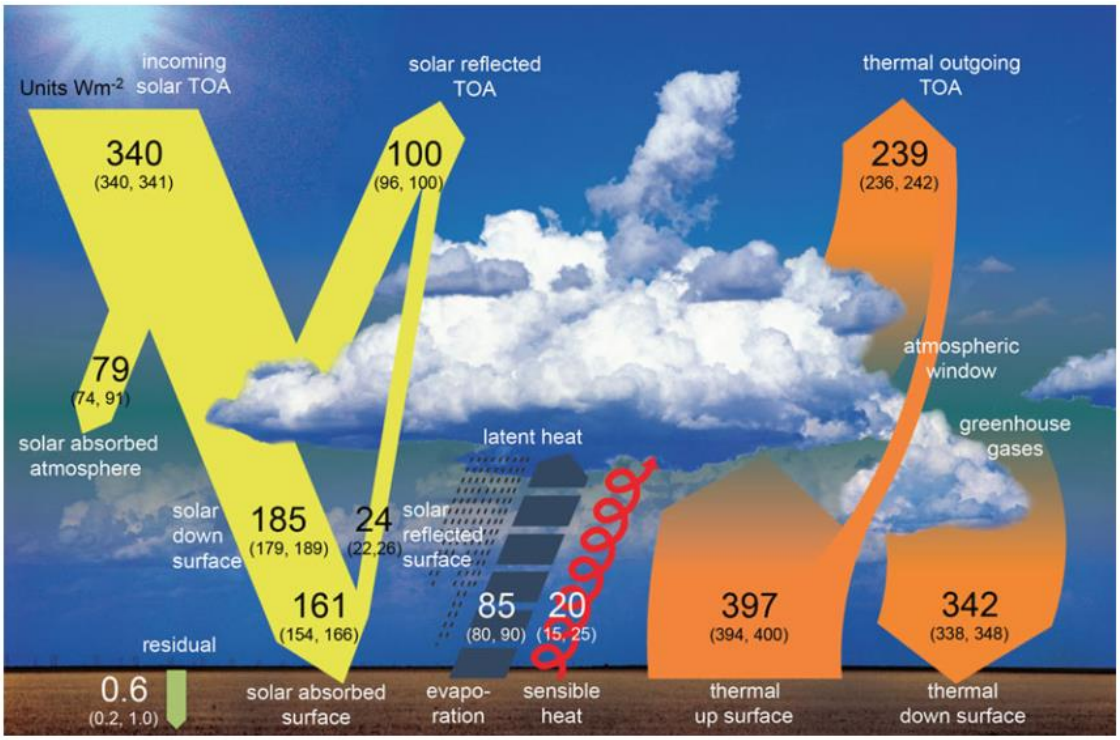

Fig 2 Schematic diagram of the global mean energy balance of the Earth. Numbers indicate best estimates for the magnitudes of the globally averaged energy balance components together with their uncertainty ranges, representing present day climate conditions at the beginning of the twenty first century, all in W m^{-2} (Wild et al., 2013).

Among other energy flows within the atmosphere and Earth's surface, the knowledge of both sensible (*H*) and latent *(LE*) heat fluxes, together with soil moisture content, are of great importance to many environmental applications, i.e. the monitoring of plant water demand, plant growth and productivity (Chahal, 2007; Verstraeten et al., 2008; Tian et al., 2010), as well as for cultivation and irrigation management systems (Kirda, 2002; Beeson, 2006; Toumi et al., 2016), or drought monitoring (Možný et al., 2012). Such information is essential for numerical modelling of atmospheric and hydrological processes and for improving the accuracy of the models used in weather forecasting (Dutta et al., 2016). Moreover, quantitative information on these parameters is highly important for land management, monitoring of land degradation and desertification on a regional scale (Liou et al., 2014).

2.1.1 Components of energy balance equation

Term energy balance of the lower part of the atmosphere in general can be expressed as an equation:

$$Rn = H + LE + G + S + Q\,, \tag{1}$$

where *Rn* is net radiation, *H* is *LE* are sensible heat and latent heat flux density, respectively, *G* is heat flux into the soil, *S* and *Q* are the rates at which heat goes into physical (heat storage in the layer of air between the soil surface and the level of the measurement instrumentation plus the storage in plant canopy) and biochemical (photosynthesis) storages

within the vegetation, respectively (all in W m^{-2}). Thom (1975) included also term "*D*" which represented the net rate at which energy is being removed horizontally (by advection). In practical experiments, however, these terms (*S*, *Q*, or *D*) are usually neglected as a small fraction of the surface energy balance (typically less than 5 % of *Rn* for individual sinks) (Meyers and Hollinger, 2004). In the three following sections net radiation, soil heat flux, and sensible heat flux will be shortly introduced followed by section 2.2 devoted to different aspects of evapotranspiration (latent heat flux).

2.1.2 Net radiation

Net radiation (*Rn*) is a dominant part of the energy balance equation (Eq. 1) not only in the absolute sense due to its size (several hundreds of watts per square meter) as Thom (1975) explained but also by its relation to all other terms of the energy balance. Every part of the equation depends to some extent on the *Rn* directly or indirectly during the day. Typically, it is changing rapidly close to dawn and dusk when it is near zero, at night reaches negative values of tens of watts per square meter, and during the clear day it changes significantly with cloudiness.

The net radiation comprises of four components: incoming and outgoing short wave (SW) and long wave (LW) fluxes; short wave incoming (SWin) or global solar radiation, short wave outgoing (SWout) or reflected solar radiation, long wave incoming (LWin) or infrared emitted by the sky and long wave outgoing (LWout) or infrared emitted by the ground surface. Short wave radiation is mainly present in the 300 to 3000 nm region while long wave in the 4500 to 50000 nm region.

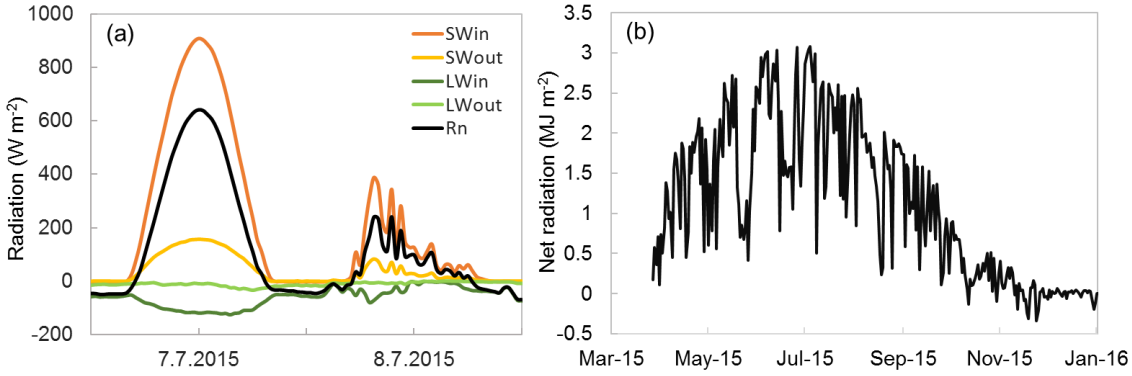

Fig 3 (a) Typical diurnal course of all components of net radiation 10-min values. Data come from the locality Polkovice one clear day and one rainy day; (b) the seasonal course of net radiation, daily sums in MJ m^{-2} during the season 2015 in Polkovice.

Typical diurnal course of all components of net radiation during clear sky and cloudy (rainy) day can be seen in Fig 3a. From four components of radiation, parameters like SW albedo, sky temperature, (ground) surface temperature and off course net radiation can be calculated. Net radiation is the difference between incoming and outgoing radiation of both SW

from the sun and LW from the earth, clouds and other material in the sky (Burman and Pochop, 1994):

$$Rn = \mathrm{SWin} - \mathrm{SWout} + \mathrm{LWin} - \mathrm{LWout} \quad (2)$$

The seasonal course of net radiation is shown in Fig 3(b). Ability to estimate net radiation is vital for prediction of evapotranspiration (ET) as the radiant heat coming from the sun is the source of energy and thus the driver of ET. Additionally, many techniques to determine ET measure sensible heat flux in the first place and latent heat is consequently calculated through the energy balance equation as a residual term. Accurate measurement of *Rn* is therefore essential.

Albedo (*α*) is defined as reflecting power of a surface. It is the ratio between reflected and incident shortwave radiation (Eq. 3) in this thesis *α* refers to combination of both direct and diffuse radiation. Albedo is a dimensionless value which enables to be expressed in percentage with values between 0 (no reflectance - completely black body) to 1 (for perfect reflection of a white surface).

$$\alpha = \mathrm{SWout} / \mathrm{SWin} \quad (3)$$

Typical value of albedo for reference grass cover is 0.23 (Allen et al., 1998). General average for other surfaces according to Burman and Pochop (1994) is as follows: soils between 0.05–0.31 average 0.18; snow depending on age between 0.29–0.95 on average 0.63; coniferous forest 0.10–0.24; deciduous forest 0.15–0.20, clouds depending on kind and configuration 0.05–0.84; water depending on sun´s angle 0.02–1.00. Albedo of plants vary throughout the growing season and albedo of bare soils will also change with different soil water content (wet soil is darker thus it has lower albedo). Foken (2008) declare albedo 0.25–0.30 and 0.10–0.12 for dry and wet soil, respectively.

2.1.3 Soil heat flux

The amount of thermal energy that moves through an area of soil in a unit of time is the soil heat flux or heat flux density (Sauer and Horton, 2005). The ability of soil to conduct heat determines how fast its temperature changes during the day or between seasons. The soil heat flux (*G*) is relatively small compared to net radiation especially when surface is covered with tall vegetation. It is always involved in the energy balance calculations. Daytime values of *G* reach only about 5–15 % of net radiation and nocturnal values 50 % of *Rn* (Stull, 1988). For its relatively small magnitudes and thus minor influence on final fluxes some of the authors neglect it for ET estimates. Others use very simple models to define *G* (Allen et al., 1998). Soil heat flux is, however, a very complex process (Heitman et al., 2010). During the field experiments, soil heat flux plates (SHFP) are commonly used to measure *G* few centimetres below the soil surface. To be able to capture variability of *G* across the experimental field it is necessary to use more SHFPs to gain an average value. Kustas et al. (2000) found that difference between individual SHFPs under similar conditions can reach 200–250 W m^{-2}. They were testing 20 sensors in the mesquite dune site in Mexico showing that even micro-topography can have a significant effect on the results. Moreover, *G* used in energy balance equation is hypothetical

value of energy stored at the soil surface. Therefore, for exact measurements it is also advisable to measure the energy stored in the layer of soil between soil surface and SHFP (Mayocchi and Bristow, 1995). This can be done, for example, by measuring the soil temperature at the surface and at the level of SHFP.

2.1.4 Turbulent fluxes

In the total balance, the earth's surface receives more radiation energy (through short wave and long wave incoming radiation) than is lost (outgoing radiation). In other words, the net radiation at the surface is positive (Foken et al., 2008). The surplus of supplied energy is transported back to the atmosphere thanks to two turbulent energy fluxes: the sensible heat flux (*H*) and the latent heat flux (*LE*). *H* is responsible for heating the atmosphere from the surface up to some 100 m during the day, except for days with strong convection (Foken et al., 2008). *LE* is the heat required to evaporate mass of water under given conditions. More on this par of the energy balance equation will be given in the following sections. *H* and *LE* are positive when transport of energy takes place from the surface aloft.

2.2 Definition of the evapotranspiration

Evapotranspiration (ET) is the process of water transport from the evaporative surface to the atmosphere (Novák, 2012). The ET consists of two parts: (i) evaporation from the surface of soil, plant surfaces (interception), water bodies, other impermeable surfaces, and (ii) transpiration through the stomata of plants.

John L. Monteith, respected British scientist who pioneered the application of physics to biology, associated the evaporation of water to commercial transaction in which a wet surface sells water vapour to its environment in exchange for heat. For each gram of water evaporated at 20 °C the surface demands 585 calories (2449 J) of heat and several forms of payment are acceptable (Monteith, 1965). Heat can be supplied by solar radiation, turbulent transfer from the atmosphere or by conduction from the soil. The relation between the rate of evaporation and state of the environment can be described by few basic principles of thermodynamic. The amount of heat in a parcel of air is equal to sum of sensible heat content (dependent on temperature) and latent heat content (dependent on vapour pressure) (Monteith, 1965). This means that any change in latent heat content must be balanced by an equal and opposite change in sensible heat content. In other words, evaporating of liquid water increases latent heat content of the air and at the same time cools down the air which means that it reduces the sensible heat content of the air. This process stops when the air reaches so called saturation vapour pressure - air saturated by water at temperature *T*. Saturated air can be replaced by drier ambient air and the process of evaporation continues. Exchange of air hence strongly depends on wind speed and turbulent mixing of air. Consequently, solar radiation, air temperature, air humidity, and wind speed are the parameters needed to calculate evapotranspiration. Additionally, turbulent mixing depends to a great extent on the surface roughness as an aerodynamic property of the surface (crop canopy, soil surface or water

surface). That is why many methods to determine ET include also the surface roughness as an important parameter.

Transpiration is also dependent on mentioned climate parameters but also takes into account plant type and other factors such as soil water content, soil type, water salinity, cultivation, management, plant environment and development (Allen et al., 1998). In agricultural field the ratio between transpiration and evaporation changes during the growing season gradually. Fig 4 adapted from Allen et al. (1998) displays how evaporation and transpiration change during the growing period of the annual field crop. At the beginning of the season or after the sowing, nearly 100 % of ET is lost through evaporation from the bare soil but when the crop covers the soil surface more than 90 % of ET comes from plant transpiration (Allen et al., 1998). Transpiration and evaporation occur simultaneously and it is not a simple task to distinguish both processes. In general, transpiration can be determined using one of the methods based on plant physiology. For example, one of the sap flow methods, porometry or other chamber methods. The focus of this thesis, however, is the water loss from the complete agroecosystem and so we will further focus on the evapotranspiration as a whole.

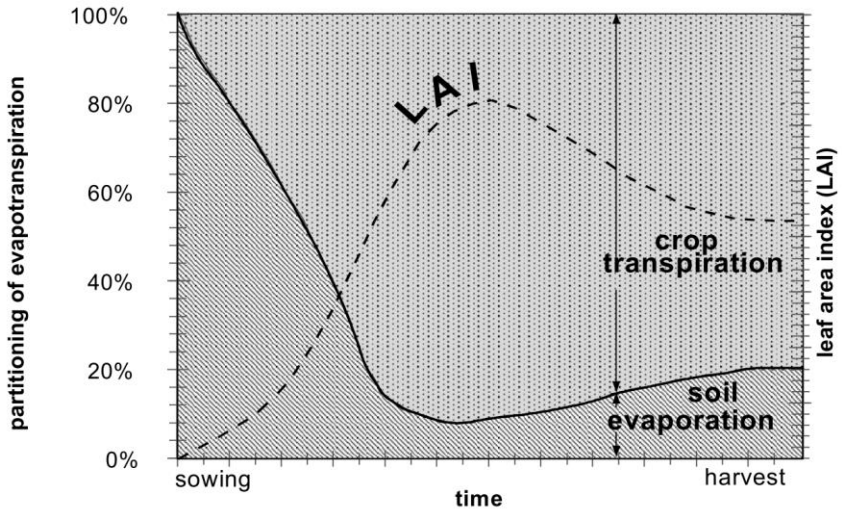

Fig 4 The evapotranspiration partitioning into evaporation and transpiration over the growing period for an annual field crop (Allen et al., 1998).

Tab 1 Conversion factors for evapotranspiration adapted from Allen et al. (1998).

	Depth	Volume per unit area		Energy per unit area
	mm day^{-1}	m^3 ha^{-1} day^{-1}	l s^{-1} ha^{-1}	MJ m^{-2} day^{-1}
1 mm day^{-1}	1	10	0.116	2.45
1 m^3 ha^{-1} day^{-1}	0.1	1	0.012	0.25
1 l s^{-1} ha^{-1}	8.64	86.40	1	21.17
1 MJ m^{-2} day^{-1}	0.41	4.08	0.05	1

As it was mentioned earlier in this section, evaporation of water takes an energy. In particular, 1 kg of water “costs” 2.45 MJ to evaporate at 20 °C. That means, for the ET rate we

can use units MJ m^{-2} day^{-1} (or mm m^{-2} day^{-1}). Eventually the latent heat flux (*LE* sometimes referred to as λET or *LvE*) can be also expressed in units W m^{-2} s^{-1}. Tab 1 adapted from Allen et al. (1998) summarizes the conversion factors used for different units: mm of water column per day, cubic meters/litres per day, or MJ of energy per different unit areas (m^2 or ha).

Water loss through ET can be either measured or modelled. Fischer (2012) summarized different approaches for estimating water loss and their development in time very well. He divided measurement approaches to three groups: hydrological (lysimetry, water balance), micrometeorological (Bowen ratio energy balance method, aerodynamic method, eddy covariance and scintillometry), and plant physiology approaches (porometry, sap flow and chamber methods). Some of these direct and indirect methods will be described in section 2.4. Theory of measurement techniques, and used in practical part of the thesis. Fischer (2012) also sorted out the modelling approaches, into three groups: empirical ET models (Penman and Priestley-Taylor approach), Penman-Monteith analytical approach (Food and Agriculture Organization (FAO) reference and crop ET), and soil water balance modelling. Our attention will be drawn to the second mentioned - FAO reference and crop evapotranspiration in the section 2.2.2. Reference evapotranspiration.

2.2.1 Potential evapotranspiration

Potential evapotranspiration (PET) is defined in different ways in the literature. According to Thomas (2000) PET is the most important climatic element next to temperature and precipitation and it plays a crucial role in the heat and mass fluxes of the global atmospheric system. Lu et al. (2005) describe PET as an important index of hydrologic budgets at different spatial scales and a critical variable for understanding regional biological processes. The concept of PET was first introduced in the late 1940s by Penman and it was defined as the amount of water that could evaporate and transpire from a vegetated landscape without restrictions other than the atmospheric demand (Penman, 1948; Thornthwaite, 1948). The vegetation was described as “a short green crop, completely shading the ground, of uniform height and never short of water”, nevertheless not a specific crop (Irmak and Haman, 2003; Matejka and Hurtalová, 2005). Hence, the concept of reference evapotranspiration was introduced in the late 1970s and early 80s to avoid ambiguities that existed in the definition of potential evapotranspiration.

2.2.2 Reference evapotranspiration

Reference evapotranspiration (*ETo*) is the evapotranspiration rate from a reference surface. This hypothetical crop surface has specific characteristics such as crop height (0.12 m), a fixed crop surface resistance (70 s m^{-1}), and albedo (0.23). This closely resembles an extensive green grass cover of uniform height, completely shading the ground, actively growing with adequate water (Allen et al., 1998; Smith, 2000). The *ETo* expresses the evaporating power of the atmosphere at a specific location and time and does not consider the specific crop characteristics and soil factors. The *ETo* can be computed from weather data because the only factors affecting *ETo* are climatic parameters (Allen et al., 1998).

Reference ET in diurnal step can be calculated using following equation:

$$ETo = \frac{0.408\,\Delta(Rn-G)+\gamma\left(\frac{900}{T}+273\right)u\,(e_s-e_a)}{\Delta+\gamma(1+0.34\,u)}, \quad (4)$$

where *ETo* is reference crop *ET* (mm per day), *Rn* is net radiation (MJ m^{-2} per day), *G* is soil heat flux (MJ m^{-2} per day), *T* is mean day temperature (°C), *u* is a wind speed measured at 2 m height (m s^{-1}), $(e_s - e_a)$ is vapour pressure deficit (kPa), Δ is slope of the vapour pressure curve (kPa C^{-1}), γ is psychrometric constant (kPa C^{-1}), and 900 is conversion factor. This equation resulted from simplification of the Penman-Monteith form of the combination equation using fixed aerodynamic (r_a) and surface resistances (r_s). Based on the assumption that crop height of reference grass is constant (h = 0.12 m) and air temperature, humidity and wind speed measurements height is also standardized (2 m) the aerodynamic resistance for the grass reference surface is equal to:

$$r_a = \frac{\ln\left[\frac{z_m-d}{z_{om}}\right]\ln\left[\frac{z_h-d}{z_{oh}}\right]}{k^2 u_z} = \frac{208}{u}, \quad (5)$$

where z_m and z_h are measurement heights (m) of the wind speed and air humidity, respectively ($z_m = z_h = 2$ m), *d* is zero plane displacement height (m), z_{om} and z_{oh} is roughness length (m) for momentum transfer and heat and vapour transfer, respectively, *k* is von Karman´s constant (0.41) and u_z is a wind speed at height *z* (m s^{-1}). When *h* is the crop height then d = 2/3 h; z_{om} = 0.123 h; and z_{oh}= 0.1 h (Allen et al., 1998).

The equation of surface resistance (r_s) is:

$$r_s = \frac{r_l}{LAI_{active}} = \frac{100}{0.5\,(24)0.12} \approx 70\ s\ m^{-1}, \quad (6)$$

where r_l is bulk stomatal resistance of well illuminated leaf (s m^{-1}), and LAI_{active} refers to active leaf area index (m^2 m^{-2}). This LAI is calculated for 0.12 m height reference grass and it is assumed that 50 % of total LAI is active. Number 24 represents the fact that LAI for clipped grass is 24 times its height. The average value of surface resistance for the whole day is then equal to 70 s m^{-1}. Allen et al. (2006) reviewed using r_s = 70 s m^{-1} for hourly or shorter periods and using a lower r_s = 50 s m^{-1} value during daytime and r_s = 200 s m^{-1} during night time. They concluded with recommendation to use these values as standardized parameters and coefficients for calculating *ETo*. On average, they will provide good agreement with computations made on a daily time step basis. No changes were suggested for the FAO-PM method for daily time steps, where use of r_s = 70 s m^{-1} should continue (Allen et al., 2006).

However, for the research purposes half hourly data are commonly used. When we do not omit surface and aerodynamic resistances, the equation has the form of the Penman-Monteith combination equation:

$$LE = \frac{\Delta(Rn-G)+\rho_a C_p \frac{(e_s-e_a)}{r_a}}{\Delta+\gamma\left(1+\frac{r_s}{r_a}\right)}, \quad (7)$$

where *Rn, G,* $(e_s - e_a)$, Δ, γ, r_a , r_s are as previously specified for Eq. 4 and Eq. 5.

In practice, the measurement of meteorological variables not always take place on the reference type of cover. But for the reference *ET* estimates the net radiation and the soil heat flux must be always calculated using global radiation. Using a measured value of *Rn* or *G* of different crop would imply an error to the estimated *ETo.* The same rule applies to wind speed measurement. Anemometer should be placed above the reference cover or if measured above a taller crop anemometer should be placed higher and then wind speed recalculated for 2 m height. This way the influence of the crop on wind velocity would be minimised.

2.2.3 Actual evapotranspiration

Contrary to reference evapotranspiration, actual evapotranspiration (*ETa*) is the ET of particular crop at particular place and time which takes into account also the plant characteristics and stress caused by non-standard conditions, i.e. pests and diseases, or soil fertility, water shortage or waterlogging etc. One of the basic approaches towards estimation of *ETa* is the use of so-called crop coefficients. Although this attitude has its drawbacks as will be described in the following section.

2.2.3.1 Crop coefficient

Estimating crop evapotranspiration have been established in Food and Agriculture Organization (FAO) Irrigation and Drainage Paper No. 56 (Allen et al., 1998). According to this methodology the crop evapotranspiration can be deduced by multiplying reference ET (*ETo*) by corresponding crop coefficient (*Kc*). Such ET represents crop evapotranspiration under standard conditions, it is denoted as *ETc*, and it is the ET from disease-free, well-fertilized crops, grown in large fields under optimum soil water conditions, and achieving full production under the given climatic conditions (Allen et al., 1998). As described, it gives us an idea of the actual ET in an absolutely "ideal world".

The crop coefficient, *Kc*, is basically the ratio between the crop ET and the reference ET:

$$K_c = \frac{ET_c}{ET_o}, \tag{8}$$

It represents an integration of the effects of four primary characteristics that distinguish the crop from reference grass: crop height, albedo, canopy resistance, and soil evaporation (Allen et al., 1998). *Kc* varies predominantly with crop characteristics and only to a limited extend with climate. That is why this approach allows to transfer standard values of *Kc* across different climate conditions and has been accepted worldwide.

The crop coefficient approach towards calculation crop ET has several levels. The *Kc* expresses the difference between reference grass and specific crop. According to Allen et al. (1998) this difference can be either combined to a single coefficient (single crop coefficient) or split between two factors describing evaporation and transpiration separately (dual crop coefficient).

Dual *Kc* is more precise since it takes into account varying soil evaporation in time. It is more advisable for research purposes and precise real time irrigation scheduling. Dual *Kc*

allows calculation of ET for shorter time steps (daily values, while single *Kc* 10-day or monthly values), hence requires higher computing capacity. Dual *Kc* can be expressed as:

$$K_c = K_{cb} + K_e, \quad (9)$$

where K_{cb} is basal crop coefficient, K_e is soil water evaporation coefficient. The K_{cb} is the ratio between *ETc* and *ETo* when the soil is dry on its surface but there is sufficient amount of the soil water content in the root zone of the plants to sustain full transpiration. On the contrary, K_e represents evaporation from the soil surface and can be large after the rain or irrigation and fairly small and drops to zero wen there is no water left for evaporation. Sum of K_{cb} and K_e can never exceed the maximum *Kc* determined by the energy available for evapotranspiration at the soil surface. Practical use of the dual *Kc* will be presented as a case study from Domaník (the Czech Republic) in 2013 entitled: Analyses of spring barley evapotranspiration rates based on gradient measurements and dual crop coefficient model (Appendix D).

2.3 Relevance of the evapotranspiration in agriculture

The yields of agricultural crops depend to a great extent on water availability. According to some projections, the likelihood of stress caused by drought is going to increase in the future climates expected for the Central Europe. Moreover, increasing global population will put a higher pressure on agriculture to feed more people. The United Nations published a projection of expected growth in World Population Prospects: The 2015 Revision. The world population is projected to increase by more than one billion people within the next 15 years, reaching 8.5 billion in 2030, and to increase further to 9.7 billion in 2050 and 11.2 billion by 2100 (Yee et al., 2015).

In agriculture evapotranspiration (ET) plays a crucial role in water management. It is a key component of the water balance as well as the energy balance. Therefore, in order to manage agrosystems properly, a high level of accuracy is necessary to estimate crop water demand of particular site. Precise evapotranspiration measurements are essential for efficient irrigation management and can even prevent significant losses of economic and water resources (Lecina et al., 2003).

Between 70 and 85 % of rainfall can be considered “lost” in agriculture (Rockström et al., 2003) through surface run-off and deep percolation (blue water) and non-productive water flow so-called green water (soil evaporation). Soil evaporation generally accounts for 30–60 % of rainfall (Wallace, 1999), and it can exceed 60 % in sparsely cropped farming systems in semi-arid regions (Allen, 1990). Cooper et al. (1983) found that up to 60 % of the seasonal rainfall evaporated directly from the soil from barley grown in Northern Syria and Brutsaert (1982) indicated that approximately 60 % of precipitation is turned into ET. Especially in arid and semi-arid regions water resources are limited. According to Molden et al. (2010) up to 90 % of rainfall evaporates back into the atmosphere in arid environments. That is why, there is a need for techniques valid in dry conditions. Such data can be used in planning and management of sustainable agriculture and drought mitigation similar to InterDrought project running in the

Czech Republic (www.intersucho.cz, www.klimatickazmena.cz) which aims for monitoring of drought in agriculture and developing an early warning system for agricultural droughts. This thesis is a part of that project.

Given the importance of good understanding of interactions between climate and water for crop production at different time and special scales (Pauwels et al., 2008; Smith, 2000) this thesis focuses on detailed study of water and energy budget of agricultural crops using a multisensory approach.

Nowadays, the most common technique to measure ET at field scale has been the eddy covariance method (Baldocchi, 2003; Simmons et al., 2007; Rosa and Tanny, 2015). As Rosa and Tanny (2015) pointed out this technique is reliable for research, however, it is quite costly, requires complex operation and intensive data analysis and thus its application at the farm level is limited. These are the main reasons for exploring other possibilities and simpler techniques to measure ET in agriculture. For example, the Bowen ratio or the surface renewal technique. The use of scintillometry in agrometeorological studies is rising, too, especially for its ability to measure at larger scales and heterogeneous surfaces and its potential for remote sensing validation.

Countless studies report on ET, however, Allen et al. (2011a,b) warn against reporting the data containing measurement biases that can confuse or mislead the water management administrators who follows the irrigation water requirements. According to these authors currently ET data are derived from variety of measurement systems and all of them require substantial experimental care and are prone to biases. In this thesis several techniques including traditional and approved methods but also state of the art techniques will be described and compared involving mentioned concerns. To our best knowledge, there has not been published any field study from the Czech Republic using the scintillometry method in the agricultural experimental field and thus it will be the main focus of the thesis as a novelty in the field.

2.4 Theory of measurement techniques

In this section a theoretical background of four techniques to determine actual evapotranspiration will be given. Starting with “The eddy covariance theory” section explaining principles of the method which is nowadays considered to be a standard technique to measure evapotranspiration worldwide. The second section 2.4.2 The scintillometry theory is further divided into three subsections describing different types of devices. The theory behind the large aperture scintillometers is defined in section 2.4.2.1 Boundary layer scintillometer theory behind the laser scintillometers is presented in subsection 2.4.2.2 Surface layer scintillometer and the microwave scintillometer is described in subsection number 2.4.2.3. This part is followed by the section 2.4.3 The Bowen ratio theory, and 2.4.4. The surface renewal theory.

2.4.1 The eddy covariance theory

The eddy covariance (EC) method is a direct measurement method for deriving the vertical transfer of water vapour proposed firstly by Swinbank (1951). The EC determines turbulent fluxes using high-frequency point-sampling measurements. It is based on the direct measurement of the specific humidity, *q,* and scalar concentration by gas analyser and wind speed components (u, v, and w) measured by the 3D sonic anemometer to assess direction of the flow. Mathematically, the vertical flux can be expressed as covariance of the vertical velocity and concentration of the entity of interest (Burba, 2013). In the framework of eddy covariance the fluxes of quantity x are defined by:

$$F_x = \overline{\rho}\,\overline{w'x'} = \overline{\rho}\,\mathrm{cov}(w, x), \tag{10}$$

where F_x is the flux of quantity x (kg m^{-2} s^{-1}), ρ is the density of air (kg m^{-3}), w' is the turbulent part of the vertical wind speed (m s^{-1}) and x' the turbulent part of scalar quantity x (Webb et al., 1980; Stull, 1988). Quantity x is usually referred to as mixing ratio (the ratio of the constituent to the dry air, i.e. mass of the substance per unit mass of dry air). Eq. 10 can be applied when two important assumptions of the eddy covariance technique are fulfilled. Firstly, air density fluctuations are assumed to be negligible. For conventional eddy covariance measurements this assumption is usually fulfilled by choosing suitable measurement site: a vast reasonably flat terrain with adequate fetch. Secondly, mean vertical flow is assumed to be negligible for horizontal homogeneous terrain (no divergence/convergence) (Burba, 2013). When these assumptions are fulfilled, the "eddy flux" is equal to the product of the mean air density and the mean covariance between instantaneous deviations in vertical wind speed and mixing ratio (second part of Eq. 10).

Sensible heat flux is equal to the mean air density multiplied by the covariance between deviations in instantaneous vertical wind speed and temperature; conversion to energy units is accomplished by including the specific heat term:

$$H = \bar{\rho} C_p \overline{w'T'}, \tag{11}$$

and latent heat flux can be expressed:

$$LE = \rho\lambda \overline{w'q'}, \tag{12}$$

where, C_p is the heat capacity of air at constant pressure (J kg^{-1} K^{-1}) and λ is the latent heat of vaporization (J kg^{-1}). In this study, both C_p and λ are modelled by taking into account their temperature dependence (Garratt, 1992; Stull, 1988).

To reduce random error in the covariance, high-frequency measurements of the wind speed, temperature, humidity, or CO_2 are needed to limit the averaging time (Lenschow et al., 1994; Bosveld and Beljaars, 2001). At the same time, the averaging time must be long enough to include the largest turbulent eddies and short enough to exclude non-turbulent motions (Lenschow et al., 1994; Mahrt, 2010). This results in an averaging time of at least 10, but

typically 30 minutes (Hartogensis et al., 2002; Sun et al., 2005; Aubinet, 2008; Finnigan, 2008; Vickers et al., 2009; Mahrt, 2010). During these 10–30 minutes, stationarity is required, a condition that is not always met, e.g. in cloudy conditions or intermittent boundary layers (Hartogensis et al., 2002). Consequently, under these circumstances the eddy covariance method has limited application (Van Kesteren et al., 2013a).

The EC method relies on many other assumptions. Some of them are related to terrain and flow. These involve: terrain is uniform and flat (average of fluctuation is zero, and two mentioned above), adequate fetch and footprint, measurement is done within a boundary layer of interest, point measurement represents an upwind area, flux is fully turbulent, instrument can detect very small changes in a very high frequency (Burba, 2013). When all the assumptions are not met the raw data must undergo a set of corrections to minimise potential sources of errors. These corrections include, e.g. coordinate rotation (tilt correction) (Lee et al., 2004), spectral correction in the high and low frequency range, sensor separation correction (Moore, 1986), correction of the buyoancy flux measured with the sonic temperature (Kaimal and Gaynor, 1991), and density fluctuation correction (Webb et al., 1980). The corrections are made in the post processing of raw data and generally result in increased LE which is usually underestimated by this technique.

2.4.2 The scintillometry theory

Scintillation or twinkling is the variation of light beam caused by turbulence in the atmosphere. This phenomenon is used to detect turbulence between an optical transmitter and a receiver of the scintillometer along the propagation path.

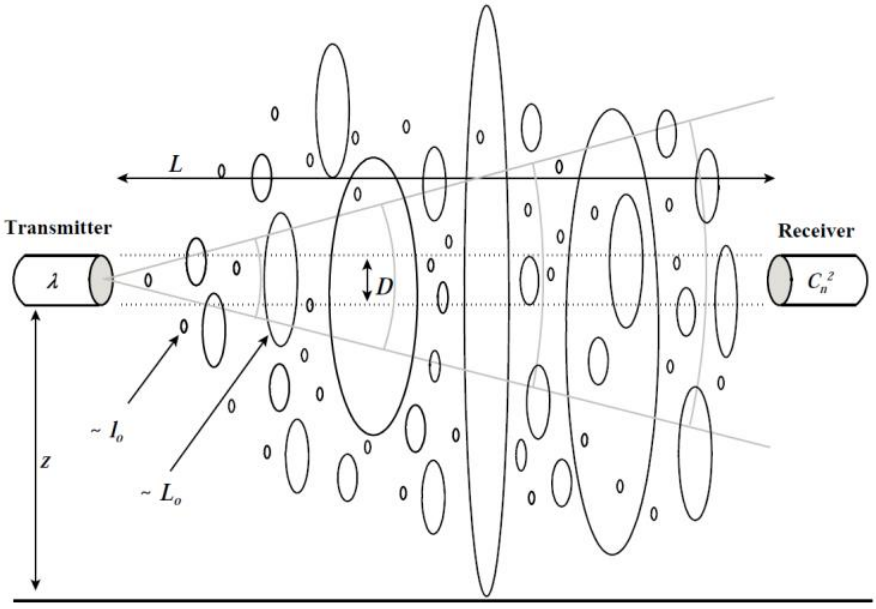

Fig 5 Schematic drawing of a scintillometer set-up where the electro magnetic beam (wavelenth λ) emitted by the transmitter is passing through the turbulent atmosphere and is scattered by eddies (circles). Also important length scales are shown (l_o, L_o) and the aperrture size of the scintillometer (D), the path length (L), and the path height (z) (Meijninger, 2003).

The path can be long between several 10s of meters to several kilometres (Fig 5). The resulting flux calculations represent an area average of this path influenced by a weighing function – centre of the path more than the edges (Fig 20). Such a footprint can be of a grid size of an airborne picture (e.g. satellite image) and thus it represents a great tool for validation of models based on remote sensing.

The scintillations are caused by the fluctuations of the refractive index of air (n) and its magnitude can be described by its structure parameter (C_n^2) which is the basic parameter derived from scintillometer data (De Bruin, 2002). The refractive index is influenced by temperature, humidity and to a minor extent by the pressure of the atmosphere. At the optical wavelengths the contribution of temperature fluctuations dominates and thus the structure parameter of temperature (C_T^2) can be deduced from C_n^2 (Moene, 2003a, Lüdi et al., 2005, De Bruin, 2009, Ward et al., 2013). For the radio wavelengths (more than 1 mm), on the contrary, water vapour fluctuations contribute to the scintillations the most and thus enable to determinate the structure parameter of the moisture (C_q^2) from the C_n^2 measurement. Eq. 13 shows the relationship between the structure parameters:

$$C_n^2 = \frac{A_T^2}{\bar{T}^2}.C_T^2 + 2\frac{A_T A_q}{\bar{T}\bar{q}}.C_{Tq} + \frac{A_q^2}{\bar{q}^2}.C_q^2, \tag{13}$$

where A_T and A_q are functions of temperature, humidity, pressure (neglected), and wavelength (Hill et al., 1982; Andreas, 1989). For scintillometers operating at visible or near-infra red wavelengths the Eq. 13 can be simplified using the Bowen ratio (β) (Moene, 2003b) to:

$$C_n^2 = \frac{A_T^2}{\bar{T}^2}.C_T^2\left(1 + \frac{0.03}{\beta}\right)^2. \tag{14}$$

By applying Monin-Obukhov similarity theory (MOST) surface flux of sensible heat flux (H) can be derived from C_T^2, and C_q^2 (Wyngaard and Clifford, 1978; De Bruin et al., 1995; Meijninger et al., 2002b). Further, latent heat flux (LE) can be determined by incorporating the surface energy balance equation. The MOST describes the relationship between structure parameters of temperature and humidity and the surface fluxes of sensible and latent heat assuming stationarity conditions and horizontal homogeneity. The similarity relationship for the vertical profile of the temperature structure parameter can be expressed by (Hill, 1997):

$$\frac{C_T^{\,2}(z-d)^{2/3}}{T_*^{\,2}} = f_T\left(\frac{z-d}{L_O}\right), \tag{15}$$

where, z is the (effective) height of the scintillometer beam, and d is the zero-plane displacement. The Obukhov length is defined as:

$$Lo = \frac{u_*^2\, T}{g\, k\, T_*}, \tag{16}$$

where u_* is friction velocity, T_* is the temperature scale, k is von Kármán constant, and g is the acceleration due to gravity. An analogous equation can be formulated for the profile of the humidity structure parameter that is then used to derive the latent heat flux (Beyrich et al., 2012).

The detailed description of the stability functions can be found, for example, in Andreas (1988) and in this work similar relations are used with the constants c_1 = 4.9 and c_2 = 6.1 (Moene et al., 2004).

A number of length scales plays its role in scintillometry (De Bruin, 2009). The Obukhov length (L_O) is the measure of atmospheric stability. The L_O is indirectly related to L_{out} – the outer length scale of turbulence which scales with large eddies generated by heated surface and wind shear, and is proportional to the height above the surface. Another length related to turbulence is inner length scale of turbulence (l_0) which is proportional to Kolomogorow microscale (De Bruin, 2009). Turbulent eddies between inner and outer length scales determine the form of a temperature spectrum in the inertial subrange where the Corrsin-Obukhov law applies (for details see De Bruin, 2009). The length scales mentioned above are instrument related and depend on: wavelength of the transmitter (λ), the aperture size of the instrument (D), the path length (L) - the distance between transmitter and receiver, and the first Fresnel zone ($F = \sqrt{\lambda L}$).

Based on these different scales different types of scintillometer can be distinguished. First of all, a small aperture scintillometer or laser scintillometer (SAS) with the aperture smaller than the first Fresnel zone. The second type is an optical scintillometer with aperture size 15 cm (large aperture scintillometer - LAS) or with 30-cm an extra-large aperture scintillometer (XLAS). These are operating on visible and near infra-red wavelengths. The third type of scintillometer is using radio wave source (micro wave scintillometer - MWS). Basic characteristics of these types are summarized in Tab 2 and more detailed description follows in the next sections.

In the presented thesis a large aperture scintillometer is referred to as BLS because in the experimental part of the study we use an instrument with a product name “Boundary Layer Scintillometer” given by the Scintec company. Similarly, for a small aperture scintillometer we use an abbreviation SLS according to product name “Surface Layer Scintillometer”.

Tab 2 Typical values for the basic characteristic length scales of different scintillometer types: dual beam small aperture scintillometer (SAS), large aperture scintillometer (LAS), and microwave scintillometer (MWS) (Beyrich et al., 2012).

Parameter	SAS	LAS	MWS
Wavelength, λ	≈ 700 nm	850–950 nm	≈ 3 mm
Aperture diameter, D	0.0025 m	0.1–0.3 m	0.4 m
Beam separation, d	≈ 2.7 mm	-	-
Path height, h	0.5–10 m	10–50 m	10–50 m
Path length, L	0.05–0.2 km	0.5–5 km	0.5–10 km
First Fresnel zone diameter, F	≈ 10 mm	≈ 50 mm	≈ 5 m

2.4.2.1 Boundary layer scintillometer

Boundary layer scintillometer (BLS) is an optical device operating on visible and near infrared wavelengths where the structure parameter is mostly influenced by temperature. That is why, we can neglect the humidity influence on the C_n^2, and the structure parameter of

temperature (C_T^2) can be deduced from the C_n^2 measurement. The C_n^2 can be deduced from the variance of the logarithm of the signal amplitude, B_i:

$$B_i = 16\,\pi^2 k_\lambda^{\,2} \int_0^L dx \int_0^\infty d\kappa\ \phi_n(\kappa, l_0, C_n^{\,2}) \sin^2\left[\frac{\kappa^2 x(L-x)}{2k_\lambda L}\right]\left[\frac{4J_1^2(\kappa Dx/2L))}{(\kappa Dx/2L)^2}\right], \quad (17)$$

where k_λ is the optical wavenumber, κ is the turbulent spatial wavenumber, ϕ_n is the three-dimensional spectrum of refractive index, l_0 is the inner-scale length of turbulence, D is the aperture diameter, L is the path length, x is the distance along the path and J_1 is a Bessel function of the first kind (Beyrich et al., 2012). Finally, assuming that $\Phi_n^2 = 0.033 C_n^2 k^{-11/3}$ leads to the relation (Wang et al., 1978):

$$C_n^2 = 1.12\,\sigma_{\ln(I)}^2 D^{7/3} L^{-3}, \quad (18)$$

where $\sigma_{\ln I}^2$ is the variance of the logarithmic intensity, D is the aperture diameter, and L is the path length.

Two more steps are needed to estimate the sensible heat flux (H) from C_n^2, and require additional measurements of pressure, temperature, humidity, and wind speed (De Bruin et al., 1995; Beyrich et al., 2002). Firstly, derivation of the structure parameter of temperature (C_T^2), from C_n^2 is necessary using Eq. 14 according to Moene (2003b), and the values of A_T and A_q as given in Andreas (1988, 1989). Secondly, H from C_T^2 is solved iteratively using Monin-Obukhov similarity theory (MOST). In our study the similarity relations by Andreas (1988) are used with the constants c_1 = 4.9 and c_2 = 6.1 (Moene et al., 2004). The friction velocity (u_*) is obtained from the standard MOST flux-profile relationship (see Eq. 12–15 from De Bruin et al. (1995)). The wind speed was measured at 3.5 m above the ground and the roughness length (z_0) was estimated as 0.123 of a crop height. The principle of sensible and latent heat flux calculation based on the methodology used for commercially available scintillometers is graphically summarizes in Fig 6. A more elaborate description of the flux calculations can be found in (Meijninger et al., 2002a,b; Moene et al., 2004; Van Kesteren, 2008).

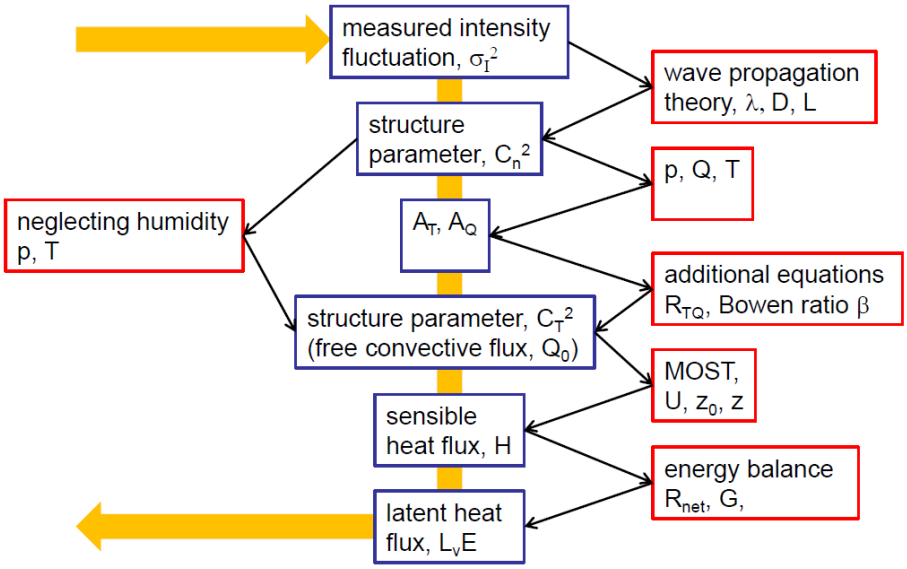

Fig 6 Summary of the process to derive a latent heat flux density using scintillometry (Scintec, 2013).

2.4.2.2 Surface layer scintillometer

Surface layer scintillometer (SLS) sometimes called also dual-beam small aperture scintillometer is a scintillometer with the aperture smaller than the first Fresnel zone ($D < F$). The name “dual–beam” reflects the fact that the beam of light (670 nm) in transmitter is split into two displaced parallel beams (approximately 2.7 mm) with orthogonal polarization. It is sensitive to eddy sizes of the order of 10 mm that are close to the inner scale length of turbulence (l_0). Its biggest advantage compared to the BLS is that it is able to directly resolve l_0.

The relation between the correlation coefficient of ln(I_1) with ln(I_2) (I_1 and I_2 are the received signal intensities) and the inner-scale length of the refractive index, l_0 (m) is described by the wave propagation and turbulence theory (Hill, 1982; Thiermann and Grassl, 1992; Hartogensis et al., 2002). Once l_0 is obtained, the structure parameter of the refractive index (C_n^2) ($m^{-2/3}$) can be obtained from the variance of ln(I_1) or ln(I_2). For the dual-beam laser scintillometer the relation is given by (Hill and Lataitis, 1989):

$$B_{12} = \frac{1}{4}\mathrm{cov}(\ln(I_1), \ln(I_2)) = 4\pi^2\kappa^2 \int_0^L \int_0^\infty \Phi_{nn}\left(k, C_{n^2}, l_0\right) J_0(kd) \sin^2\left(\pi \frac{\Lambda^2}{l^2}\right) \left(\frac{2J_1\left(\frac{kDx}{2L}\right)}{\frac{kDx}{2L}} \right)^2 dk dx \quad (19)$$

where B_{12} is the covariance of the logarithmic amplitude of the beams, $\kappa = 2\pi/\lambda$ is the wave number of the emitted radiation, L is the path length between transmitter and receiver, Φ_n^2 (k, C_n^2, l_0) is the three-dimensional spectrum of the refractive index, $k = 2\pi/l$ is the eddy wave number, J_0 and J_1 are Bessel function of the first kind (zeroth and first order respectively), d is the displacement between the two beams (2.7 mm), D is the aperture size of the receiver (2.5 mm), and $\Lambda^2 = \lambda x(L-x)/L$ is the square of the radius of the first Fresnel zone at position x along the path (Van Kesteren et al., 2014).

Firstly, the l_0 and C_n^2 are solved with the scintillometer using Eq. 18, subsequently, the structure parameter of temperature (C_T^2) ($K^2\ m^{-2/3}$), can be derived from C_n^2 (Moene, 2003a). Afterwards, friction velocity (u_*) and the turbulent scale of temperature, θ_*, can be iteratively solved using Monin-Obukhov similarity theory:

$$u_* = \nu \left(\frac{7.4}{l_0}\right)^{4/3} \left(k_{kar} z_{eff}\right)^{1/3} f_\varepsilon \left(\frac{z_{eff}}{L_O}\right)^{-1/3}, \quad (20)$$

$$\theta_* = \left(C_T{}^2\right)^{1/2} \left(k_{kar} z_{eff}\right)^{1/3} f_T \left(\frac{z_{eff}}{L_O}\right)^{-1/2}, \quad (21)$$

where ν is the kinematic viscosity of air, $k_{kar} = 0.4$ is the von Kármán constant, z_{eff} is the effective measurement height of the scintillometer, L_O is the Obukhov length, and f_T and f_ε are similarity functions for temperature and for the dissipation rate of turbulent kinetic energy that depend on z_{eff}/L_O (Van Kesteren et al., 2014).

Finally, after finishing the iteration, H can be obtained via equation:

$$H = \rho c_p \, u_* \theta_*, \tag{22}$$

where ρ is the density of air and C_p is the heat capacity of air at constant pressure, u_* is the friction velocity, and θ_* is the turbulent scale of temperature.

2.4.2.3 Microwave scintillometer

Different versions of the visible and near-infrared scintillometers are commercially available over the last 10–20 years and are becoming the research tool of an increasing number of scientists. However, the microwave scintillometer remained in the background compared to BLS and SLS. Probably this is due to the technical challenges, sophistication, and the high of cost (Green et al., 2001).

The optical scintillometer is mostly sensitive to temperature, on the other hand, radio wave scintillometer to the humidity of air. The combination of a near-infrared scintillometer and a microwave wave scintillometer is also known as the two-wavelength method and appeared in 1980s (Hill, 1982; Andreas, 1989). The method was used by Green et al. (2000, 2001) and Meijninger et al. (2002a,b) and recently its popularity slowly grows (Beyrich and Mengelkamp, 2006; Meijninger et al., 2006; Ward et al., 2013, 2015a,b).

There are several ways to determine fluxes by this method. Briefly, the two-wavelength scintillometer system provides three refractive index structure parameters (C_n^2), denoted C_{n1n1} from the optical scintillometer, C_{n2n2} from the millimetre-wave scintillometer and C_{n1n2} from the correlation between optical and millimetre-wave signals. Conversion to the temperature and humidity structure parameters involves either the single-wavelength, two wavelength or bichromatic-correlation method (Ward et al., 2015b). For a schematic summary see Fig 7, detailed description including equations can be found, for example, in Ward et al. (2015a,b).

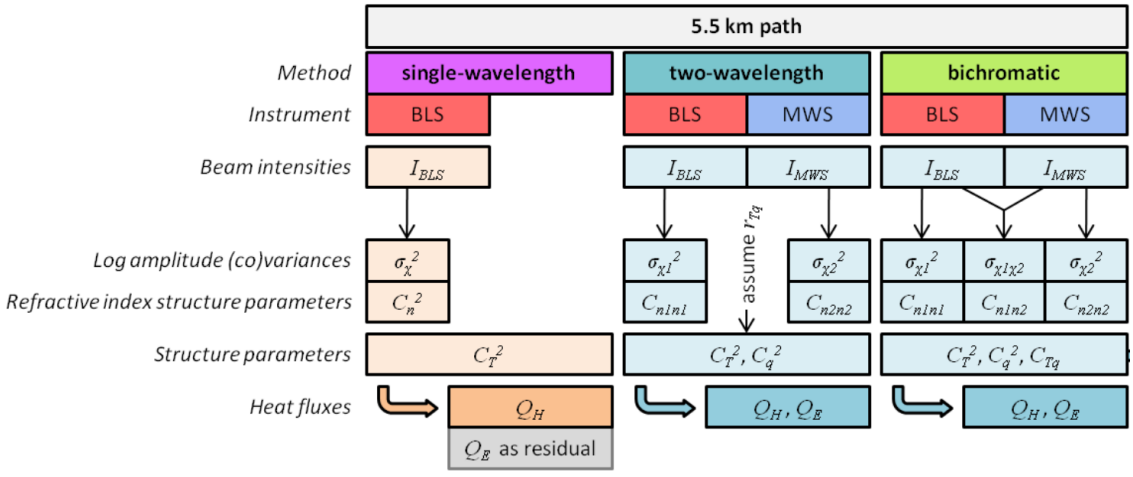

Fig 7 Schematic of the methods to obtain heat fluxes from scintillometry including an optical large aperture scintillometer (BLS) and a millimetre-wave scintillometer (MWS) (Ward et al., 2015b).

2.4.3 The Bowen ratio theory

One of the standard techniques to determine latent heat flux density (*LE*) indirectly is the Bowen ratio energy balance (BREB) method (Heilman and Brittin, 1989). The BREB determines *LE* and *H* fluxes based on the rearrangement of simplified surface energy balance equation given by:

$$Rn = H + LE + G \tag{23}$$

where *Rn* is the net radiation flux, *G* is soil heat flux, *H* and *LE* are sensible heat and latent heat flux, respectively (all in W m^{-2}) (Bowen, 1926). The Bowen ratio is basically the ratio between *H* and *LE*, and can be expressed as:

$$\beta = \frac{H}{LE} \tag{24}$$

The combination of energy balance and the Bowen ratio are then following equations:

$$LE = \frac{Rn-G}{1+\beta} \tag{25}$$

$$H = \frac{\beta\,(Rn-G)}{1+\beta} \tag{26}$$

To divide available energy between the sensible and the latent heat flux we use the measurements of air temperature and air humidity at two heights above the surface (Savage, 2010) to gain the temperature and vapour pressure gradients (Perez et al., 1999; Peacock and Hess, 2004; Guo et al., 2007; Savage, 2010). These are used to further calculate *LE* and *H* as follows:

$$LE = \rho c_p \gamma^{-1} K_{LE} \left(\frac{\partial e}{\partial z}\right), \tag{27}$$

where, *γ is* the psychrometric constant, K_{LE} is the exchange coefficient for latent energy flux ($m^2\ s^{-1}$), *∂e* is the difference in vapour pressure (kPa), and *∂z* is the difference in height (m).

Similarly, the sensible heat flux can be determined by:

$$H = \rho c_p \gamma^{-1} K_H \left(\frac{\partial T}{\partial z}\right), \tag{28}$$

where K_H is the exchange coefficient for sensible heat flux ($m^2\ s^{-1}$), and *∂T* is the air temperature difference (°C) between the two heights. According to Bowen ratio similarity principle $K_H = K_{LE}$ (Verma et al., 1978), and thus the Bowen ratio can be expressed in the simplified form:

$$\beta = \frac{\gamma \partial T}{\partial e}, \tag{29}$$

which enables determination of *LE* and *H* using Eq. 25 and Eq. 26.

The BREB method is relatively simple to use, affordable, and gives reasonable results, however, there are limitations that need to be addressed. For adequate flux results, data when $\beta \approx -1$ must be rejected (denominator in Eq. 25 and Eq. 26 would be 0). Data should be rejected when the wind velocity is lesser than 1 m s^{-1} and the difference between upper and lower wind speed is larger than 0.3 m s^{-1} (Foken et al., 1997). Such a filtering should ensure sufficient turbulent regime. Although the measurement height itself or the difference in the measurement heights is not included in the calculation directly, it does have an influence on the measurement and thus attention should be payed to correct choice. The more distant the sensors are the bigger gradients will be recorded and larger fluxes calculated. The height of the sensors above the crop surface also influences the footprint and fetch requirements.

2.4.4 The surface renewal theory

The surface renewal method measures the sensible heat flux (*H*) by analysing the temperature changes in turbulent coherent structures (small parcels of air) that directly interact with the crop surface (Paw U et al., 2005). The exchange of scalars between the surfaces and the atmosphere results in creation of a ramp-like structures in the scalar trace. For some time after the interaction of an air parcel with the surface its temperature does not change. This period is called the quiescent period (s) and it is followed by the warming period (d) when the energy is transported from the canopy to the air parcel. The warming stops when a cool air parcel from aloft sweeps down and replaces the warmer air in the canopy represented by a sudden drop of the temperature. This “renewal” event on the surface of plant canopy gave a name to the surface renewal (SR) method.

The temperature ramps are characterized by an amplitude (a) and inverse ram frequency (d + s) (Snyder et al., 1996; Spano et al., 1997). The scheme of the temperature ramp is shown in Fig 8.

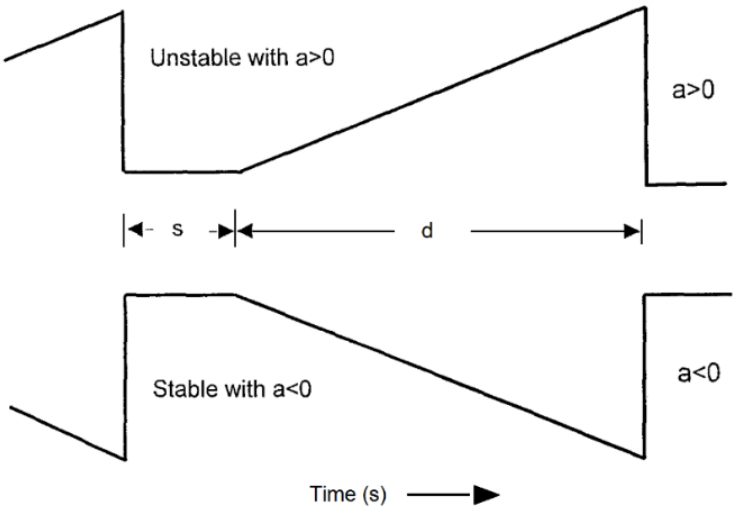

Fig 8 Schematic temperature ramps with amplitude a > 0 for unstable and a < 0 for stable atmospheric conditions. The inverse ramp frequency (d + s) is the sum of the quiescent period (s) and the ramp (d) (in seconds) (Snyder et al., 1996).

The ramp characteristics of the high frequency signal need to be identified in order to quantify scalar flux density. According to Paw U et al. (1995), sensible heat flux density (*H*) can be expressed as a function of mean ramp amplitude (a) and mean ramp duration ($d + s$) as follows:

$$H_{SR} = \alpha z C_p \rho \frac{a}{(d+s)}, \tag{30}$$

where *α* is correction factor for unequal heating of the air column, *z* is the height (m) of the measurement, C_p is the specific heat of air, *a* is the ramp amplitude, and (*d* + *s*) is the ramp duration. The estimate of mean value for amplitude during the interval is determined by following equation for real roots:

$$a^3 + \left(10S^2(r) - \frac{S^5(r)}{S^3(r)}\right) a + 10S^3(r) = 0. \tag{31}$$

Inverse ramp frequency can be calculated using:

$$d + s = \frac{a^3 r}{S^3(r)}\,. \tag{32}$$

The ramp duration (*d* + *s*) can be according to Van Atta (1977) determined via combining the second, third and fifth order structure functions, although other alternatives like wavelet analysis and model fitting (Katul et al., 1996) have been successfully used, as well. The correction factor *α* is usually derived by comparing to independent measurement such as eddy covariance (Paw U et al., 1995; Spano et al., 1997), or is quantified as a function of stability by applying MOST theory using additional measurement of the wind speed (Castellví, 2004).

In presented study, the two-scale ramp model was used since we prefer to have an independent method with the simplest instrumentation possible, i.e. only fine wire thermocouple (Fischer, 2016, pers. comm.). In this two scale procedure the gradual rise of the scale one determines the time lag for resolving the scale two. The gradual rise period is obtained by solving the third order structure function at two time lags (Paw U et al., 2005; Shapland et al., 2012a).

Afterwards, a ramp duration is determined based on the intermittency of the scale one characteristics (Shapland et al., 2012a,b). After the choosing proper time lag, scale two ramp characteristic are obtained from the expanded Van Atta procedure (Shapland et al., 2012a,b) and H can be obtained from Eq. 30 without the need of any calibration.

2.5 Comparison of methods

Tab 3 starting on page 32 contains the selection of case studies focused on the comparison between different measurement methods for latent heat flux (*LE*) or sensible heat flux (*H*) estimation. The list is not comprehensive however, it shows a relatively wide range of work that have been done on the evapotranspiration related topic since 1990s. The most of the presented studies compared two measurement techniques, some of the papers listed below are the reviews summarizing and comparing several methods. Not only measurement techniques but also modelling approaches like Penman-Monteith combination equation or Priestley-Taylor

approximation (Rana and Katerji 2000; Drexler et al., 2004) were used in listed studies. Moreover, papers describing important milestones in research and development of individual methods or their implementation are also cited.

The comparison of different methods provided by Drexler et al. (2004) and Rana and Katerji (2000) are presented in Tab 4 starting on page 38. The main advantages and disadvantages of individual approaches are summarized and highlighted there. At the beginning of the table, there are three methods used in the experimental part of this thesis: the eddy covariance technique, the Bowen ratio energy balance method, and the surface renewal method. Further, reader can find benefits and drawbacks of soil water balance approach, weighing lysimeter, aerodynamic method or the sap flow method. These were not used in our study however, they are widely used and important tools for water balance studies in different ecosystems. Besides these methods LIDAR is mentioned followed by empirical and combination equations, weighted canopy methods, and crop canopy coefficient method (CCC).

Another important aspect mentioned repeatedly in the literature is the competence of the personnel performing the measurements. Allen et al. (2011a) tried to quantify the error caused by qualified or non-qualified operator and their results are presented in Tab 5 (page 41).

Tab 3 The selection of case studies comparing different methods to estimate sensible (*H*) and/or latent heat (*LE*) flux densities over different covers and their main conclusions. Abbreviations of methods: EC – the eddy covariance, BREB – the Bowen ratio energy balance, SR – the surface renewal, VAR – Flux-variance method, Sci – scintillometry, SAS – surface layer scintillometer, LAS – large aperture scintillometer.

Author	Methods	Cover	LE	H	Conclusions
Barr et al. (1994)	EC BREB	Deciduous forest	✓	✓	The EC estimates of *H* and *LE* underestimated day-time surface available energy by 11 %. The EC also partitioned available energy differently than BREB. The most plausible causes for the failure of EC to close the energy balance are a low frequency loss of flux and the failure to account for the spatial dispersive flux.
Katul et al. (1996)	SR VAR	Pine forest	✓	✓	The SR theory in conjunction with a two-stage time-frequency filtering scheme reproduced the direct eddy-correlation measurements well for *H* and *LE*.
Anandakumar (1999)	Sci (SAS) EC SR	Wheat		✓	Good agreement between H_{EC} and H_{SAS}; SAS exhibiting smoother variations than EC; SLS was better correlated with net radiation than EC and variations in *H* due to the shadowing effect of the clouds are well reflected (5 days of measurement). The SR provided reliable estimates of *H* but with low temporal resolution.
Rana and Katerji (2000)	A review	Different surfaces	✓		Summary of the advantages and disadvantages of the evapotranspiration (ET) measurement methods (Tab 4).
Spano et al. (2000)	SR	Grapevine	✓	✓	The results indicated that the SR technique provides good estimates of *H* under all stability conditions without the need for calibration when the data are measured at about 90 % of the canopy height. The SR technique offers an

Tab 3 (Continued)

Author	Methods	Cover	LE	H	Conclusions
					inexpensive alternative for estimating evapotranspiration with good accuracy.
Todd et al. (2000)	BREB Lysimeter	Alfalfa	✓		Disagreement between the BREB and lysimeter, daytime *LE* was greatest during the first and the second cutting, when the relative RMSD was 24 and 29 %, respectively. Daytime relative RMSD decreased during subsequent cuttings, and ranged from 16 to 19 %. Greatest disagreement was when the *LE* was greater than 400 W m^{-2}. Night-time *LE* disagreed more than the daytime fluxes. Relative RMSD, by cutting, ranged from 86 to 118 %.
Zapata and Martínez-Cob (2001)	SR EC	Wetland	✓	✓	The SR method was used to estimate H near the lagoon and LE was obtained by solving EB equation for both EC and SR method.
Drexler et al. (2004)	A review: EC BREB SR LIDAR	Wetland	✓		Each measurement and estimation method has advantages and disadvantages based on cost, theoretical approach, underlying assumptions, calibration, and data requirements. Another result of the review is that, because individual methods have strengths and weaknesses, it seems prudent to use two or more measurement and estimation methods and compare the results.
Beyrich et al. (2006)	EC Sci (LAS)	Different surfaces: forest, lake, grassland, agro systems	✓	✓	The LITFASS-2003 experiment on heterogeneous terrain. Measurements from the 13 sites were composed into a time series of the area-averaged surface flux by taking into account the relative occurrence of each surface type in the area. Comparison of these aggregated surface fluxes with area-averaged

Tab 3 (Continued)

Author	Methods	Cover	LE	H	Conclusions
					fluxes from scintillometer and from airborne measurements showed good agreement.
Pauwels and Samson (2006)	EC BREB	Wet grassland	✓		The objective was to compare methods under non-ideal conditions – a wet sloping grassland. The comparison resulted in a good agreement.
Hoedjes et al. (2007)	EC Sci (LAS)	Olive orchard		✓	During irrigation events spatial variability in soil humidity was large. This heterogeneity caused large differences between the source area characteristics of the EC system and the LAS, resulting in a large scatter when comparing sensible heat fluxes obtained from LAS and EC.
Castellví et al. (2008)	EC SR	Grassland	✓	✓	The energy balance closure was analyzed using two methods. Regardless of the weather conditions, the EC closure underestimated the available energy by about 10 %, but the performance was slightly better during dry rather than humid conditions. In contrast, the SR closure was always good and did not favour wetness conditions. The SR analysis provided reliable Bowen ratio estimates.
Shi et al. (2008)	EC BREB Penman-Monteith	Forest	✓		The LE estimated with the three methods showed similar diurnal and seasonal courses. PM usually gave the highest *LE* among the three methods. Sum of the half hourly values from BREB and PM methods of the three growing seasons took 81.2 % and 131 % of that from EC measurement.

Tab 3 (Continued)

Author	Methods	Cover	LE	H	Conclusions
Savage et al. (2010)	EC Sci (SAS) BREB	Grassland	✓	✓	The SAS estimates of *H* and the estimates of evaporation rate as a residual compared favourably with those obtained using the BREB and EC methods for cloudless days, cloudy days and days with variable cloud. There was no evidence for the EC measurements of *H* being underestimated in comparison to the BREB and SAS measurements. The agreement between estimates of *LE* obtained using EC and SLS was poor. However, this study adds to the discussion of MOST and uncertainties induced by choosing different functions.
Liu et al. (2011)	EC Sci (LAS)	Different surfaces		✓	The *H* measured by LAS were larger than EC. This difference seems to be caused by the so-called energy imbalance phenomenon, the heterogeneity of the underlying surfaces, and the difference between the source areas of the LAS and EC measurements.
French (2012)	EC SR VAR	Cotton, grassland	✓	✓	Estimation of surface energy fluxes using SR and VAR over an advective irrigated agricultural site. Surface flux conditions ranged widely and include episodes of latent heat fluxes exceeding net radiation. Overall, flux estimates from SR and FV were similar to simultaneously obtained eddy covariance observations on most days. During strong advection neither approach closely agreed with EC data.
Shapland et al. (2012c)	EC SR	Vineyards	✓	✓	Estimation of actual ET in vineyards on hillside terrain was estimated using SR analysis. They calibrated SR data against EC for *H* estimation. *LE* was

Tab 3 (Continued)

Author	Methods	Cover	LE	H	Conclusions
					estimated from the residual of the energy balance.
Liu et al. (2013)	EC Sci (LAS)	Different surfaces	✓		The differences in ET among the years and sites were primarily connected with the difference in soil moisture and crop growing conditions (different crops, varieties, tillage practice, etc.). The heterogeneity of the underlying surfaces in the EC and LAS source areas are the primary reasons causing the difference in measurements.
Van Kesteren et al. (2013a)	Bowen-variance Structure-parameter VAR Energy balance	Wheat	✓		The accuracy of the flux results from a correct representation of the turbulence variables. Furthermore, a 30-min flux validation shows that the methods compare well to the independent EC fluxes. They found that the structure-parameter method performs best. During the night the VAR methods were influenced by non-stationarity. They suggest using the correlation coefficients between temperature and scalar quantities to acquire the sign of the fluxes.
Van Kesteren et al. (2013b)	Bowen-variance Structure-parameter VAR Energy balance	Wheat	✓		Estimates of *LE* both the EC and the energy balance are unsuitable for estimating fluxes over 1-min averaging intervals. The three other combined methods are more successful. The structure-parameter method performs best of all methods and also under dry conditions the method accurately resolves CO^2 flux, although *LE* was more difficult to resolve.
Suvočarev et al. (2014)	EC SR	Orchard	✓	✓	There was a high agreement between the 30-min turbulent fluxes independently derived by EC and SR. Estimation of fluxes determined by SR

Tab 3 (Continued)

Author	Methods	Cover	LE	H	Conclusions
					resulted in higher values (around 11 % for LE). According to the EBC, the SR method was as reliable as the EC in estimating the turbulent fluxes related to irrigated agriculture, even when applied in heterogeneous cropping systems.
Rosa and Tanny (2015)	EC SR	Cotton	✓		A maximum deviation of 7 % was found between daily ET obtained by EC and SR methods during validation. Reducing the frequency of data analysis from the commonly used 10 Hz down to 1 Hz, increased the weighting factor but did not much affect the ET results, which indicates that the SR technique could be realised by using low-cost data acquisition systems.

Tab 4 Advantages and disadvantages of the selected evapotranspiration measurements and estimation methods adapted from Drexler et al. (2004) and from Rana and Katerji (2000).

Method	**Advantage**	**Disadvantage**
Eddy covariance	A clear advantage is that if the water vapour covariance is measured, it provides a direct measure of *LE*. In addition, if *Rn*, *G* and *H* are measured at the same time, energy balance closure can be computed to provide some verification of the measurements. None of the other methods have this self-verification. Direct method with fast hygrometer.	The greatest disadvantages of using eddy covariance are the cost, the complexity and the sensitivity of instruments to damage. Eddy covariance instrumentation generally requires high maintenance to ensure good results. Delicate sensors, difficult software for data acquisition, hygrometer very delicate and expensive.
Bowen ratio energy balance	The system is quite robust and the instrumentation is less costly than an eddy covariance system. If the wetland is of large extent, relatively smooth, and uniform, the BREB method can give good results. Simple sensors to be installed, suitable also for tall crops. It can be also used when the fetch is 20:1. Not very expensive if psychrometers are used.	It is assumed that the transfer coefficients for sensible and latent heat are equal. This is generally true during neutral and unstable atmospheric conditions near the surface, but may not be true during stable (inversion) conditions. In the arid west, stable conditions are common during afternoon periods with high ET, so some error may occur during crucial periods because of invalid assumptions. Difficult to have correct measurement of the wet temperature if psychrometers are used. The sensors need to be inverted to reduce bias. Difficult maintenance.
Surface renewal	The relatively low cost, portability and ease of maintenance. It is based on short-term energy transfer between canopy elements and air parcels passing through the canopy, rather than flux gradient theory. Therefore, it is less dependent on	Currently, the main disadvantage is that it must be calibrated against an independent measure of sensible heat flux density. As with all of the energy balance measurements and equations (e.g. Bowen ratio energy balance, Penman-Monteith – PM,

Tab 4 (Continued)

Method	**Advantage**	**Disadvantage**
	fetch, and it may provide a useful method for determining ET along the edges of wetlands, in small wetland patches, along narrow wetland corridors and anywhere else with fetch limitations.	Penman – PE, Priestley-Taylor – PT), the overall accuracy of the method depends on accurate measurement of *Rn* and *G*.
Soil water balance	Soil moisture simple to be evaluated with gravimetric method. Not expensive if the gravimetric method is used.	Large spatial variability. Difficult to be applied when the drainage and capillary rising are important. Difficult to measure soil moisture in cracked soils.
Weighing lysimeter	Direct method.	Fixed. Difficult maintenance. It could be not representative of the plot area. Expensive.
Aerodynamic method	Simple sensors to be installed. It does not need humidity measurements. Not very expensive.	It needs to be corrected for the stability. Not suitable for tall crops.
Sap flow	Direct measurement of transpiration. Suitable for small plots. It takes into account the variability among plants.	Difficult scaling-up. Probe spacing and stem geometry are the most significant source of error.
LIDAR	A great advantage is that it provides an averaged, horizontal cross-section of the water vapour content of air. In so doing, it provides a weighted measure of the latent heat flux from the variety of surfaces that may exist within variable terrain and/or plant communities.	The main drawbacks are the complexity and high cost. In addition, because the surfaces of most wetlands are variable, the Monin-Obukov similarity function may vary across the surface, whereas only one similarity function is typically used to calibrate the LIDAR measurements.
Empirical equations	Empirical methods require easily measurable parameters for which data are typically available from local climate stations.	The most empirical equations are quite crude, implying a high amount of error, especially when applied outside the original

Tab 4 (Continued)

Method	Advantage	Disadvantage
	The convenience and low expense makes this approach highly desirable for managers and researchers.	climatic area for which they were developed. When ET estimates are required for an entire watershed or region, however, empirical methods may be the only practical way to generate estimates for the area needed.
Combination equations	A great advantage of using combination equations (i.e. PM and PE) is that the data requirements are minimal and collection at several heights is unnecessary. Combination equations accounts for wind speed, which is an improvement over the Priestley–Taylor equation. The PM equation has an advantage over the PE equation in that it accounts for surface resistance.	The PM equation assumes that the surface is uniform and 'nearly' wet with known canopy and aerodynamic resistances. In many wetlands, the assumption that the surface is nearly wet is reasonable; however, it may not be true for wetlands that dry up during part of the year. Because wetland canopies tend to be rough due to the presence of a mixture of vegetation, surface and aerodynamic resistances are difficult to determine and are likely to change with vegetation characteristics and weather conditions.
Weighted canopy methods	The weighted canopy method has similar advantages and disadvantages as the combination equations. However, an additional advantage is that the method accounts for energy balance and aerodynamic and surface resistance differences over the soil, water and plant canopy surfaces.	It is theoretically a better approach than treating a wetland like a large, uniform surface (e.g. the PM equation), it does require aerodynamic and surface resistance estimates and available energy measurements over the canopy, soil and water surfaces. Because measurements are replicated over several surfaces, the method is more expensive than combination equations and the CCC method.

Tab 4 (Continued)

Method	**Advantage**	**Disadvantage**
Crop canopy coefficient method (CCC)	If the biological and environmental conditions are nearly the same at a particular wetland as where the Kc values for particular plant species or plant communities were developed, then using the Kc values to estimate wetland. ET in the new location is justifiable. Because no on-site measurements are required, the CCC method is the most cost-effective.	Wetlands often have variable, non-uniform surfaces and they may have differences in water quality and water temperature from one site to another. Therefore, the CCC method should be used only where accurate reference ET data are available and in wetlands with largely uniform stands of vegetation.

Tab 5 Error, expressed as one standard deviation from the true mean value, expected for various types of ET methods (Allen et al., 2011a).

Method	Typically (%)	An experienced expert, trained and steeped in the physics of the process (%)	A novice or a person working outside their specialty area (%)	Additional error caused by physical or equipment malfunction (%)
Lysimeter	5–15	5	20–40	5–40
Soil water balance	10–30	10	20–70	10–40
Bowen ratio	10–20	10	20–50	5–40
Eddy covariance	15–30	10–15	30–50	10–40
Remote sensing energy balance	10–20	5–15	30–40	5–10
Sap flow	15–50	10–40	40–200	20–100
Scintillometers	10–35	10–15	20–50	5–30

2.6 Energy balance closure

The surface energy balance closure (EBC) cannot be omitted when speaking about energy fluxes in the surface layer of the atmosphere. Some of the methods used to determine evapotranspiration (latent heat flux – *LE*) highly depend on the EBC. For example, in scintillometry sensible heat flux is calculated from structure parameter of refractive index of air measured directly and subsequently, *LE* is calculated using energy balance equation. In such case, final flux directly depends on the accuracy of measurement of the remaining terms of the energy balance equation. In such cases, EBC gives us reliable feedback on how well our energy balance "closes", i.e. how is the available energy in the system distributed between sensible and latent heat flux.

The EBC refers to equation between available energy (the sum of the net radiation and the ground heat flux), and the sum of turbulent fluxes of sensible and latent heat. This equation results from radiation budget and can be written as Eq. 23. EBC is based on a formulation of the first law of thermodynamics which requires that the sum of the estimated sensible (*H*) and latent (*LE*) heat flux be equivalent to all other sinks and sources:

$$Rn - G = H + LE\,, \tag{33}$$

where *Rn* is net radiation, *G* is the ground heat flux, *H* and *LE* is sensible and latent heat flux, respectively. An imbalance between the remaining independently measured terms on the left- and right-hand sides of Eq. 33 may indicate inaccurate estimates of scalar fluxes (Wilson et al., 2002).

Standard way of evaluating EBC is statistical regression of turbulent energy fluxes (*H*+*LE*) against available energy (net radiation, less the energy stored) and by solving for the energy balance ratio, the ratio of turbulent energy fluxes to available energy (Wilson et al., 2002). An ideal regression (closed energy balance) is represented by slope equal to 1 with intercept of 0. However, according to Foken (2008b) since 1980s it became obvious that experimental data cannot close the energy balance (EB). This topic is still very lively although a lot of effort was made to solve this issue (Wilson, et al, 2002; Heusinkveld et al., 2004; Liu et al., 2011). In 2008 Foken summarized that (*Rn*–*G*) was found higher that (*H*+*LE*) in the majority of conducted experiments and the energy balance closure reached approximately 80 %. The detailed discussion on the reasons for EB disclosure will be given in section 6.1 Energy balance closure problem.

Generally, according to literature the lack of EBC is mainly due to measurement errors (Li et al., 2005), different footprints (Liu et al., 2011), advection (Wilson et al., 2002) and other reasons as it was suggested in the past studies (Barr et al., 1994). Most commonly, disclosure is related to sampling errors. These are associated with different measurement source areas demonstrated in Fig 9 adapted from Foken (2008a). In the picture the non-identical balance

layers of the measurements for particular terms are displayed as a reason for possible measuring errors. The quantification of such errors is summarized in Tab 6.

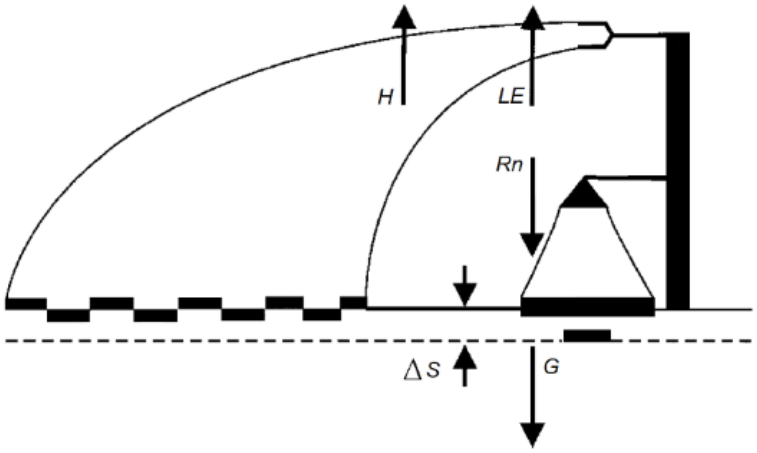

Fig 9 Measurement height and horizontal scale of the measurement of the energy balance components. The bar on the right of the figure is a tower; the cone with a black top is a radiation sensor showing the radiation footprint; arrows show the direction of flux. Rn is net radiation, G is soil heat flux, H is sensible heat flux, LE is latent heat flux, and ΔS is heat storage (Foken, 2008a).

Tab 6 Typical errors of the components of the energy balance equation and horizontal scales and heights for the measurements of these components adapted from Foken (2008b).

Component	Error (%)	Energy (W/m^2)	Horizontal scale (m)	Height (m)
Latent heat flux	5–20	20–50	100	2–10
Sensible heat flux	5–20	10–30	100	2–10
Net radiation	5–20	20–100	10	1–2
Ground heat flux without storage	20–50	20–50	0.1	-0.02 to -0.1
Storage term	20–50	20–50	0.1–1	-0.02 to -0.1

Possible measurement errors include soil heat flux underestimation caused by neglecting the heat stored in the layer of soil above the soil heat flux plate. This issue was addressed by several experiments (Kustas et al., 2000; Heusinkveld et al., 2004; Liebethal et al., 2005) where influence of heterogeneity of the soil was also recognized as an important issue significantly influencing the result. Further, energy stored in the air column between the sensors and the soil surface as well as energy heating the biomass. Another part of the energy balance usually neglected is energy used for photosynthesis. These and other issues will be described in more detail in section 6 Discussion.

3 OBJECTIVES OF THE THESIS

The objective of my Ph.D. studies was to study evapotranspiration (ET). In particular, to revise the theory behind different methods to determine actual ET, and to implement new state-of-the-art method (scintillometry) in the Czech Republic. This ambition included selection of appropriate localities within the Czech Republic and Austria and expand existing network of micrometeorological measurement sites studying the water balance. My responsibility was to deploy the measuring devices at experimental sites with respect to the footprint and fetch requirements, and run the measurements for several seasons. Not only the scintillometers were used but also the eddy covariance technique, the Bowen ratio systems, and other methods. Moreover, we carried out regular auxiliary measurements and had to service the installed equipment. Consequently, using the experience gained during my studies, the main objective of presented thesis was to find answers to following questions:

(i) Which method is the most suitable for measuring evapotranspiration in our field conditions based on the comparison of the scintillometry, the eddy covariance technique, the Bowen ratio energy balance method, and the surface renewal method during the experimental study carried out in Polkovice agricultural site?

(ii) What are the suggestions for improving the network of ground based measurements for assessment of evapotranspiration in the Czech Republic and Austria? Taking into account installation and operation issues, maintenance requirements, cost, applicability for field measurements, and reliability which methods should be further implemented or avoided in order to increase our effectivity?

(iii) What is the influence of the field heterogeneity on the results of energy fluxes and which of the methods represents the area of the potential grid size the best? Which method would be the most suitable for validation of models based on satellite images?

4 MATERIALS AND METHODS

The experimental part of presented study was conducted using the instrumentation of the CzechGlobe (Global Change Research Institute of the Czech Academy of Sciences). CzechGlobe is in charge of 8 ecosystem sites across the Czech Republic including agrosystems, forests, wetlands, and meadows, at which the eddy covariance technique is used for long term monitoring of water and CO_2 fluxes. On the top of these, CzechGlobe is running laboratories and other infrastructure (Fig 10).

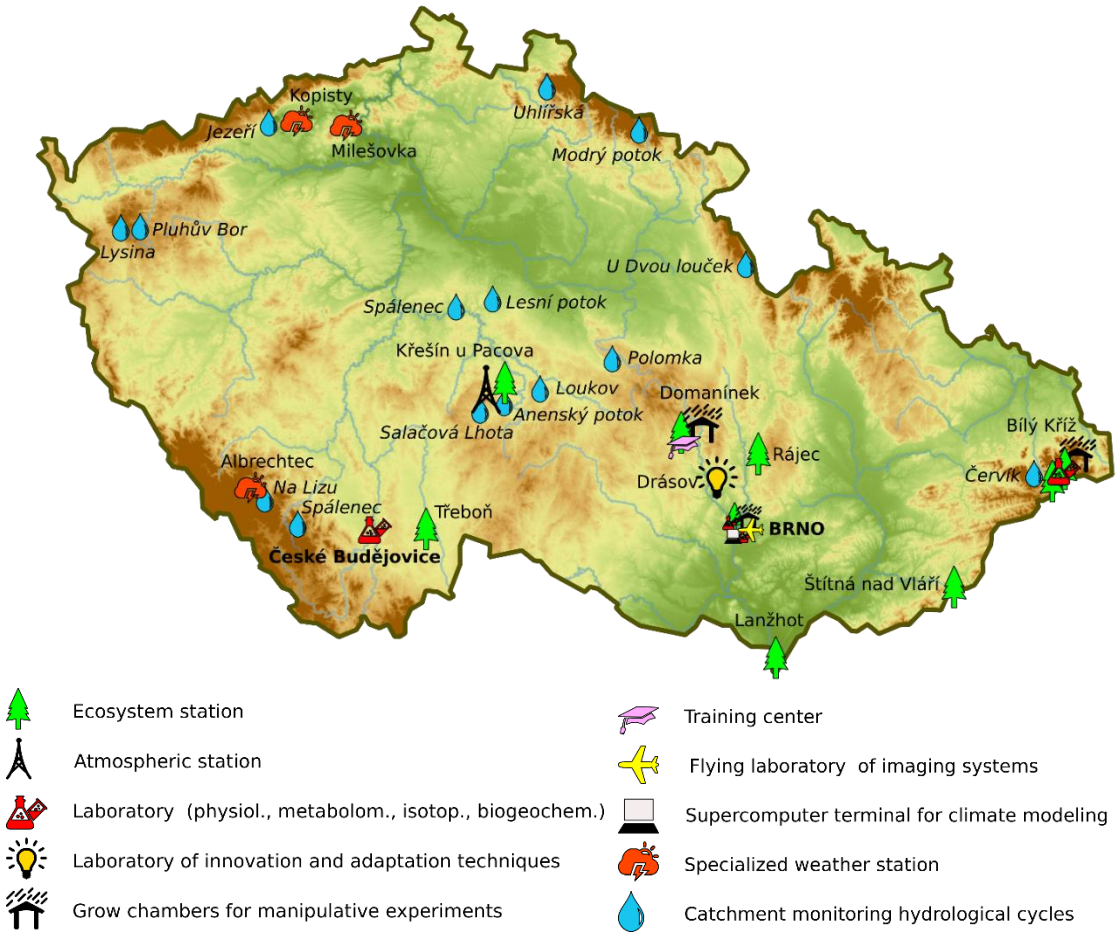

Fig 10 Schematic layout of the CzechGlobe network consisting of ecosystem and atmospheric stations, laboratories and other units of the institute´s infrastructure (Image by L. Krupková).

For several years we are benefiting from the collaboration and improve the network of field sites by running 11 more experimental localities around the Czech Republic but also in Austria. Our aim is to monitor actual evapotranspiration and other meteorological variables across the country to cover different climatic conditions. Our network (Fig 11) consists of meteorological stations adapted for the Bowen ratio energy balance method (BREB systems), the eddy covariance systems and since 2013 also scintillometers (boundary layer scintillometers (4x) and since 2015 also SLS (2x)). The list of sites we are running is summarized in Tab 7.

These experimental localities are part of a larger project focusing on quantification of evapotranspiration within agricultural landscape in context of water management and drought. The ground based measurements will serve for further research and will be used for calibration and validation of remote sensing-based evapotranspiration data, water balance models, bio-climatological models, and drought monitoring. The project focusing on drought within this scheme is called InterDrought and you can find more about the project in English as well as the map of the Czech Republic with actual drought intensity on the following web page: http://www.intersucho.cz/en/.

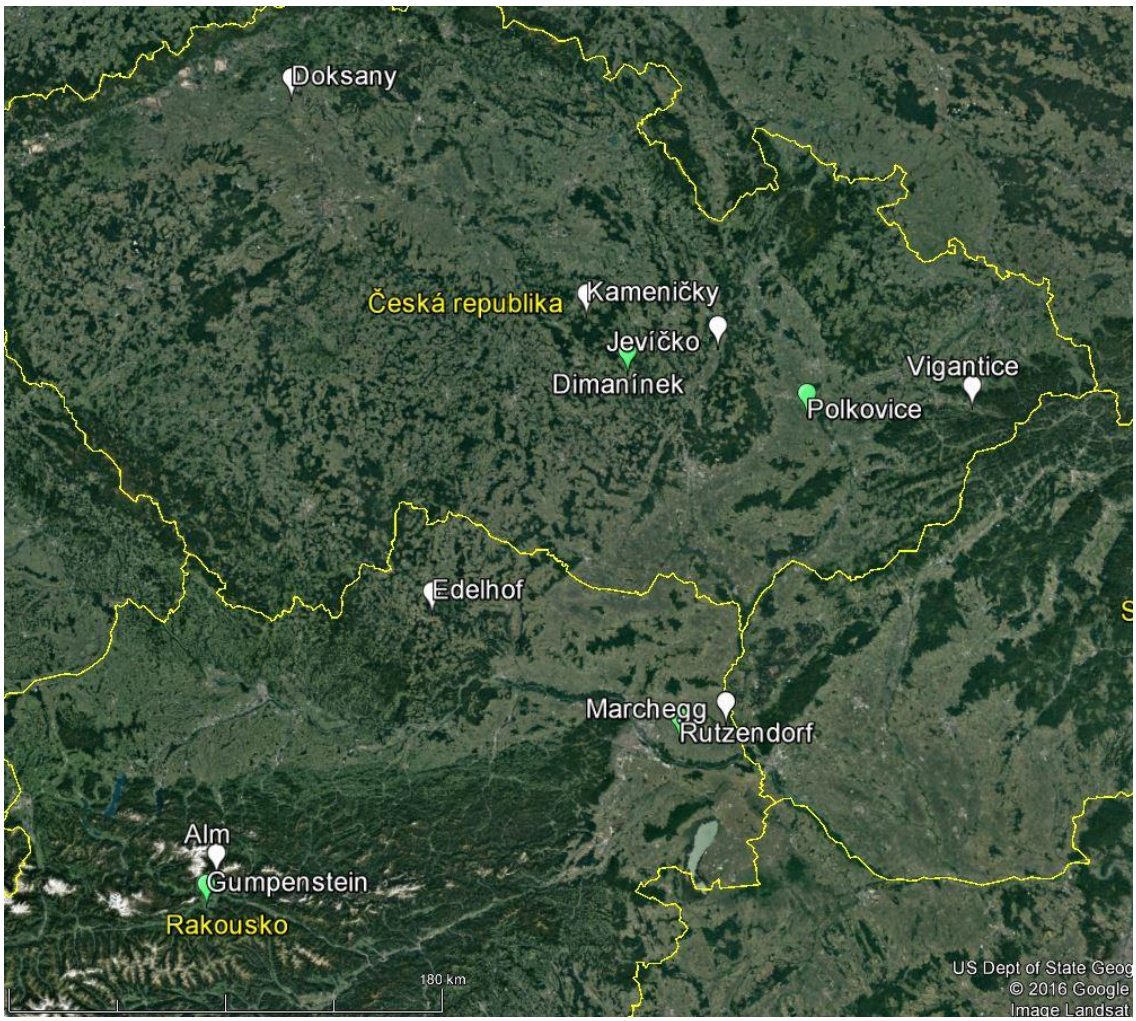

Fig 11 The network of experimental localities to measure actual evapotranspiration in the Czech Republic and Austria run by our team. The green marks identify sites with scintillometry measurements and white marks denote BREB systems (figure created using software Google Earth 2016).

After three years of experience with setting up the field experiments using various techniques under different climate conditions within the frame of network described above we have decided to optimise our network. For this purpose, the results of method comparison

presented in this thesis will be used. Some suggestions will be made to improve, further develop and stabilise the network for monitoring of water balance across the Czech Republic and Austria with an overall goal to have a representative ensemble of ET measurements at various covers and different altitudes.

Tab 7 The list of experimental sites operated by our team which are part of the network for water balance monitoring in the Czech Republic and Austria.

Locality	Type of system	First installation	Cover	Elevation m a.s.l.
Doksany	BREB system	6. 5. 2013	Grassland	155
Domanínek	Eddy covariance	28. 9. 2010	Agrosystem	590
	BREB systems	24. 6. 2008	Grassland	
	Scintillometer	? 2016	Poplar plantation	
Jevíčko	BREB system	22. 5. 2014	Grassland	350
Kameničky	BREB system	2. 5. 2013	Grassland	635
Polkovice	Scintillometer	27. 9. 2013	Agrosystem	200
	BREB system	25. 9. 2013		
	Eddy covariance	2. 7. 2015		
Vigantice	BREB system	20. 12. 2014	Grassland	455
Alm	BREB system	22. 7. 2015	Grassland	1802
Edelhof	BREB system	7. 8. 2013	Grassland	400
Gumpenstein	Scintillometer	17. 10. 2013	Experimental site	690
	BREB system	17. 10. 2013	Grassland	
Marchegg	BREB system	25. 7. 2013	Grassland	150
Rutzendorf	Scintillometer	11. 3. 2014	Agrosystem	150
	BREB system	11. 3. 2014		

4.1 Site description

The field experiment presented further in this thesis took place in Polkovice (49°23'42.8"N 17°14'47.3"E), village near Kojetín in very fertile agricultural region Haná in the Moravian part of the Czech Republic (Fig 11). It is located in the altitude of 200 m. The field has approximately 26 ha and its local name is “Nivy”. It is surrounded by other agricultural fields, to the north there is a similarly large field always growing the same crop separated only by the dirt road. From the south west and the south east, the field is bordered by the asphalt road. In the west direction, a small stream flows along the field and it is lined with trees. They serve as a shelterbelt. The field is relatively large and fairly flat providing a promising site for micrometeorological measurements (Fig 12). The homogeneity of the field from different perspectives was a subject of analysis and its results will be presented in the subsections 4.5.5 Variability of the field, and 5.6 Homogeneity of the site.

Fig 12 The experimental location and the position of the instrumentation on the field in Polkovice (the Czech Republic) in 2015; star indicates an automatic weather station (AWS), black points indicate scintillometers: boundary layer scintillometer (BLS) and surface layer scintillometer (SLS) letters “T” and “R” stand for transmitter and receiver, respectively. Position of the soil pits (SP1 and SP2). The image was created using https://mendelu.maps.arcgis.com (1. 5. 2016).

The climate is moderate in Polkovice with average daily air temperature 8.3 °C and average precipitation 552.5 mm per year. The soil type of this typically agricultural region is fertile chernozem. Soil survey of the experimental field was carried out 19. 8. 2014. Two soil pits (80 cm and 110 cm deep) were dug within a field and the soil profiles can be seen in Fig 13. Soil type is luvic chernozem on the bedrock material loess. In the first pit carbonates were present in the whole profile in the second pit down to 40 cm. Topsoil is 30 cm thick, soil type is loam, clay-loam with granular structure.

Our study started in autumn 2013 when there was maize (*Zea mays*) in the field. Next season the field was sown with oil-seed rape (*Brassica napus*) and in 2015 – the final and most important year of the experiment – there was winter wheat (*Triticum aestivum*). Experimental set–up (positions of individual instruments) for the season 2015 can be seen in Fig 12. The majority of instruments was deployed in the centre of the field. This way we ensured the largest footprint with respect to prevailing wind direction.

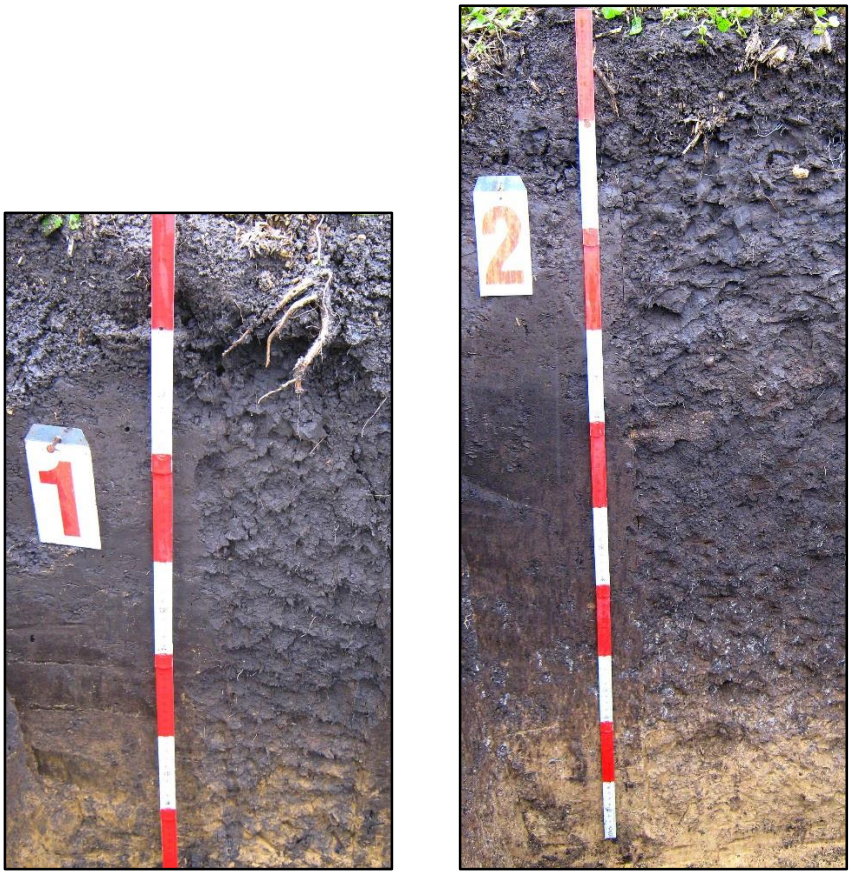

Fig 13 Two soil pits from the study area, first 80 cm deep, second 110 cm deep. Soil type luvic chernozem. (Images by M. Brtnický).

4.2 Fetch and footprint

Given the aim of this study, comparison of different methods to determine evapotranspiration, it was necessary to ensure similar footprints for all of them. The footprint of point measurements: the eddy covariance (EC), the Bowen ratio energy balance (BREB), and the surface renewal (SR) method, is given primarily by the distance between sensor and edge of the field against the wind (fetch) and the height of the sensor above the soil surface or crop. For the area averaging methods (scintillometry), footprint is influenced by the weighing function along the path between transmitter and receiver (Fig 20) and of course by the wind patterns at the locality. The wind patterns during the season 2015 are captured in Fig 14 in the form of a wind rose. The main wind directions are northwest and southwest. That is why orientation of the scintillometers was chosen from northwest (transmitter) to southeast (receiver).

The fetch for different coordinates is displayed in Tab 8. Maximum and minimum fetch is 555 m and 183 m, respectively. The same crop was sowed on the neighbouring field situated in the north from our field and it is separated from our site only by a small dirt road. The fetch in the north and northeast directions can therefore be theoretically doubled if we neglect the road. Considering the rule of thumb 100:1 fetch-to-height ratio (using the upper sensor height) we can

argue sufficient fetch in direction of prevailing wind. In particular, 315–337 m between sensor (3.5 m high) and nearest roughness element (obstacle). In the west direction from our field there is a small stream lined with trees. They serve as a shelterbelt so we deployed the transmitter of the large aperture scintillometer further from the edge of the field towards its centre. Hence, the scintillometer path is not influenced by the trees as a turbulent obstacle. Moreover, Heilman and Brittin (1989) conducted an experiment and proved that much less than the often-quoted value of 100:1 is required for sufficient use of the BREB method and they substantiated the fetch-to-height ratios as small as 20:1. With such argument we can justify all our fetch conditions regardless wind direction.

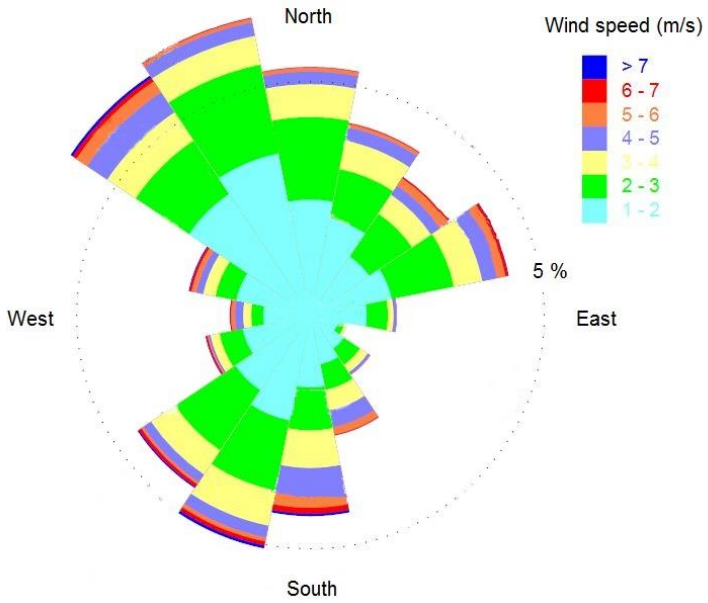

Fig 14 Wind rose for the Polkovice site during the measurement period in 2015 recorded in 3.5 m height above the soil surface. The image was created using WindRose PRO3 by Enviroware.

Tab 8 Fetch lengths for 16 wind directions in m, value in parenthesis is the distance towards a dirt road in the middle of the field.

Direction (deg)	Fetch (m)	Direction (deg)	Fetch (m)
0.0 (N)	555 (170)	180.0 (S)	202
22.5	490 (145)	202.5	183
45.0 (NE)	510 (148)	225.0 (SW)	192
67.5	475 (176)	247.5	240
90.0 (E)	340 (270)	270.0 (W)	391
112.5	301	292.5	505
135.0 (SE)	314	315.0 (NW)	474
157.5	273	337.5	554 (250)

4.3 Instrumentation

The major part of instrumentation used during the field experiment was an automatic weather station (AWS). Not only it carried the sensors for basic meteorological variables but also it wass a platform for the eddy covariance and surface renewal method. We used the AWS by EMS Brno (the Czech Republic) consisting of the 3.5 m tall aluminium mast with three parallel vertical arms at heights 0.5 m, 2 m, and 3.5 m above soil surface, solar panel and batteries, data logger and set of sensors (Fig 15). The AWS was equipped with sensor for measurement of four components of radiation: short wave and long wave incoming and outgoing (net radiometer), combined sensors for air temperature and relative humidity at three levels, 2D wind speed and wind direction measurement at three levels, air pressure, precipitation (rain gauge), soil temperature and soil moisture profiles (three depths), and two soil heat flux plates. The detailed description of the sensors is listed in Tab 9. Data were stored on the data logger RailBox RailBox V32P6 (EMS Brno, the Czech Republic). Measuring interval of the AWS was 20 s and the data were stored as 10 min averages. These data served for calculation of the fluxes by the BREB method but also as an input data for scintillometry.

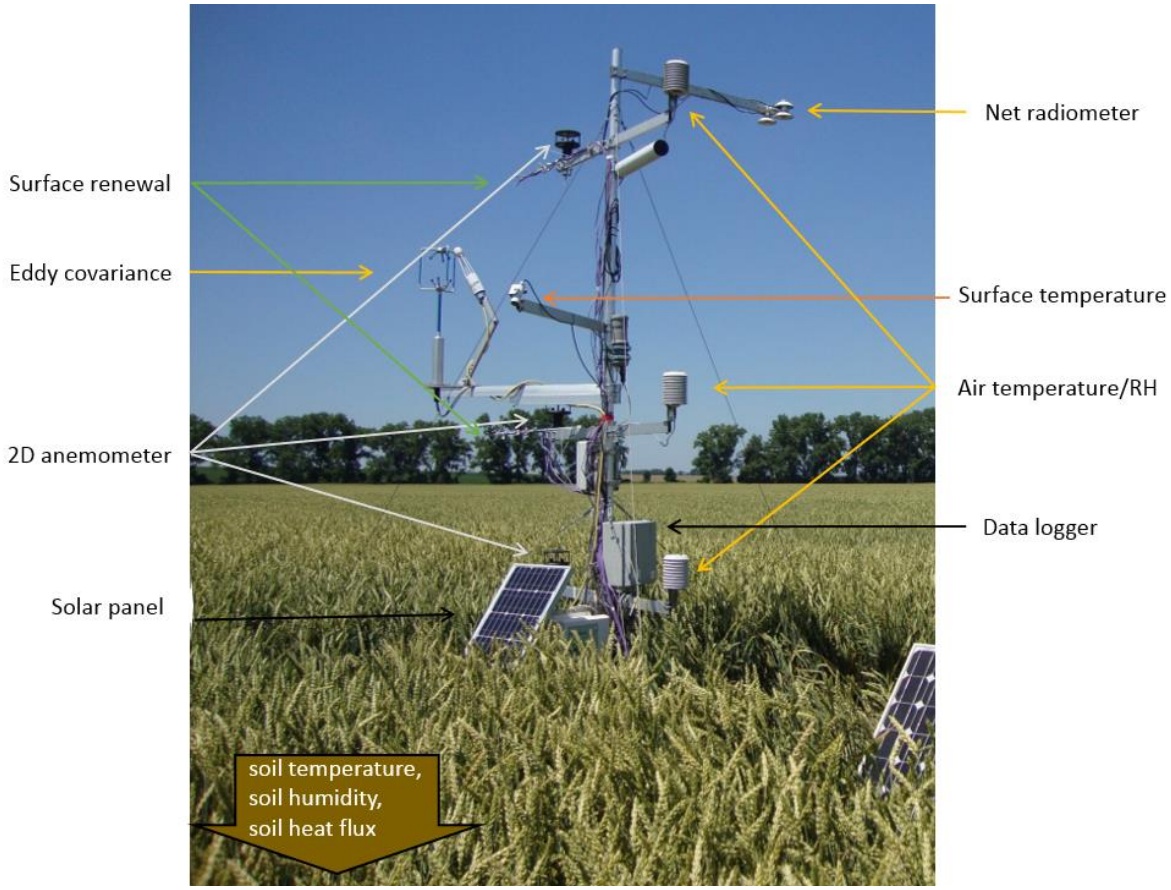

Fig 15 The automatic weather station (EMS Brno, CR) located in the middle of the experimental field in Polkovice, description of the sensors, photo 2. 7. 2015.

Tab 9 Detailed description of the sensors used for field measurements.

Observed item	Height/depth of sensor (m)	Sensor type
Sensible and latent heat flux	Height 2.70	LI-7500A, LI-COR, NE, USA WindMaster, Gill, Lymington, UK
Sensible heat flux	Height 4.25	BLS900, Scintec ltd, Rottenburg, Germany
Sensible heat flux	Height 2.70	SLS20, Scintec ltd, Rottenburg, Germany
Sensible heat flux	Height 1.90, 3.35	Thermocouples E type, Omega, Stamford, CT, USA
Radiation balance	Height 3.60	NR01, Hukseflux, Delft, Netherlands
Air temperature/humidity	Height 0.50, 2.00, 3.50	EMS33R, EMS Brno, CR
Wind speed/direction	Height 0.50, 2.00, 3.50	Ultrasonic 2D wind sensor, Gill, Lymington, UK
Soil heat flux 2x	Depth 0.05	HFP01, Hukseflux, Delft,Netherlands
Soil temperature	Depths 0.10, 0.25, 0.50	Pt 100, EMS Brno, CR
Soil water content	Depths 0.10, 0.25, 0.50	CS616, Campbell Scientific Inc., Logan, UT, USA
Liquid precipitation	Height 1.00	MetOne 380/386, Campbell Scientific Inc., Logan, UT, USA
Data logger of AWS		RailBox V32P6, EMS Brno, CR
Data logger of SR method		CR1000, Campbell Scientific Inc., Logan, UT, USA

Fig 16 The eddy covariance system an open path CO_2/H_2O gas analyser Li7500A (LI-COR Inc., Lincoln, NE, USA) and 3D sonic anemometer WindMaster (Gill, Lymington, UK).

The eddy covariance (EC) system used in the study consisted of an open path CO_2/H_2O gas analyser Li7500A (LI-COR Inc., Lincoln, NE, USA) and 3D sonic anemometer WindMaster (Gill, Lymington, UK) (Fig 16). The EC raw data were stored in the Li-7550 Analyser Interface

Unit (LI-COR Inc., Lincoln, NE, USA) at the sampling frequency of 10 Hz. The system was mounted to an arm of the AWS and the measurement height of the EC was 2.7 m above the soil surface. Northward, eastward and vertical separation of the gas analyser was 1 cm, 18 cm, and 0 cm, respectively.

For the scintillometry measurements we used two types of scintillometers. Firstly, a dual-disk type of the Boundary Layer Scintillometer (BLS) in particular, BLS900 by Scintec (Rottenburg am Neckar, Germany) (Fig 17). Its aperture diameter is 0.15 m and it operates at a wavelength of 880 nm. This scintillometer emits light with two disks of light-emitting diodes (462 at each disk, d_t = 0.186 m), and at the receiver side a single convex glass lens focuses the beams onto two silicon photodiodes (Scintec, 2013). It was installed in the fixed height of 4.2 m above the soil surface and the 617.0 m long path was oriented northwest-outheast. The set-up and alignment were done via the SRun software (Fig 18). The measurement interval of BLS was 1 min and the data were stored to a built-in data logger in Signal Processing Unit (SPU) of BLS900. The post-processing of the signal requires additional input data which were sent to The SPU from the AWS by the Wi-Fi antenna every 20 s to enable calculation of the sensible and latent heat flux with 1-min interval. The data needed for calculation of the sensible heat are air temperature, air pressure, wind speed, the Bowen ratio, relative humidity, surface roughness, and displacement height (summarized in Tab 11). Subsequently, to derive final latent heat flux, the net radiation and soil heat flux need to be added so the energy balance equation can be used.

Fig 17 The transmitter (left) and receiver (right) of the boundary layer scintillometer (Scintec, Germany) deployed in winter wheat field in Polkovice 2015.

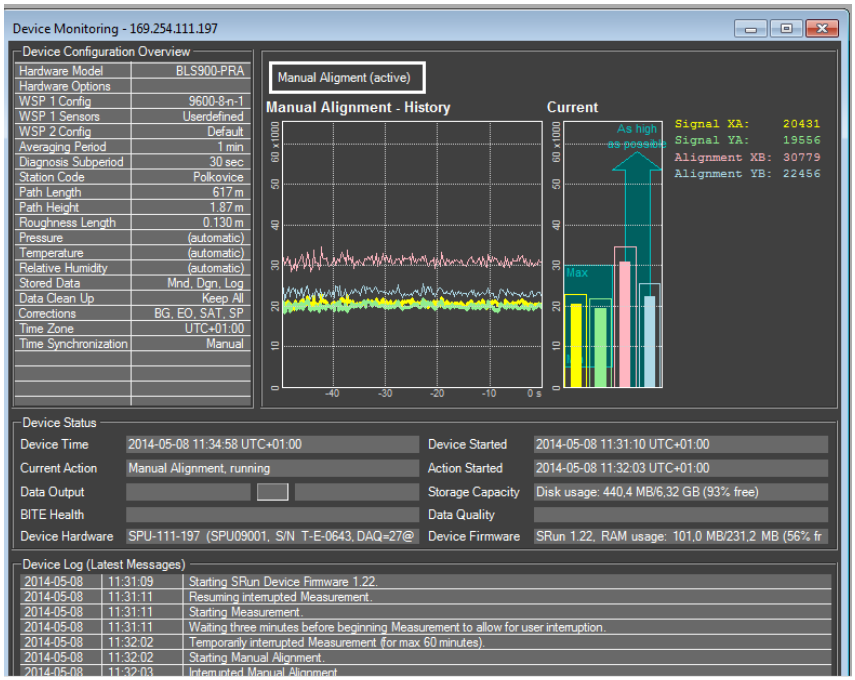

Fig 18 The SRun software version 1.22 by Scintec (Germany), manual alignment mode as an example of the set-up and alignment process of the boundary layer scintillometer (BLS 900).

Secondly, the surface layer scintillometer (SLS) type SLS20 (Scintec, Rottenburg, Germany) (Fig 19). It was installed in the same height as the EC system (2.7 m above the soil surface). Path length of the SLS was 106 m with the northwest to southeast orientation. The set-up characteristics of both scintillometers are summarized in Tab 10 and visually demonstrated in Fig 20 together with weighing functions.

Fig 19 Transmitter near the AWS (left) and receiver of the surface layer scintillometer (right) deployed in Polkovice winter wheat field in 2015.

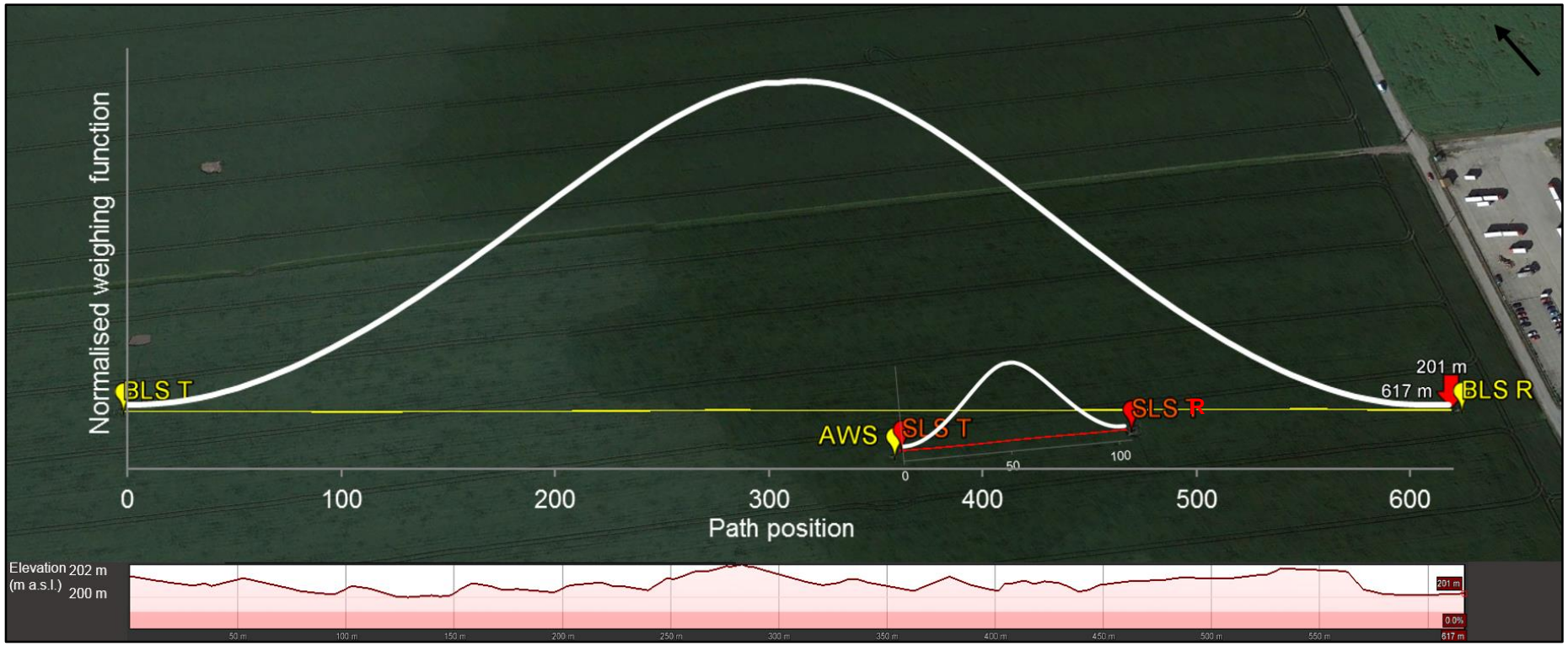

Fig 20 The normalised path weighing function for boundary layer scintillometer (BLS) and surface layer scintillometer (SLS) T and R denoting transmitter and receiver, respectively. Chart at the bottom shows elevation along the BLS path with maximum elevation change of 1 m.

Tab 10 Set-up characteristics of the scintillometer measurements.

Type	BLS	SLS
Orientation	northwest → southeast	northwest → southeast
Path height (m)	4.2	2.7
Path length (m)	106	617

The last method was the surface renewal (SR) method. It is based on the high frequency measurement of temperature by very fine thermocouples. The thermocouples type E (CHROMEGA®Constantan) with diameter of wires 0.013 mm (CHCO-0005), 0.025 mm (CHCO-001), 0.05 mm (CHCO-002), and 0.076 mm (CHCO-003) were installed in 1.90 m and 3.35 m heights on the arms of the AWS (Fig 21). The measurement frequency was 10 Hz and the data were stored to a data logger CR1000 (Campbell Scientific Inc., Logan, UT, USA) with CP flash memory extension 2GB.

Fig 21 Thermocouples for the surface renewal method (left), position on the arms of AWS (right).

4.4 Data processing

All the above mentioned data were processed with the data averaging interval 30 min for the final comparison of the methods.

4.4.1 The eddy covariance data processing

The raw eddy covariance data were sampled at 10 Hz frequency and stored to in build data logger. The EC data were processed by EddyPro® (version 6.0.0) open source software (LI-COR Inc., Lincoln, NE, USA) in the basic mode including compensation for density fluctuations, time lags compensation, axis rotation for tilt correction and quality check: flagging policy according to Foken et al. (2004). The EC data processing included spike detection. Final

data were processed for 30 min averages and the half-hourly flux data were screened according to the following criteria: (i) data were rejected when the sensor was malfunctioning, (ii) data were rejected when precipitation occurred, (iii) data were rejected when the wind direction indicated an air flow from the direction of the mast construction as a huge obstacle (60°–80°), (iv) data were rejected at night when the wind speed was below 1 m s^{-1}, and (v) data were also rejected for stable conditions when the net radiation was below 100 W m^{-2}.

4.4.2 The boundary layer scintillometer data processing

The raw BLS instrument signals were collected with an internal data logger using a sampling frequency of 500 Hz and processed with the SRun software package provided by the manufacturer (version 1.27) (Fig 18). Before being analysed, the signal was demodulated and processed through a band-pass filter with a range set to 0.03–190 Hz (personal communication, Scintec, 2014). The high-pass filter frequency depends on the interval length of the diagnosis data files. However, for removing undesired scattering and absorption effects the BLS instrument essentially relies on a correction algorithm based on $C_{12}(0)$: the extinction and outer scale correction (Solignac, 2012; Scintec, 2013).

The basic statistical data stored by SRun include the diagnosis data, the interval length which was set to the recommended 30 sec. Principal variables stored in the corresponding diagnosis-data files are average intensity ($\bar{I}$) and the log-intensity variance of the signal (σ_I^2) for each of the beams, as well as the correlation, $r_{I1/2}$, between the beams. Based on these diagnosis data files, the statistics of any desired time interval can be reproduced using the SRun software. Our main data interval length was set to 1 min. In this final processing step of generating the main data files, C_n^2 is obtained through application of Eq. 18 with the variance of the logarithmic intensity ($\sigma^2_{\ln(I)}$) arithmetically averaged over both disks (Scintec, 2013).

4.4.3 The surface layer scintillometer data processing

The structure parameter of the refractive index of air was measured and stored to a built-in data logger of the signal processing unit of the SLS every minute. The post processing was done using the additional meteorological data from the AWS similarly to large aperture scintillometer. The final fluxes were calculated for 30-min averages. Data were screened according the same rules as EC data except filtering out according to wind direction – for an area average fluxes it does not make sense, no such obstacles as for EC are present.

4.4.4 The Bowen ratio energy balance method

The sensible and latent heat flux densities were calculated according to Eq. 25 and Eq. 26 presented in section 2.4.3 The Bowen ratio theory. The meteorological data used for the calculation were recorded by the BREB system, (AWS in the middle of the field) and post-processed in software Mini32 by EMS (Brno, CR). Firstly, the 30-min averages were made of the raw data stored at 10-min intervals for all necessary variables (air temperature, RH, net

radiation, soil heat flux). Then, the gradients of air temperature and humidity were calculated followed by calculation of the Bowen ratio (Eq. 29) for different combinations of sensors (up – bottom, up – middle, middle – bottom). After the comparison the best results (up – bottom) sensors were used due to the highest gradients and reliability. Finally, the Bowen ratios larger than -1.3 and smaller than -0.7 were rejected (Ortega-Farias et al., 1996). Such values imply that the LE ≈ -H and thus available energy equals around zero. This is why such values are filtered out. Subsequently, *LE* and *H* was calculated and unrealistic data were filtered out. Especially during the dawn and dusk when the stability conditions change and gradients change their slope – occurrence of so-called "kink" (Oke, 1987). More details about this phenomenon can be found in the case study in Appendix E.

4.4.5 The surface renewal data processing

For calculating *H* using surface renewal method (H_{SR}) high frequency air temperature measurement are used. For quantifying H_{SR} we used 75 μm fine wire bead welded chromel-constantan thermocouples. For determination of their time constant we used a methodology described by Shapland et al. (2014). Since their study consider the cylindrical and spherical geometry and our thermocouples were bead welded we additionally estimated the time constant of bead (τ_b) as a function of cylinder time constant (τ_c) according to the relation $\tau_b = \tau_c (D/d)^{3/8}$ where *d* is the wire diameter and *D* is the bead dimeter (McGee, 1988). When the time constant was known, the measured temperature was corrected for the high frequency loss (Moore 1986, Shapland et al. 2014). Data were processed with the data averaging interval 30 min.

4.5 Auxiliary measurements

Before the flux measurement started in 2013 we visited a potential site several times at the beginning of the field campaign and thought over the positioning of meteorological station, individual instruments with respect to fetch and footprint and prevailing wind direction, but also the placement of the spots for auxiliary measurements was thoroughly considered. The decision was made in 2014 when there was an oil seed rape growing in the field based on the Landsat satellite image of NDVI (Fig 22) from 18. 4. 2014 prepared by Dr. Lukas.

We intentionally chose contrasting spots within a field with the potential to represent different vegetation states. We were lucky (or unlucky) that in 2014 the growth of the oil-seed rape was not uniform and quite large differences occured across the field. Points P1–P5 on Fig 22 mark the positions of a leaf area index (LAI) measurements and will be described in more detail in section 4.5.3 Leaf area index measurement. Further, Fig 22 shows the positions of 12 access tubes in the soil to measure soil water content by PR2 probe assigned by "Tx". More details will be given in section 4.5.4 Soil moisture measurement. Net radiation and soil heat flux were measured by a meteorological station marked "Met" in Fig 22 however, in the next season (2015) AWS was deployed 100 m further towards the middle of the field.

Scintillometer (BLS) remained approximately at the same position than in 2014, exact positions of AWS and BLS during experiment in 2015 can be seen in Fig 12.

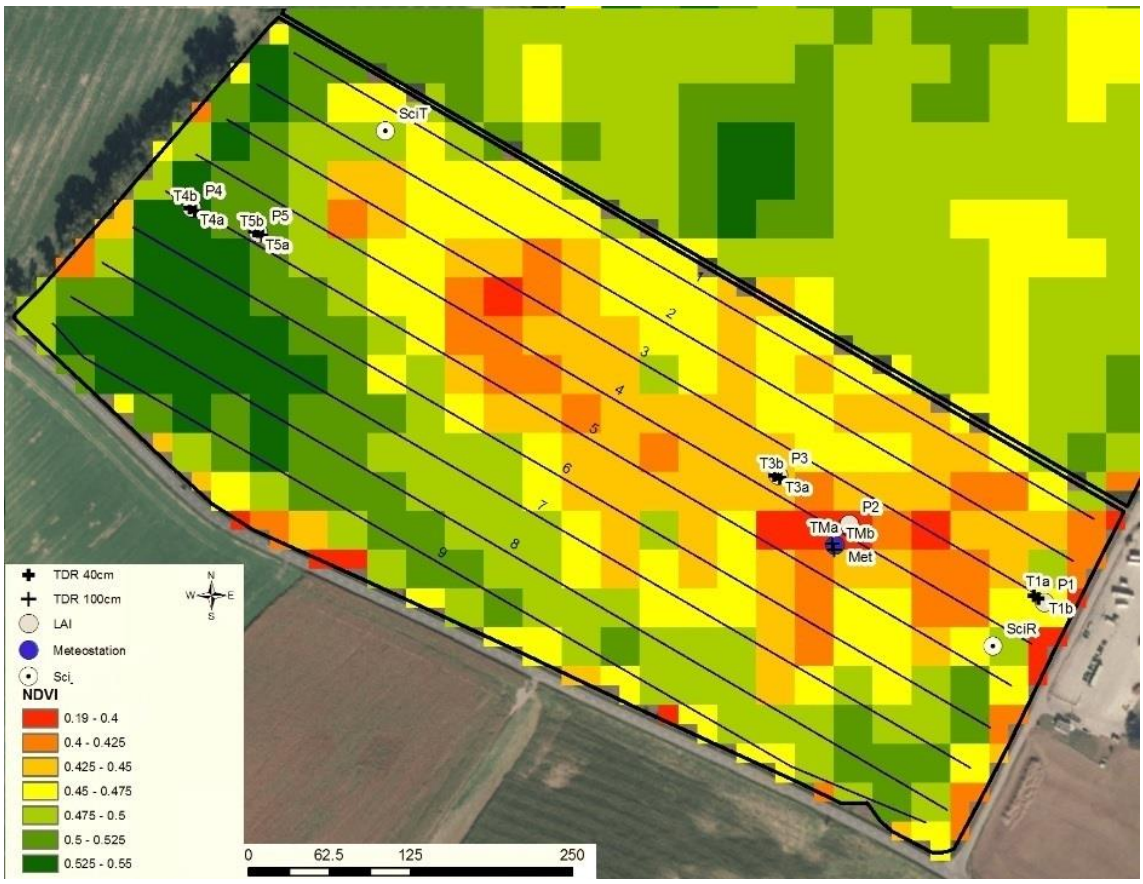

Fig 22 Layout of the measurement spots across the experimental field based on the NDVI image (Landsat, 18. 4. 2014). SciT and SciR mark the position of the boundary layer scintillometer transmitter and receiver, respectively; Met assigns the position of an automatic weather station; P1–P5 mark the position of regular LAI measurement; and the points assigned T1a–T5b show the positions of 10 access tubes (40 cm) and TMa–TMb two 100 cm long tubes to measure soil moisture profile.

4.5.1 Net radiation measurement

For the measurement of radiation, net radiometrer type NR01 by Hukseflux (Netherlands) was used to determine four components of radiation with in-built thermometer to measure pyrradiometer temperature. The instrument was placed 3.5 m weigh above the soil surface at the AWS. The glass domes of the instrument were cleaned regularly. Net radiation was calculated using software Mini32 by EMS Brno (the Czech Republic) using a script (Fig 23) prepared by Dr. Fischer.

```
Var1 = Chan1 ; Pyrradiometer temperature [°C]
SWin = Chan2
Var2 = SWin ; SW incoming radiation [W/m2]
SWout = Chan3
Var3 = SWout ; SW outgoing radiation [W/m2]
LWin_un = Chan4
Var4 = LWin_un ; LW incomming uncor. [W/m2]
LWout_un = Chan5
Var5 = LWout_un ; LW outgoing uncor. [W/m2]
T = Chan1 + 273.16 ; Pyrradiometer temperature [K]
LWin = LWin_un+(5.67*10^-8)*T^4
Var6 = LWin ; LW incoming radiation [W/m2]
LWout = LWout_un+(5.67*10^-8)*T^4
Var7 = LWout ; LW outgoing radiation [W/m2]
Rn = SWin-SWout+LWin-LWout
Var8 = Rn ; Net radiation  [W/m2]
```

Fig 23 The script used in Mini32 software (EMS Brno, CR) for the calculation of the net radiation from the raw data sampled by net radiometer (Hukseflux, Netherlands).

4.5.2 Soil heat flux measurement

Soil heat flux (*G*) was measured by two soil heat flux plates (SHFP) type HFP01 by Hukseflux (Delf, Netherlands) connected to data logger of the AWS installed in 5 cm under the soil surface. Because of acceptable homogeneity if the vegetation and soil across the site and due to technical limits we used only two SHFP. The sampling interval was 20 s and data were stored as 10-min average. During the data processing suspicious values (non-realistic, when the sensor was malfunctioning) were rejected and the final *G* was calculated as an average of both sensors. The energy stored in the layer of the soil above the SHFP was neglected as well as the energy into the biomass.

4.5.3 Leaf area index measurement

During the experiment, plant height as well as leaf area index (LAI) was measured periodically across the field using the ceptometer SunScan by Delta-T Devices (Cambridge, England) (Fig 24). Five measurement spots across the field were regularly sampled fo assessment of within field variability. The spots were chosen based on the heterogeneity survey mentioned above in subsection Auxiliary measurements. The differences in NDVI from satellite image in 18. 4. 2014 were reflected in the position of the sampling spots (Fig 22 P1–P5). Measurements were conducted weekly or biweekly and each spot was sampled 20 times to get and average value. Reference was always measured at the beginning of the sampling session and subtracted from the average value. Since we were measuring oil-seed rape or winter wheat and for the agricultural crops it is difficult to separate leaves from stems in the results we use a term leaf are index (LAI) as an integrated value for all above ground biomass of plants (m^2/m^2). Moreover, stems of these plants are also green and contribute to evapotranspiration. Tab 10 summarizes the plant height development, LAI, displacement height, and effective heights of both scintillometers and the eddy covariance.

Fig 24 The ceptometer (SunScan by Delta-T Devices, England) (left), field measurement of LAI in oil-seed rape in 2014 in Polkovice (right).

Tab 11 Plant height development, LAI, displacement height, and effective heights.

Date	DOY	Plant height (m)	LAI (m^2 m^{-2})	Displacement height (m)	Effective height (m)			Wind sensor height (m)
					BLS	SLS	EC	
2.7.2015	183	1.0	7.7	0.67	3.53	2.03	2.03	2.83
5.8.2015	217	1.0	7.6	0.67	3.53	2.03	2.03	2.83
6.8.2015	218	0.2	0.1	0.13	4.07	2.57	2.57	3.37
14.9.2015	257	0.1	0.1	0.07	4.13	2.63	2.63	3.43

4.5.4 Soil moisture measurement

Different methods were used to evaluate soil water content at the experimental field. Firstly, a thermo-gravimetric method was used while installing the time domain reflectometry based on soil dielectric constant (TDR) probes. The TDRs were measuring continuously throughout the measuring campaign. TDR sensors were measuring in depths 10, 25 and 50 cm in the middle of the field connected to the data logger of the AWS. The third method used for soil moisture measurement was a portable probe PR2 (Delta-T Devices, England). The sampling was done periodically (weekly or biweekly) in 12 tubes that were installed across the field. Location of the tubes can be seen in Fig 22 marked “T” and it is a result of decision described earlier at the beginning of the “Auxiliary measurements” section.

4.5.5 Variability of the field

On the top of the regular measurements across the field, the variability of the experimental area was assessed using airborne pictures and satellite data (Landsat, Modis). Two times during the field campaign, plane crossed the field scanning the surface by thermovision and spectral cameras to evaluate surface temperature and NDVI with high resolution. These pictures were used to analyse the field homogeneity and results are

presented in section 5.6 Homogeneity of the site. Colleague of mine at Mendel University Dr. Lukas was in charge of this part of Polkovice field study. Thus satellite and airborne pictures presented in this thesis as well as maps in Fig 25 were prepared within our cooperation. The conductivity was measured using CMD-1 instrument (GF Instruments, Brno, CR) 4. 8. 2014.

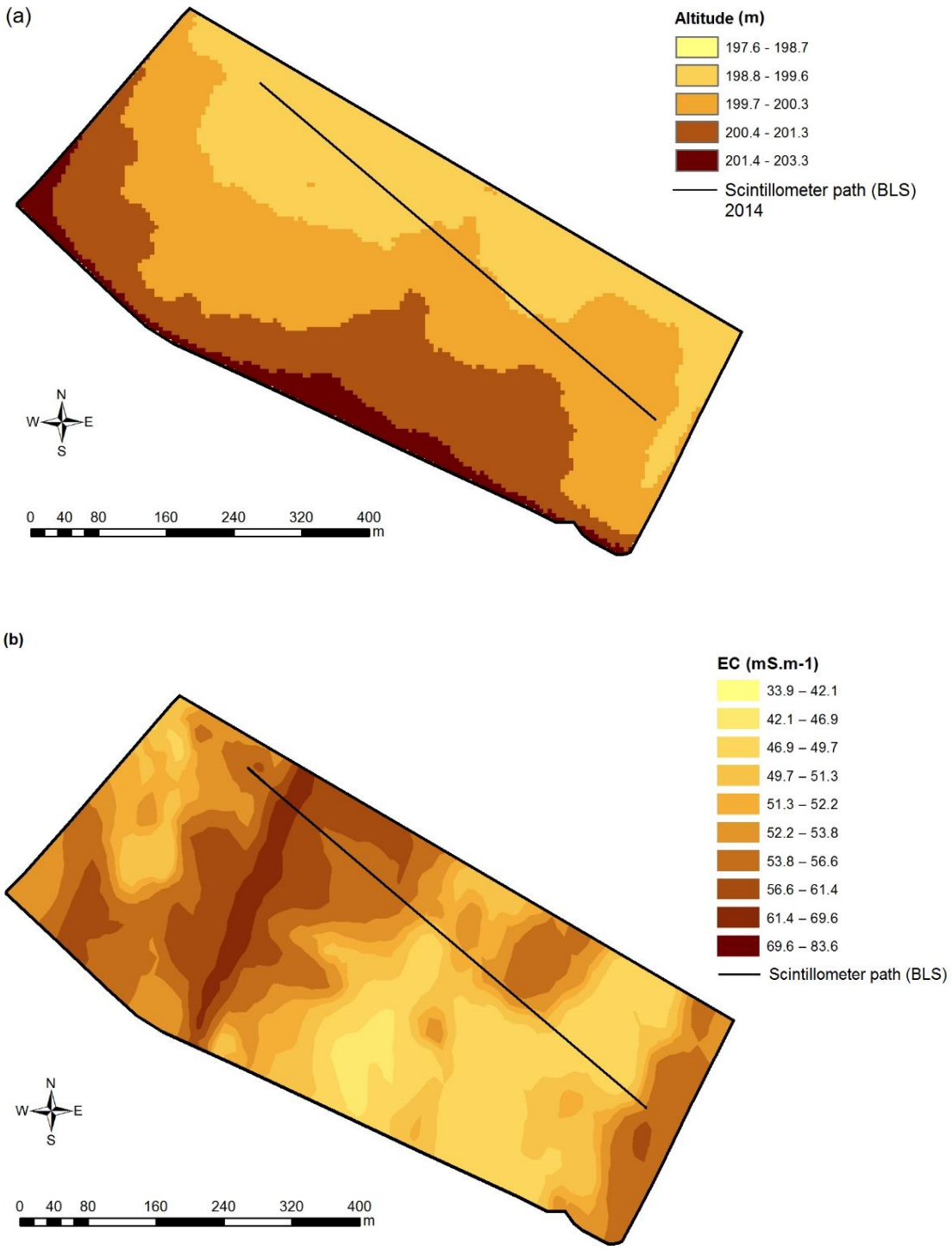

Fig 25 (a) Altitude above sea level (m) of the field, and (b) the electric conductivity of the soil up to 1 m depth measured by CMD-1 (GF Instruments, Brno, CR) in Polkovice 4. 8. 2014.

5 RESULTS

5.1 Environmental conditions

The environmental conditions during 77 days of our experiment are shown in Fig 26.

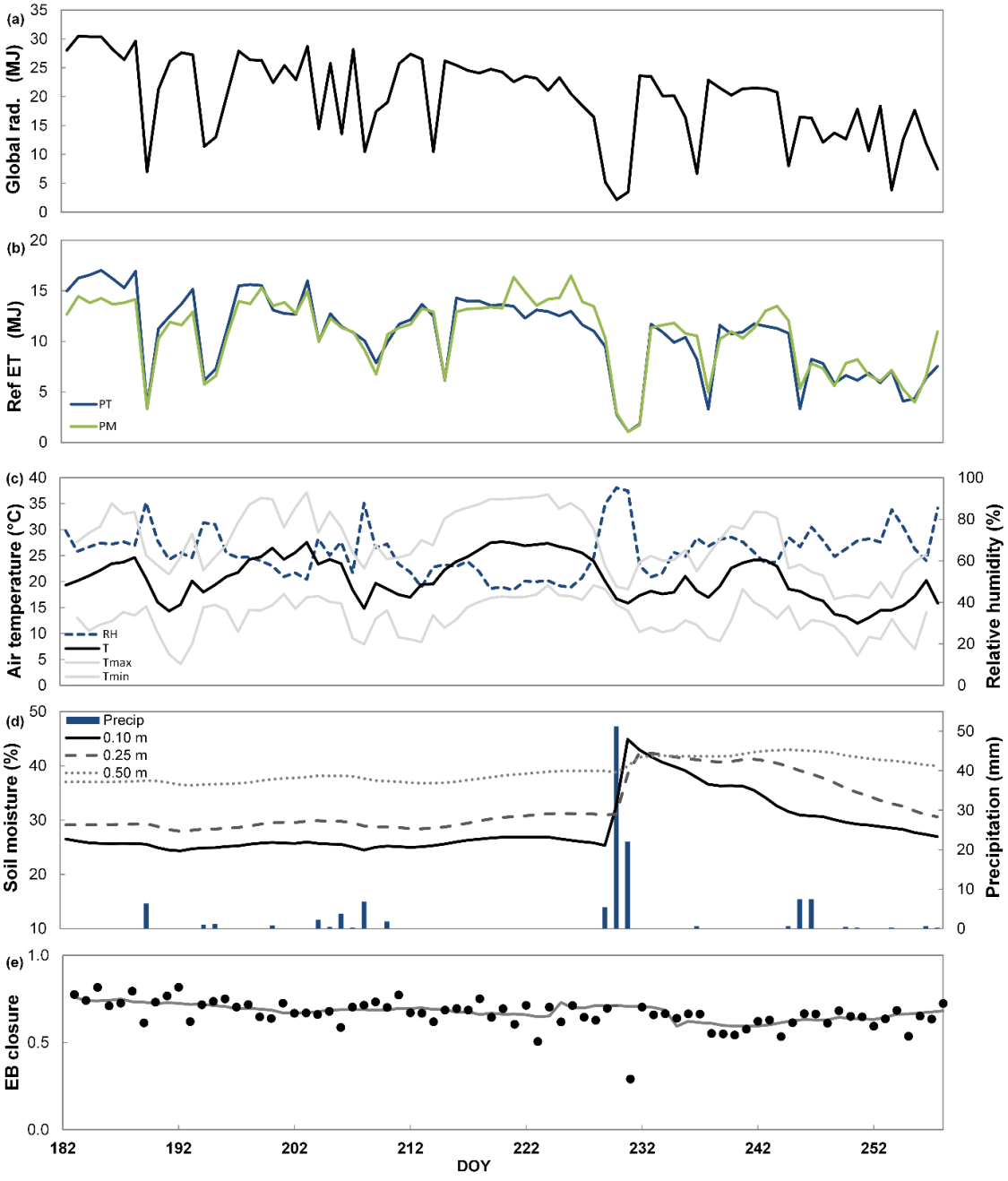

Fig 26 The climatic conditions during the study period: (a) global radiation, (b) the reference evapotranspiration according to Priestley–Taylor (PT) and Penman-Monteith (PM), (c) air temperature (min a max day temp - grey lines, and relative humidity of air; (d) soil moisture by TDR sensors in three depths and precipitation, (e) energy balance closure: points represent the slope between (*Rn-G*) and (*H+LE*), green line is a running mean of 10-days window.

Fig 26 shows the evolution of observed average day temperatures (plot c) together with min and max daily values throught the study period. The highest maximum values were recorded during the third period of the study (mid August) reaching 35 °C whereas towards the end of the season temperatures were lower reacching 15 °C on average. This decreas reflects reduction of the global radiaton shown in plot (a). The relative humidity of air logically follows development of air temperature and so the lowest RH was recorded in August. Plot (d) of the Fig 26 shows precipitation events and development of soil moisture profile measured by TDR sensors. Relatively low rainfall in the first part of the study (first and second period together 24.6 mm) was followed by no rain at all for the third period, and the last period started with heavy rains of 96.2 mm. This was reflected by the increase in soil water content by 17.3 % in the top layer (10 cm), by 12.3 % and 4.4 % in 25 cm and 50 cm, respectively. Low rainfall at the beginning of the study agreed well with the physiological need of winter wheat which was already 1 m tall and maturing at that moment. This plant phase is characterized by grain formation and thereby production of a crop yieald. Straws were already dry and not transpiring so the lack of water did not influence the harvested production which was in the end above average. After the harvest there was 11 days period of dry conditions interrupted by mentioned rain event. This situation allowed us to divide the time with bare soil into two periods, “dry” and “wet”. It is also interesting to see development of the reference ETo (plot b) calculated according to both Priestley–Taylor (PT) and Penman-Monteith (PM), and compare it to actual evapotranspiration. Plot (e) shows development of energy balance closure during the study. The best closure was calculated for the first period with slope between (*Rn-G*) vs. (*LE+H*) equal to 0.79 and coefficient of determination equal to 0.96. On the other hand, the highest disclosure occurred in the last period. More detailed results on EBC can be found in the following subsection 5.2. Energy balance closure.

Tab 12 Description of environmental conditions during four periods of field measurement.

	I period Green wheat	II period Mature wheat	III period After harvest dry	IV period After harvest wet
Period	2. 7.–15. 7.	16. 7.–4. 8.	6. 8.–16. 8.	20. 8.–15. 9.
Period (DOY	183–196	197–216	218–228	232–258
Number of days	14	20	11	26
Mean day temp. (°C)	20.0	21.8	26.4	17.9
Sum of precip. (mm)	8.6	16.0	0.0	96.2
Med Bowen ratio	0.33	1.75	2.55	0.83
Mean ET rate (mm/day):				
ETo PT	5.30	5.02	5.33	3.11
ETo PM	4.63	4.87	5.85	3.36
LAI	7.7	7.6	0.1	0.1
EBC: Slope	0.79	0.73	0.70	0.68
R^2	0.96	0.97	0.92	0.93

Based on the meteorological conditions presented in Fig 26 four periods of the experiment were determined and their characteristic are defined in Tab 12 including energy balance closure (EBC) statistics. From the perspective of the crop the first period was characterised by green transpiring wheat, crop height was about 1 m (Fig 27a). To determine the end of the first period a tipping point had to be found from which sensible heat flux during the day exceeded evapotranspiration identifying the start of winter wheat´s maturing phase. Fig 28 demonstrates this moment clearly in the middle of 15 days of energy flux data measued by the eddy covariance ploted against net radiation. The end of first period was determined for 15. 7. 2015 according to decreasing evapotranspiration (*LE*) and increasing sensible heat flux (*H*). The second period was determined by mature crop, wheat started to senesce (Fig 27b). At the end of this period spikelets were yellow and dry. The third period started after the harvest (5. 8. 2015) and till the end of the experiment there was a stubble (Fig 27c) field with some greenery appearing as intercrop in the fourth period (Fig 27d). The third "dry" period was ended by a heavy rain lasting for three days (17. – 19. 8. 2015) which determined the beginning of the final "wet" period.

Fig 27 Pictures from the field documenting each period: transpiring wheat (a), mature wheat (b), field after the harvest (c), and greenery appearing after the harvest wet period (d).

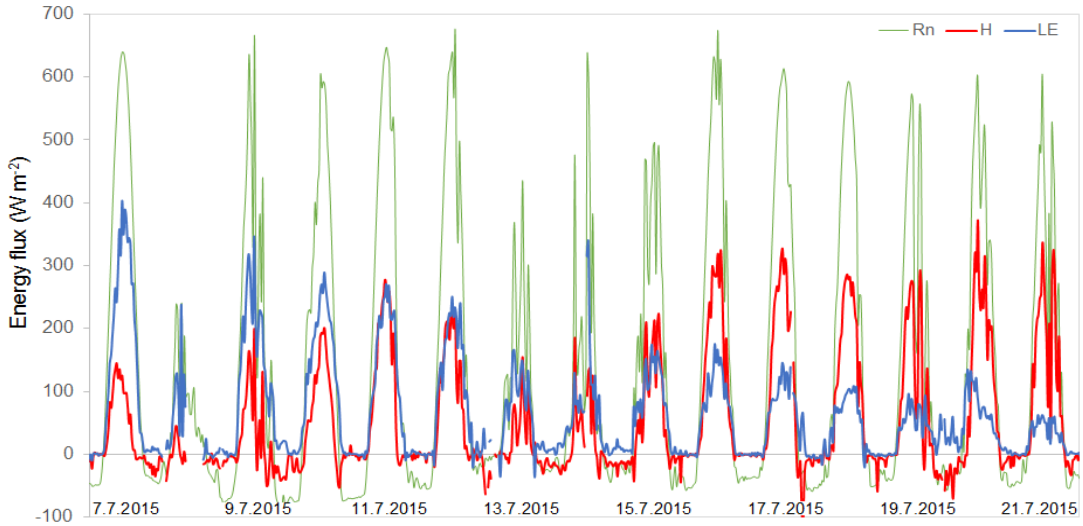

Fig 28 The course of 30-min values of the sensible (red line) and latent heat flux (blue line) densities (W m^{-2}) measured by eddy covariance used for determination of the end of first period (15. 7. 2015) at the winter wheat field in Polkovice experimental site.

5.2 Energy balance closure

Energy balance closure (EBC) is a typical measure to evaluate reliability of eddy covariance (EC) measurements. Fig 29 presents plots of EBC linear regression of half-hourly data for the whole experimental period (a) and a temporal variation of the daily linear regression slopes (b). Rainy days were excluded. The analyses outcome is relation $LE+H = 0.73(Rn-G)$ and the coefficient of determination is equal to 0.95. Our result indicate a disclosure of 27.4 % which is quite high but not uncommon (Wilson et al., 2002). Such disclosure idicates an underestimation of turbulent fluxes or on the contrary overestimation of available energy. This kind of imbalance has been reported in many studies and will be discussed in section 6.1 Energy balance closure problem.

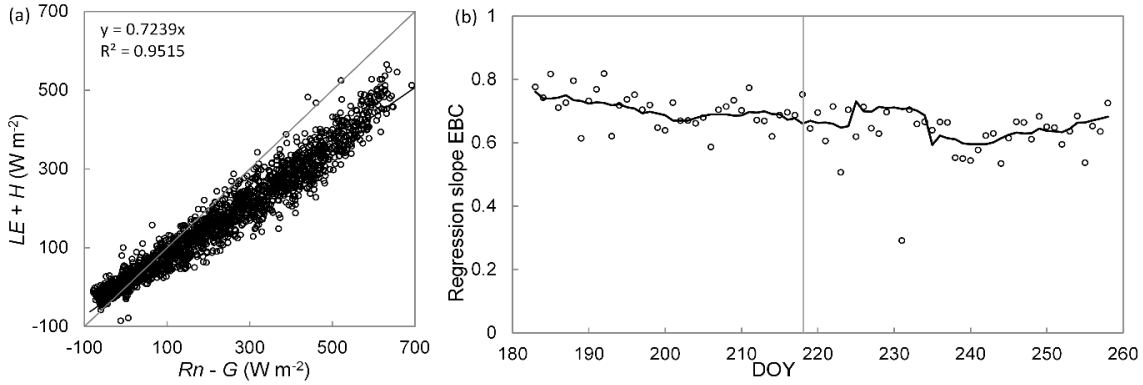

Fig 29 Energy balance closure analyses (a) temporal variation of the energy balance closure (b)using non-gap-filled data – daily linear regression slopes and 10 days running mean – solid line. *LE* and *H* are latent and sensible heat flux measured by EC system. *Rn* and *G* are net radiation and soil heat flux.

5.3 The surface renewal - ramp characteristics

The surface renewal method is based on very fast (10 Hz) measurement of temperature. An example of a 15-min time series of temperature fluctuation is plotted in Fig 30. The time series of temperature fluctuations create a periodic structures, so-called ramps. The 1-min sample of these typical features is shown in Fig 31 measured by one thermocouple during the day (a) and at night (b). By contrast, Fig 32 shows the difference in recorded temperature fluctuations during 1-min interval measured by 8 thermocouples in two heights (1.90 m and 3.35 m) during unstable (left) and stable (right) conditions. The magnitude of temperature change is around 4.8 °C during the 1-min interval under unstable conditions and all 8 sensors show similar course – caused by the mixing of the air column near the ground. On the other hand, in the right plot (Fig 32) the difference is about 1.8 °C for lower sensrs (1.90 m) and 1 °C for higher sensors (3.35 m) indicating sable atmospheric conditions as the change itself is small and air is not mixing so much between the layers.

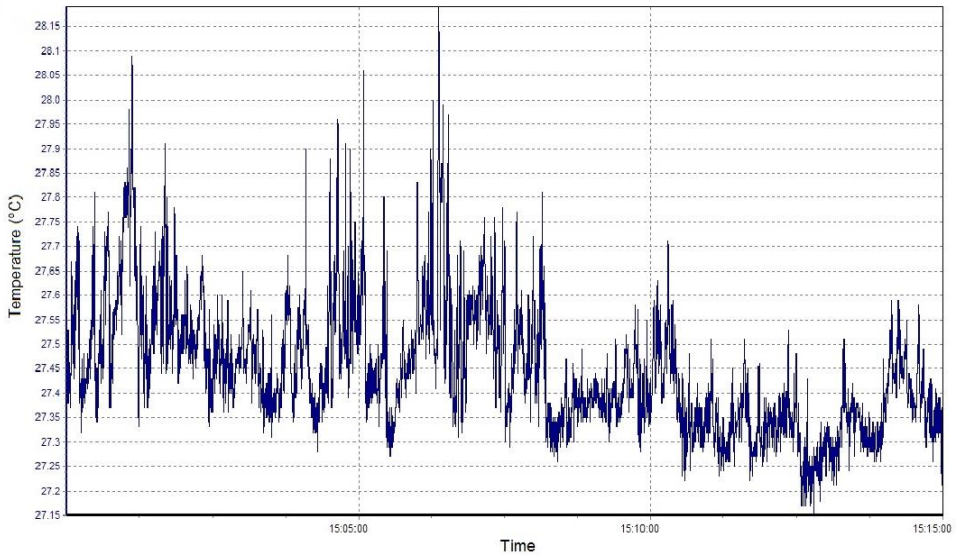

Fig 30 The sample of high temporal resolution (10 Hz) temperature fluctuatuins over winter wheat showing the ramp structures for stable conditions duration of 15 min 2. 7. 2015.

(a)

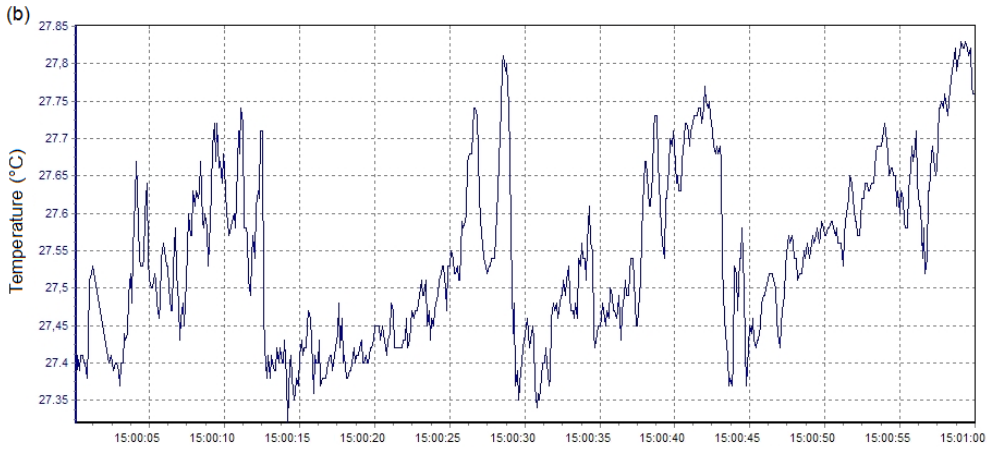

(b)

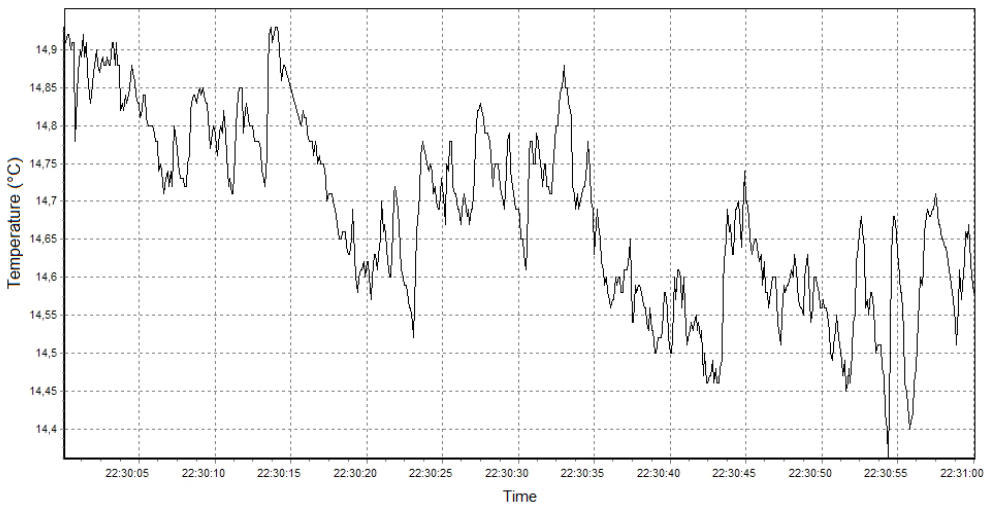

Fig 31 The 1-min sample of temperature fluctuations over wheat canopy (frequency 10 Hz) showing the ramp structures for period during unstable conditions 2. 7. 2015 (a) and stable conditions 27. 7. 2015 (b).

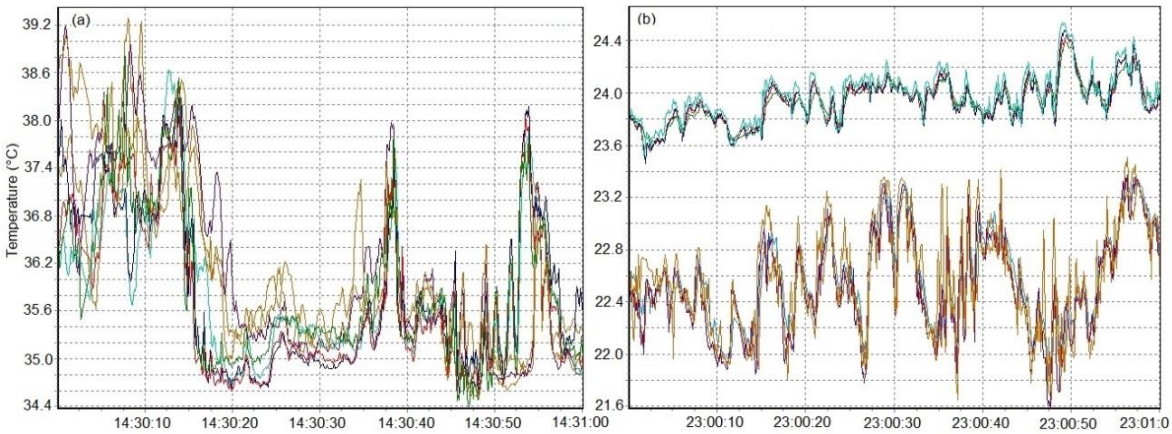

Fig 32 The 1-min sample of the temperature recorded by 8 thermocouples at two heights (1.90 m and 3.35 m). (a) unstable conditions 7. 8. 2015; (b) stable conditions 22. 7. 2015.

5.4 The sensible heat flux - comparison

Tab 13 summarizes the statistical results of intercomparison between sensible heat flux derived by the eddy covariance and four other methods for measurement periods of the study as explained in previous sections. A typical day for each of four periods is shown in Fig 33.

Tab 13 Comparison of sensible heat flux density derived by five methods; results for four periods. Intercept - a, slope - b, and R^2, and RMSE correspond to a linear regression between the eddy covariance (EC) and particular method: boundary layer scintillometer (BLS), surface layer scintillometer (SLS), the Bowen ratio energy balance method (BREB), and the surface renewal method (SR).

	I period Green wheat					**II period** Mature wheat				
	a	b	R^2	n	RMSE	a	b	R^2	n	RMSE
EC	-	-	-	145	-	-	-	-	329	-
BLS	7.99	0.84	0.94	129	18.76	-4.96	1.09	0.93	268	36.90
SLS	4.20	0.93	0.98	124	29.20	-1.37	1.21	0.95	294	54.38
BREB	26.18	1.30	0.90	142	59.31	-14.37	1.23	0.95	327	51.05
SR	14.18	1.40	0.78	130	72.89	9.57	1.38	0.74	92	141.92
	III period After harvest dry					**IV period** After harvest wet				
	a	b	R^2	n	RMSE	a	b	R^2	n	RMSE
EC	-	-	-	151	-	-	-	-	401	-
BLS	10.99	0.88	0.91	118	22.89	6.69	0.94	0.96	344	12.80
SLS	8.18	0.98	0.94	117	18.21	8.03	0.94	0.96	337	13.22
BREB	13.30	1.14	0.83	147	53.77	2.00	1.35	0.88	392	54.14
SR	27.42	0.87	0.42	151	76.05	22.30	1.01	0.55	88	65.86

During the whole study period the Bowen ratio energy balance (BREB) method always overestimated sensible heat flux compared to the eddy covariance (EC) method (H_{EC}). In general, compared methods showed the best fit during the first period of the experiment. Scintillometers rather underestimate final H_{EC} (7–16 %) compared to EC, BLS slightly more than SLS, the BREB method, and surface renewal (SR) overestimated H_{EC} by 30–40 %. Correlation was good (R^2 equal to 0.90–0.98) for the first three mentioned methods and lowest for the SR method (0.78). The SR measurements are the least smooth of all methods (Fig 33–34).

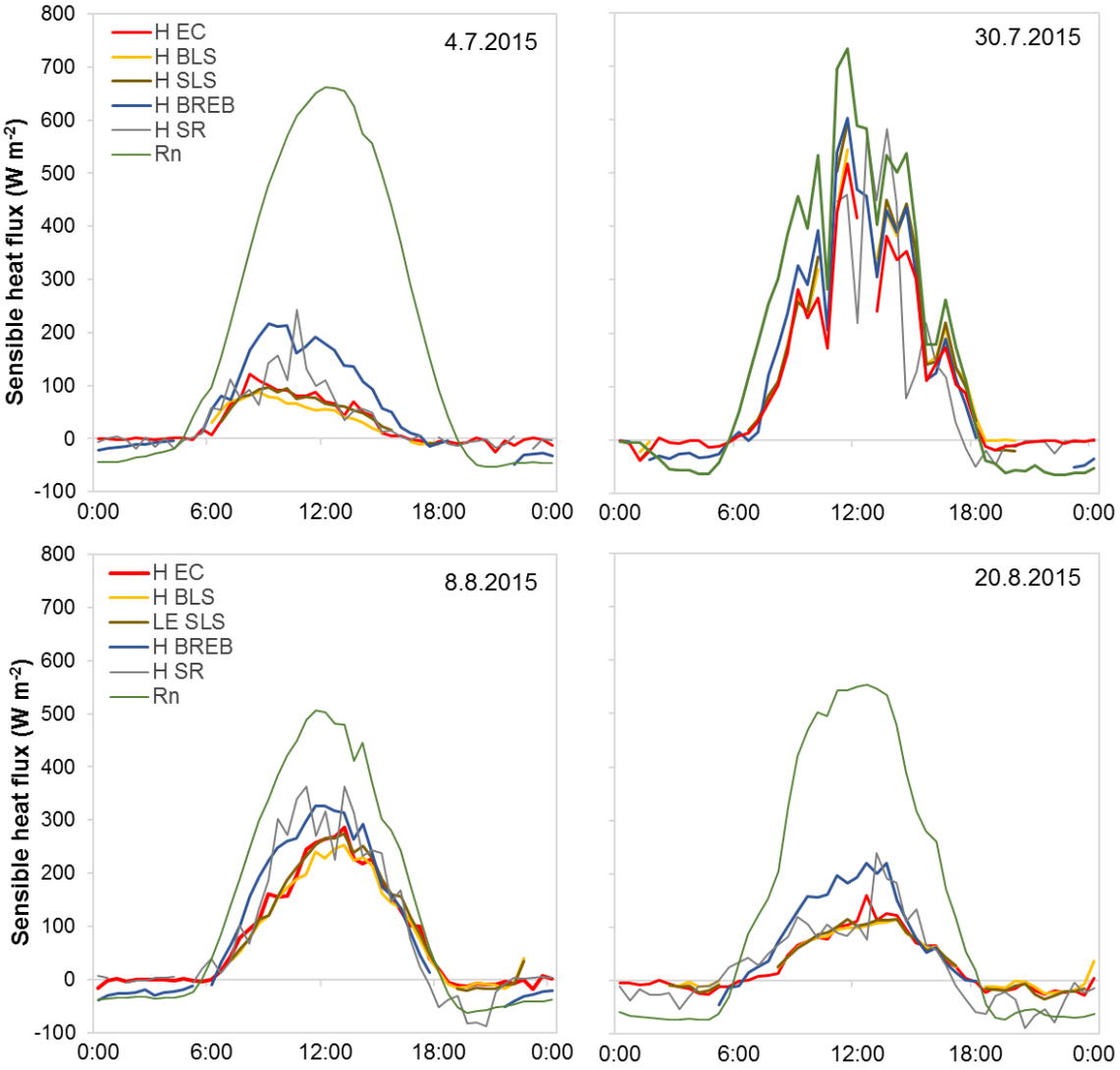

Fig 33 The sensible heat flux (H) obtained by the eddy covariance (EC), the boundary layer scintillometer (BLS), the surface layer scintillometer (SLS), the Bowen ratio energy balance method (BREB), and the surface renewal method (SR). Displayed days are typical examples of four stages of the experiment: top left - green plants, top right - mature plants, bottom left - bare soil with low soil moisture, bottom right - bare soil higher with higher soil moisture content.

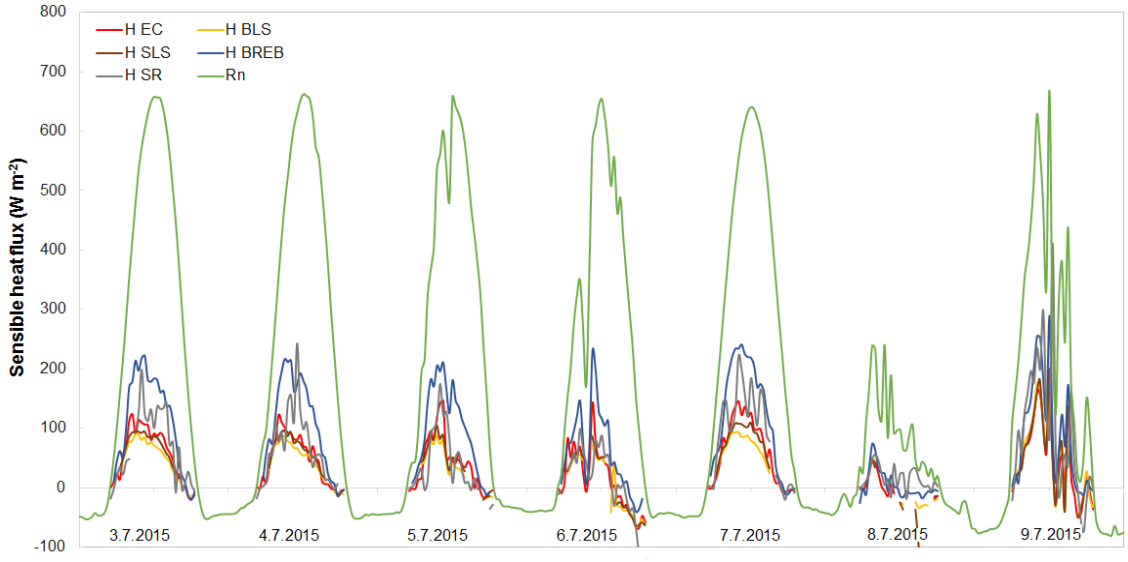

Fig 34 The 1-week flux data obtained by all methods durinfg the first period over winter wheat in Polkovice.

During the mature stage of winter wheat (the second period) differences between methods are smaller, all of them overestimate the H_{EC} (9–38 %). However, due to malfunction of the SR method (issues with memory card), the SR was analysed only based on 6 days of measurement during this period. The scintillometers overestimated H_{EC}, SLS more than BLS quantified as RMSE 54.38 and 36.9 W m^{-2}, respectively.

The third period started after the harwest (5. 8. 2015). All compared methods show reasonable agreement. Scintillometry underestimated H_{EC}, BLS slightly more than SLS, RMSE 22.89 and 18.21 W m^{-2}, respectively. The BREB method overestimated H_{EC} by 14 %. However, the largest discrepancy was recorded between EC and the SR method, which agreed well for four days, overestimated another four days and slightly underestimated EC during three days. Third period finished when the intensive precipitattion started and lasted for three days (17. – 19. 8. 2015). These data were rejected from the statistics.

In the fourth period, similarly to second one the SR results were available only for limited time period. However, slope between H_{EC} and H_{SR} for this period (6 days of comparison) is the best of all season equal to 1.01 althought the R^2 is low. Both scintillometers (H_{BLS} and H_{SLS}) showed very good fit with H_{EC} equal to 0.94 with intercept 6.69 and 8.03 for BLS and SLS, respectively. The coefficient of determination reached 0.96 for both scintillometers. The BREB method overestimated H_{EC} by 35 % with the coefficient of determination equal to 0.88.

Sensible heat flux was very low at the beginning and at the end of the study period (max 200 W m^{-2} in midday). In the first period the energy partitioning was considerably disposed towards latent heat flux. The mean Bowen ratio (β) of 0.33 indicated that only one third of the available energy pertained to H. In the last period, the β reached 0.83 and the distribution of available energy between LE and H was more equal but LE still prevailed. Contrariwise, during the second and third perod H dominated with Bowen ratios 1.75 and 2.55, respectively, with

maximum values reaching 4 before the harvest when the weather condiitions were dry and after the harvest on the bare soil.

5.5 The latent heat flux - comparison

Tab 14 summarizes statistical results of the comparison between the latent heat flux (*LE*) determined using four different methods, namely: the eddy covariance (LE_{EC}), the scintillometry (LE_{BLS} and LE_{SLS}), the Bowen ratio energy balance method (BREB) method (LE_{BR}), and the surface renewal method (LE_{SR}). Generally, the methods agreed the best in the first period. Fig 35 shows a diurnal course of *LE* derived by four methods and net radiation of a typical day of each period.

Tab 14 Comparison of latent heat flux density derived by four methods; results for four periods. Intercept (a), slope (b) and R^2, and RMSE correspond to a linear regression between eddy covariance (EC) and particular method: the boundary layer scintillometer (BLS), the surface layer scintillometer (SLS), the Bowen ratio energy balance method (BREB), and the surface renewal method (SR).

	I period Green wheat					**II period** Mature wheat				
	a	b	R^2	n	RMSE	a	b	R^2	n	RMSE
EC	-	-	-	182	-	-	-	-	333	-
BLS	22.44	1.27	0.89	153	99.83	35.20	1.59	0.59	269	97.50
SLS	26.55	1.24	0.90	145	94.40	19.44	1.51	0.69	284	70.30
BREB	16.17	1.04	0.94	181	39.37	56.05	0.96	0.60	333	62.93
SR	35.08	0.72	0.87	163	68.61	63.30	0.66	0.02	56	89.10
	III period After harvest dry					**IV period** After harvest wet				
	a	b	R2	n	RMSE	a	b	R^2	n	RMSE
EC	-	-	-	142	-	-	-	-	400	-
BLS	73.68	1.49	0.39	108	103.90	53.20	1.35	0.64	344	109.79
SLS	64.79	1.40	0.35	108	92.65	61.32	1.28	0.63	335	108.88
BREB	51.72	0.88	0.62	142	50.31	39.52	1.07	0.78	395	57.42
SR	101.81	0.63	0.06	135	114.62	36.74	0.43	0.49	88	104.45

During the first period of experiment, when winter wheat was green the latent heat flux determined the sensible heat flux (Bowen ratio on average 0.33). The LE_{BR} (the BREB method) showed the highest agreement with the LE_{EC} (slope 1.04 and R^2 0.94). Similarly scintillometry overestimated LE_{EC}, BLS more than SLS, by 27 % and 24 %, respecively. In terms of root mean square this represents an error of 99.83 and 94.40 W m^{-2} for BLS and SLS, respectively. The surface renewal method underestimated LE_{EC} with regression slope 0.72 and R^2 0.87.

In the second period of the study the Bowen ratio was higher than one and thus more enerrgy flowed through sensible heat, the latent heat flux gained roughly 50 % of H and 30 % of

available energy (Fig 35 top right plot). Also in this period LE_{BR} fited LE_{EC} the best especially in the seconf part of the sample however, at the beginning of the period it overestimated similarly to scintillometry. Overall scintillometry (both BLS and SLS) fitted well with BREB but overestimated EC by 59 % and 51 %, respectively. After the rain events the agreement between LE_{EC} and the rest of the methods was better than before (Fig 36). Data of LE_{SR} cover only five days of compared period. In Fig 36 LE_{SR} covers days 30. 7. – 1. 8. 2015. These data show large scatter and unrealistic flux.

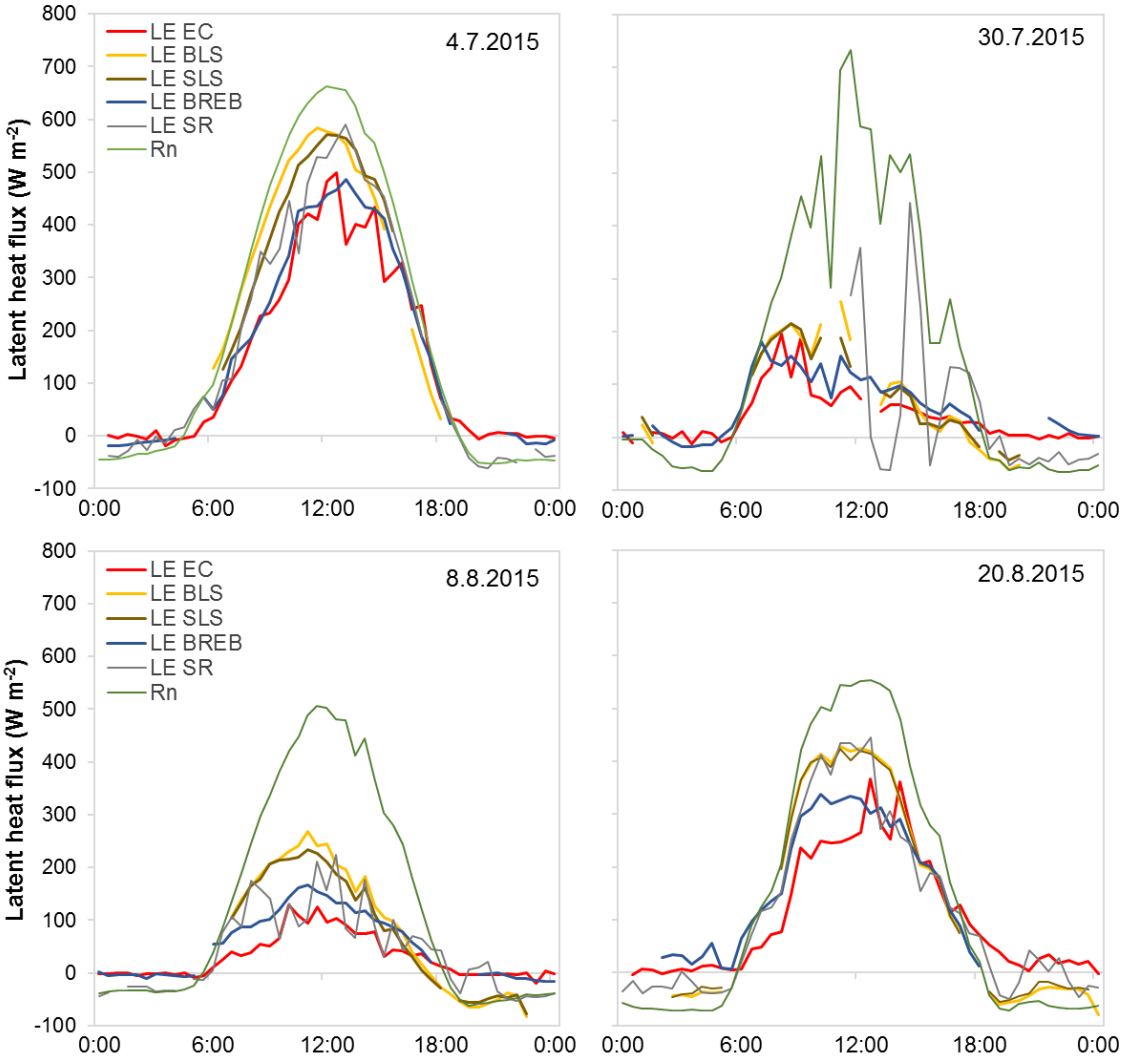

Fig 35 The latent heat (*LE*) flux obtained by the eddy covariance (EC), the boundary layer scintillometer (BLS), the surface layer scintillometer (SLS), the Bowen ratio energy balance method (BREB), and the surface renewal method (SR). Displayed days are typical examples for four stages of the experiment: top left – green plants, top right – mature plants, bottom left – bare soil with low soil moisture, bottom right – bare soil with higher soil moisture content after the rain.

The third period is represented by bottom left plot in Fig 35 (8. 8. 2015). It was after the harwest and there was stubble on the field under relatively dry conditions. LE_{EC} was lower than *LE* by other methods with highest overestimation by scintillometry. Both scintillometers agreed well. The BREB method overestimated EC and the SR method was again scatered more than the rest of fluxes (Fig 37).

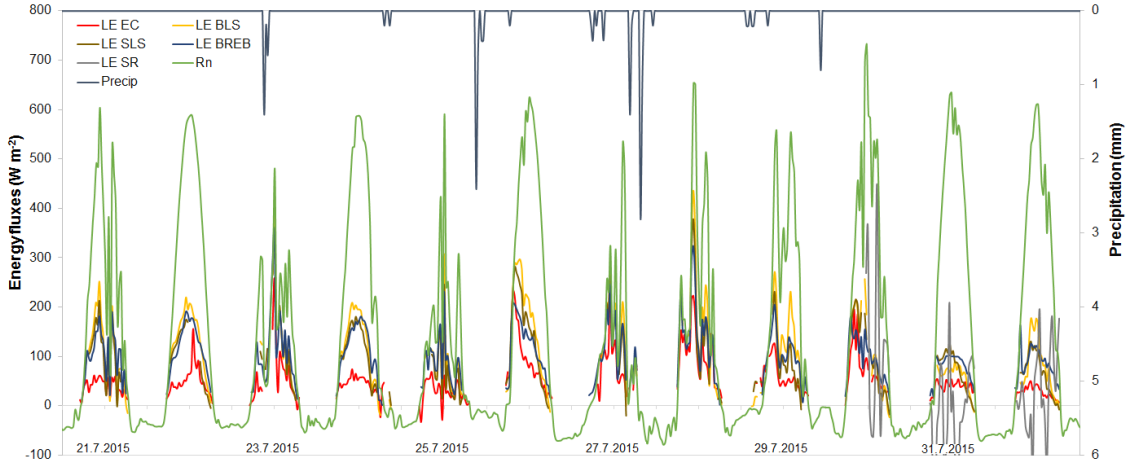

Fig 36 The 12-days long time series of diurnal course of net radiation and latent heat flux densities derived by four methods: EC – eddy covariance, BLS and SLS – boundary and surface layer scintillometer, BREB – the Bowen ratio enerfy balance method, SR – the surface renewal method, and precipitation during the second period of the study, nocturnal values were exculded.

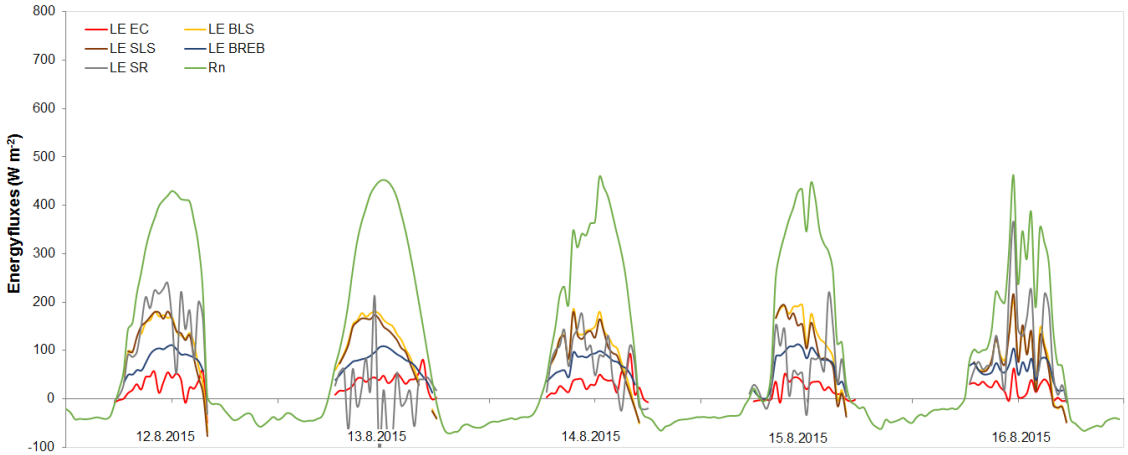

Fig 37 Diurnal courses of five days of third period, latent heat flux measurements by four methods: EC – eddy covariance, BLS and SLS – boundary and surface layer scintillometer, BREB – the Bowen ratio energy balance method, SR – the surface renewal method, nocturnal values were left out.

The last period was the longest one. The field was still covered by stubble but because of the wetter conditions some greenery appeared - second growth. Methods fittet better after the rain events otherwise they overestimated LE_{EC}. The scintillometry and the BREB method overvalued *LE* the most signifficantly. The BREB method showed the closest agreement with

EC (slope 1.07 and R^2 equal to 0.78). For the SR method we had limited number of days for comparison, however, 20. 8. 2015 and 21. 8. 2015 it agreed very well with SLS and BLS (Fig 38).

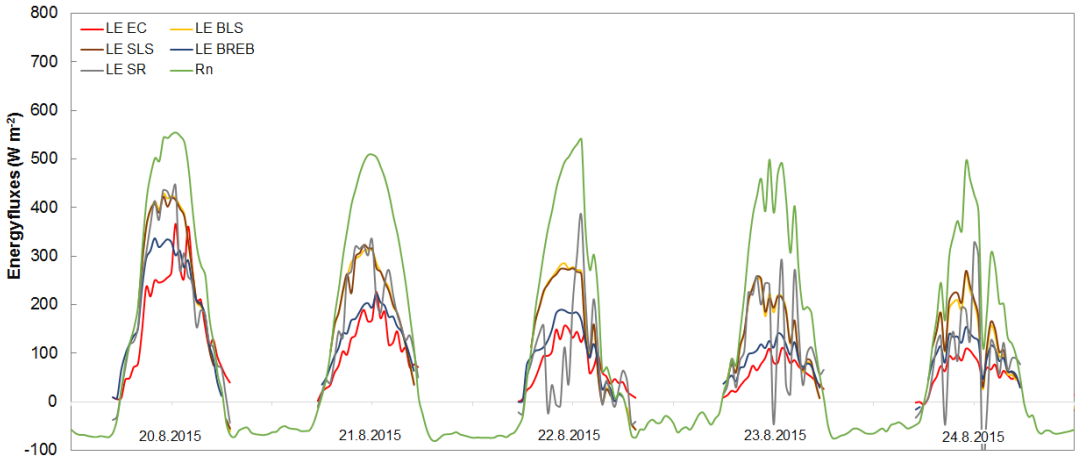

Fig 38 Diurnal course of the latent heat flux density (*LE*) measured for five days of the last period by four methods: EC - eddy covariance, BLS and SLS - boundary and surface layer scintillometer, BREB - the Bowen ratio energy balance method, SR - the surface renewal method, nocturnal values were left out.

5.4 Comparison of boundary layer and surface layer scintillometer

The intercomparison of the scintillometer data was conducted. BLS and SLS were compared based on the measurements between 2. 7. 2015 and 14. 9. 2015. Fig 39a shows the relationship between sensible heatl flux density calculated by both scintillometers and it can be characterized by equation H_{BLS} = 0.92 H_{SLS} with R^2 = 0.99. Latent heat flux, on the other hand, can be expresed as LE_{BLS} = 1.02 LE_{SLS} with R^2 = 0.96 (Fig 39b). The C_n^2 data obtained by SLS were reprocessed as BLS data to see the correlation in final sensible heat flux and their esult is ploted in Fig 39c, where the slope is 0.97 and coefficient of determination is equal to 0.98.

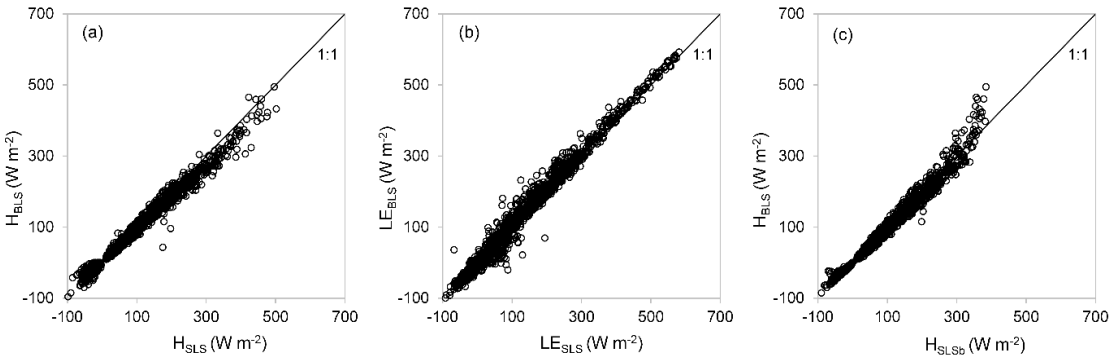

Fig 39 Comparison between SLS and BLS technique (a) sensible heat flux (*H*), (b) latent heat flux (*LE*) densities. (c) *H* calculated from C_n^2 measured by SLS using BLS procedure. The results of regression show good agreement of slope 0.92, 1.02, and 0.97 for (a), (b) and (c) respectively. The R^2 equal to 0.99, 0.96, and 0.98 for (a), (b), and (c) respectively.

5.5 Evapotranspiration: reference vs. actual

Fig 40 shows cumulative evapotranspiration (ET) by eddy covariance and reference ETo calculated according to Penman-Monteith (PM), and cumulative sums of daily precipitation (mm) for the study period. It should be mentioned that zero at the beginning (1. 7. 2015) is relative because of the previous precipitation and soil moisture content.

It is apparent from the plot that actual evapotranspiration never reached hypothetical demand of the atmosphere – reference ET (ETo). It should be noted here that mostly during all four periods of measurement eddy covariance had tendency to underestimate other methods and thus there is an assumption that scintillometry or the BREB method would give larger value of the ET sum for the season. However, actual ET was 58.87 % of the reference ET. The sum of precipitation for studied period reached 57.35 % of the actual ET. It needs to be repeated that ET is influenced not by rainfall itself but rather soil water content (SWC) which is dependent on precipitation but also other factors. Of course, there was some SWC present before 1. 7. 2015 prior to this comparison which is not included in the statistics.

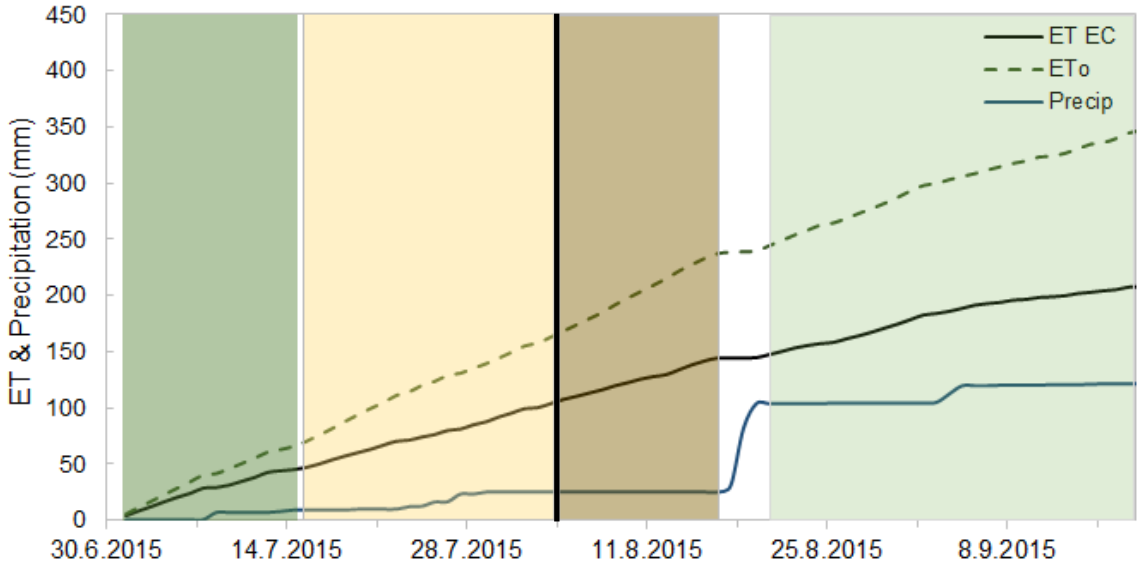

Fig 40 Cumulative ET by eddy covariance, reference ETo according to Penman-Monteith, and precipitation (mm) for the whole study period. Four sub-periods are delimited by different colours: I. period - green, II. period – yellow, III. period – brown, IV. period – light green, harvest is marked by vertical black solid line.

Fig 41 shows daily sums of actual evapotranspiration measured by the eddy covariance (ET_{EC}) and ETo according to Penman-Monteith (*ETo PM*), and Priestley-Taylor (*ETo PT*) in mm for a study period between 1. 7. 2015 and 23. 9. 2015. The sum of ET_{EC} for the whole period was 211.36 mm, *ETo* was 361.54 mm and 355.63 mm for Penman-Monteith (PM) and Priestley-Taylor (PT), respectively. Which means *ETo PT* was lower than *ETo PM* only by 1.8 %. *ETo PM* fitted ET_{EC} better during whole study period. Fig 42 shows linear regressions between ET_{EC} and *ETo* by PT and PM for four periods.

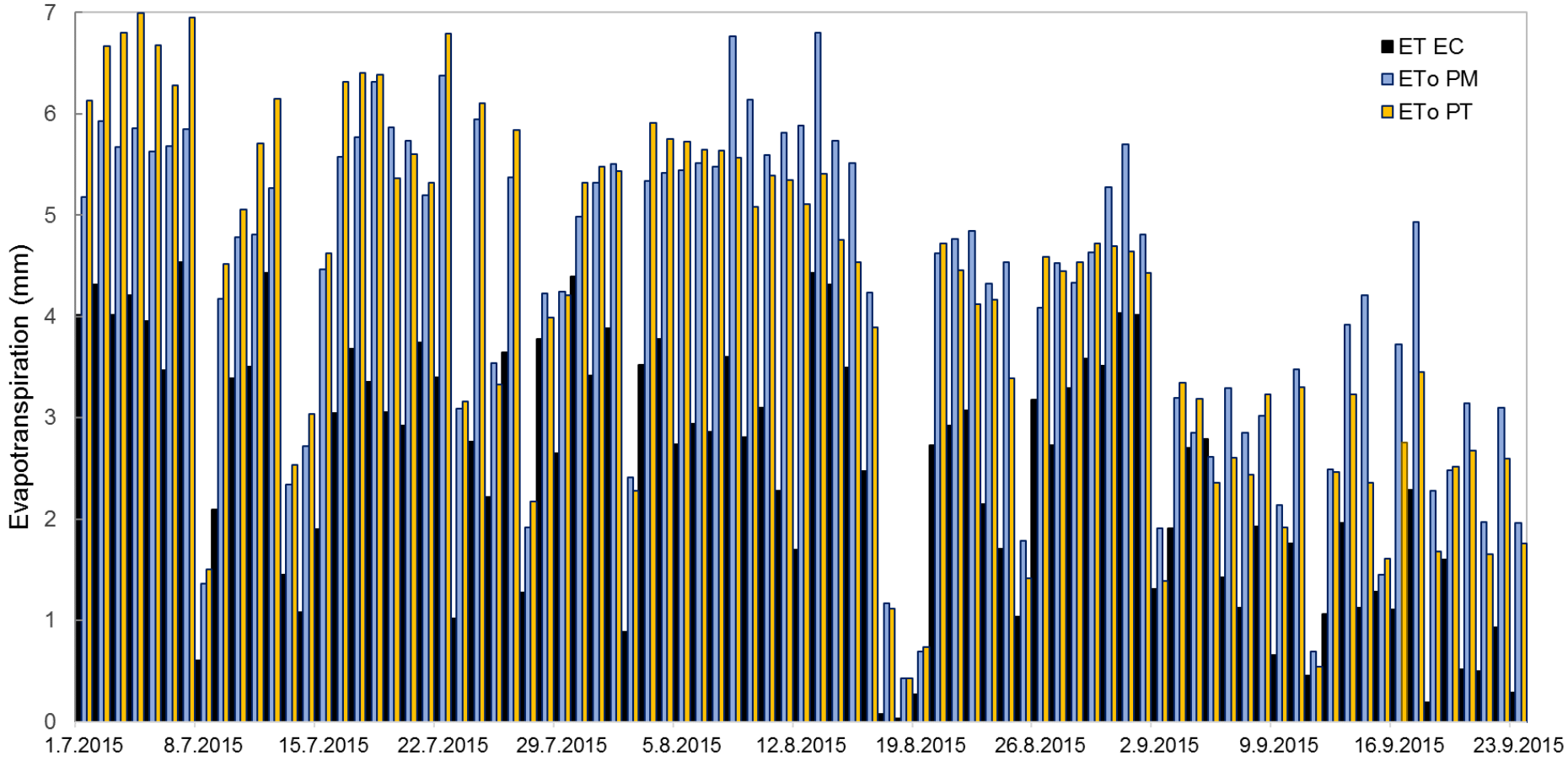

Fig 41 Daily sums of actual evapotranspiration (mm) calculated by eddy covariance (ET EC) and reference ET by the Penman-Monteith method (ETo PM) and the Priestley-Taylor method (ETo PT).

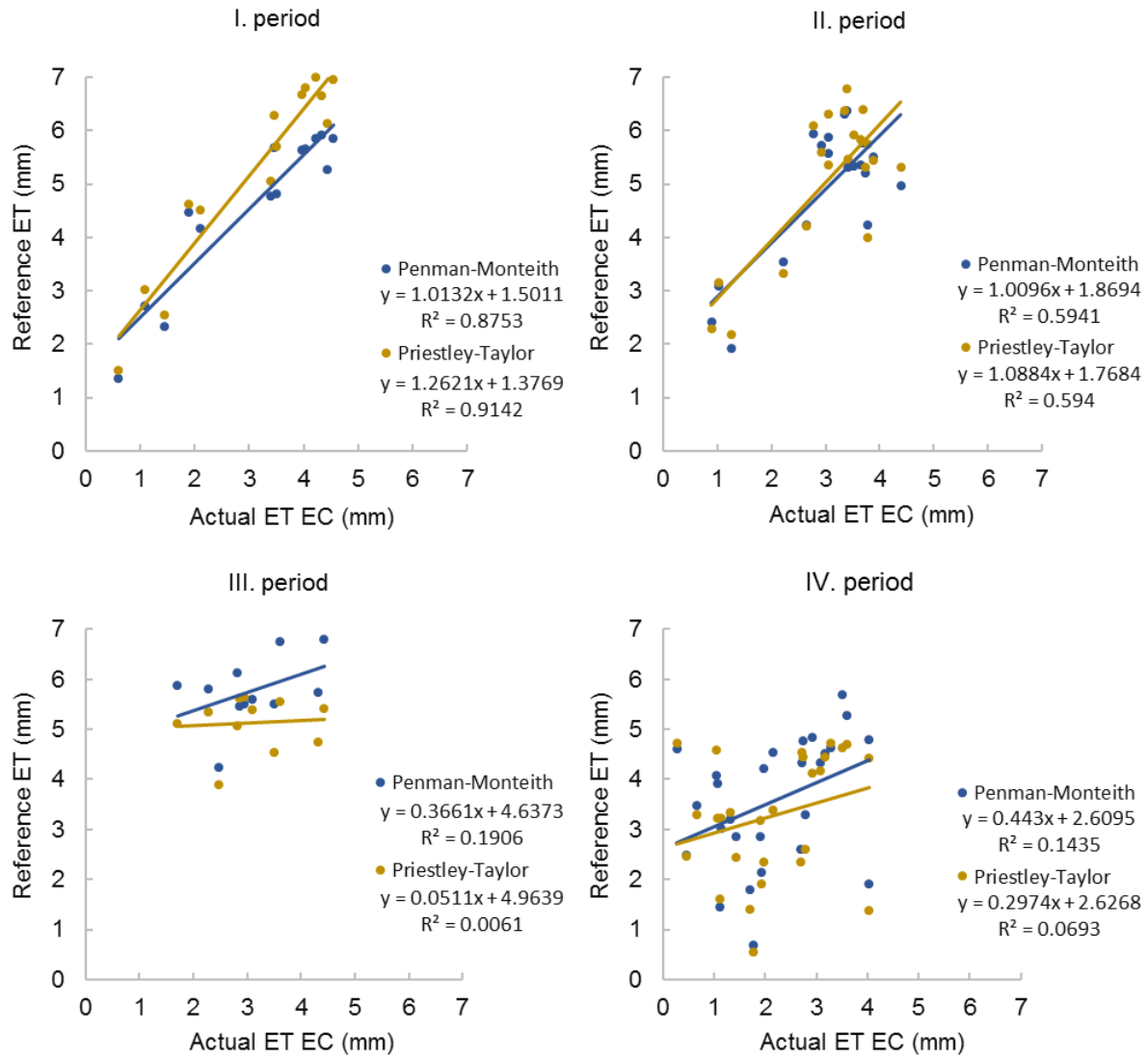

Fig 42 Linear regressions between actual evapotranspiration (ET) by the eddy covariance (EC) vs. reference ET by Penman-Monteith and Priestley-Taylor for four periods of the experiment in Polkovice between 2. 7. 2015–15. 9. 2015.

5.6 Homogeneity of the site

Fig 43 shows the aerial thermal image made during the plane campaign 5. 6. 2015 above the experimental field in Polkovice. Marks show position of AWS (Meteostation), scintillometers (blue points), and access tubes for regular ground measurements of soil water content and LAI (white points). Red line pinpoints the transect of boundary layer scintillometer (BLS). Green stripes at the upper and yellow stripes at the bottom part of the field show location of the tramlines used by tractors.

Fig 44 is an aerial image showing the NDVI of the same field scanned at the same time during the plane campaign. In the Fig 45 and Fig 46 there are detailed views on the scintillometer (BLS) transect with graphical display of the temperature gradient (Fig 45) and NDVI (Fig 46) along the path. Graph in Fig 45 shows rapid increase of surface temperature 140 m far from the receiver where

transect crosses spot of bare soil and also some increase when passing through a tramline. Similarly, in Fig 46 the NDVI drops when crossing tramline 180 m or 460 m far from receiver.

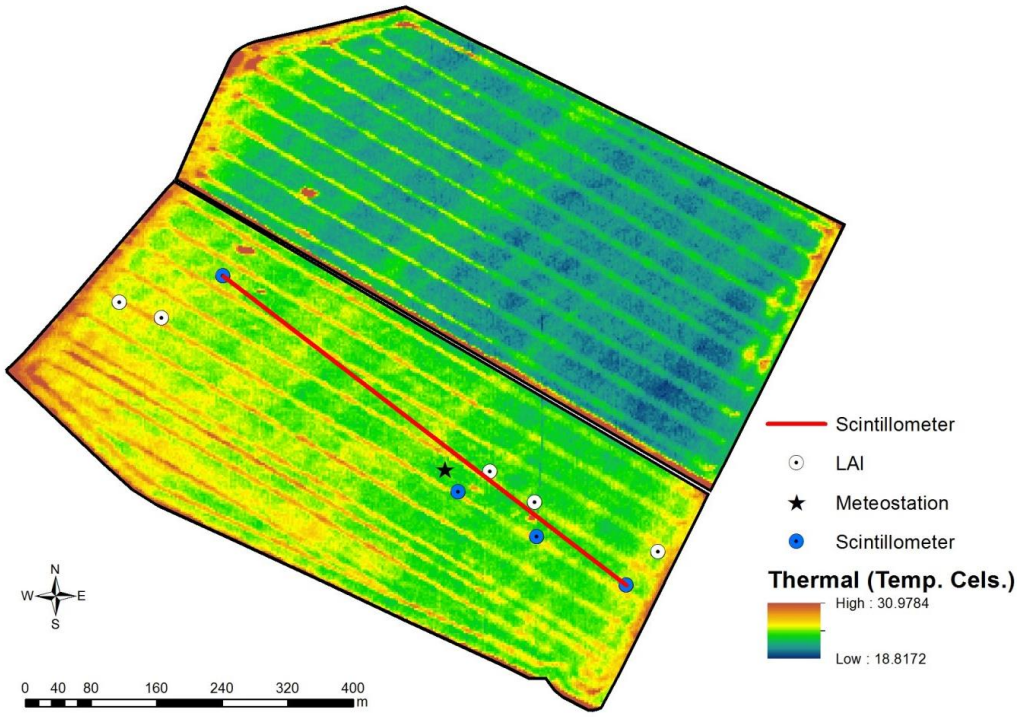

Fig 43 Thermal aerial image of the experimental field in Polkovice measured from the plane during the campaign 5. 6. 2015.

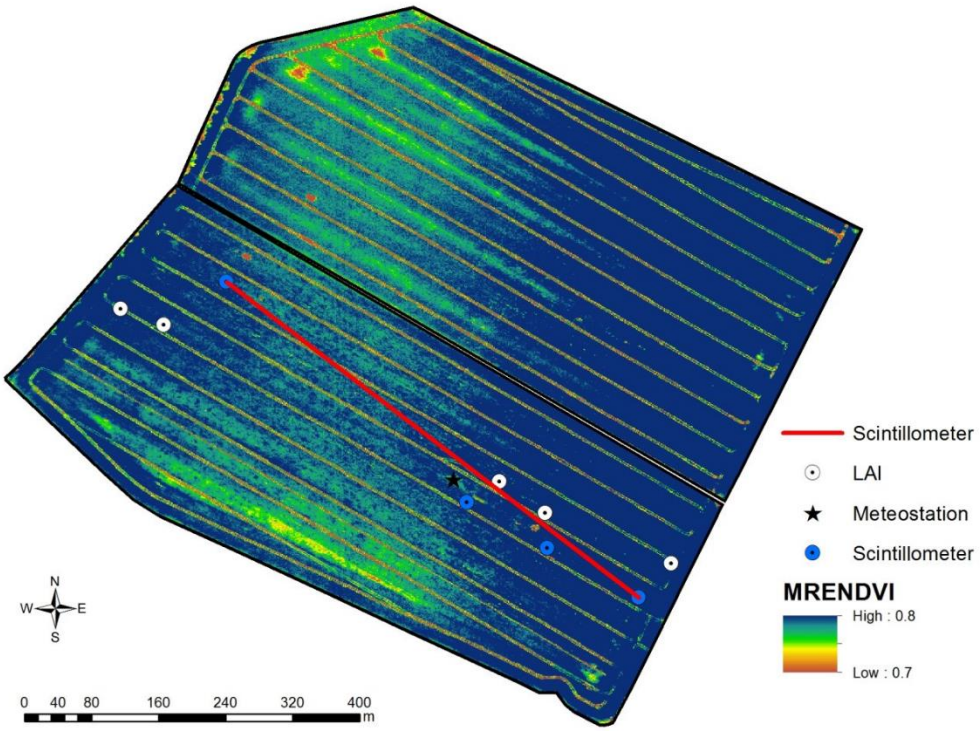

Fig 44 An aerial image of the experimental field in Polkovice scanned from plane image showing the Normalized Difference Vegetation Index (NDVI).

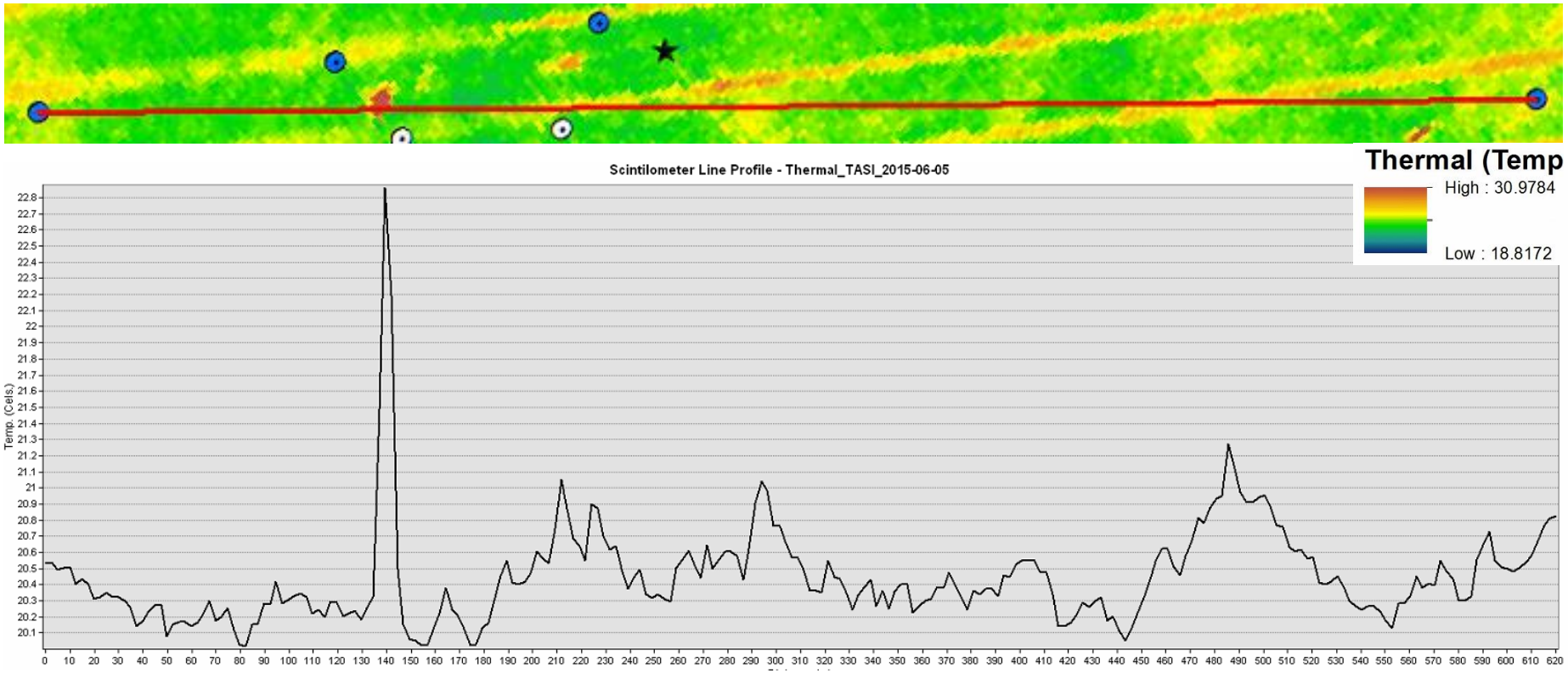

Fig 45 Thermal image of the boundary layer scintillometer transect (upper plot) and surface temperature profile along the 617-m long path from receiver to transmitter (lower plot). Image by TASI. Picture made during the plane campaign in Polkovice 5. 6. 2015.

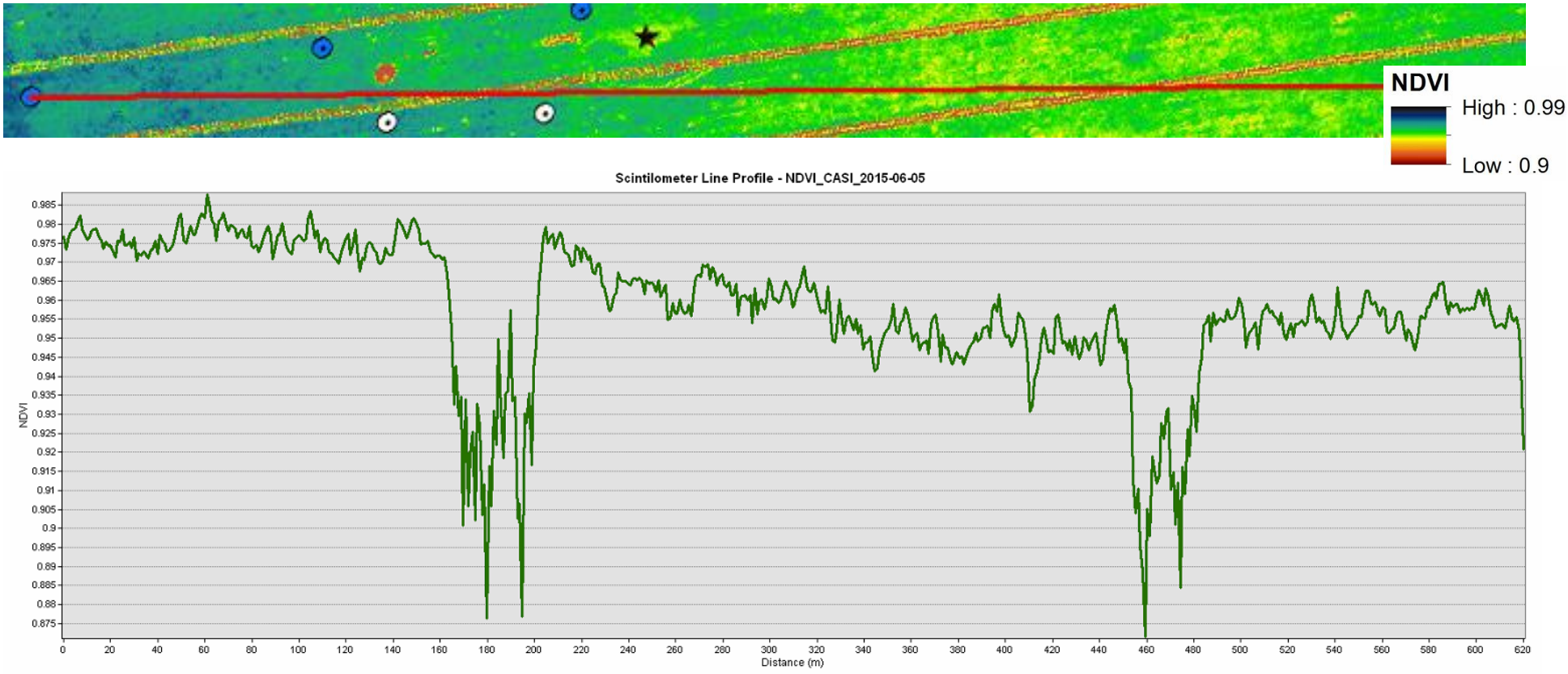

Fig 46 Areal image of NDVI of the boundary layer scintillometer transect (upper plot) and profile of NDVI along the scintillometer path (617-m long) from receiver to transmitter (lower plot) in Polkovice, Image by CASI visible and near IR radiation. Picture made during the plane campaign 5. 6. 2015.

During the plane campaign scintillometer (BLS) and the BREB system were running simultaneously measuring energy fluxes and the results are plotted in Fig 47a. The actual ET rate for BLS was 0.013 mm/min and thus 0.40 mm per 30 min, and the BREB method measured 0.012 mm/min which means 0.37 mm per 30 min. The overflight by plane is marked by red arrow. Fig 47b shows the surface temperature measured in the middle of the field by IR thermometer (Apogee instruments, Logan, UT, USA). At the moment of the plane passing it showed 20.7 °C.

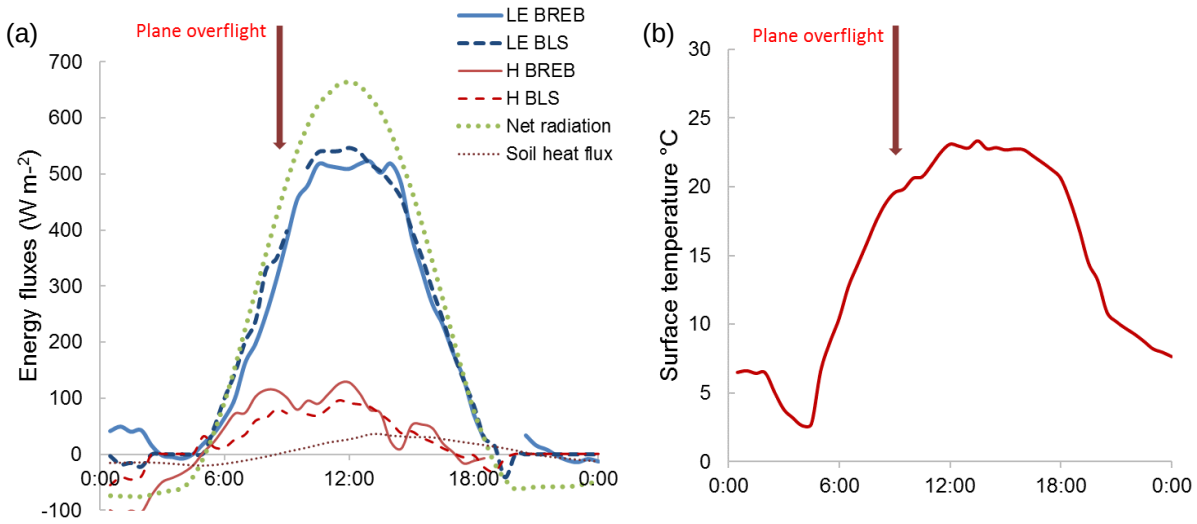

Fig 47 Energy fluxes during the plane campaign in Polkovice, 5. 6. 2015 (a), surface temperature measured by IR radiometer (SI-121, Apogee instruments, Logan, UT, USA) at AWS (b).

5.6.1 Leaf area index

The leaf area index (LAI) was measured periodically since 2014. During the growing season on the weekly or bi-weekly basis and after the harvest only the plant height was measured. In 2014 there was an oil-seed rape growing in the field and as it was mentioned in methodology the sampling spots were chosen based on the NDVI satellite image (for more detail see section 4.5 Auxiliary measurements). The position of measurement spots is plotted in Fig 22. The results of LAI measurements according to sampling spot in the field (different colour of the column) are shown in Fig 48 for oil-seed rape and winter wheat in 2014 and 2015, respectively. It is apparent from the chart that variability observed in 2014 was larger and reflected the spots (oilseed rape did not grow evenly across the field, lower LAI recorded for red spot). However, next season winter wheat did not show similar variability (crop was growing more uniformly). Fig 49 shows variability of LAI within 5 measurement spots distinguished by colour. To sum up, the field measurements and also airborne images confirmed that the field variability was higher in 2014. Surprisingly, the absolute value of LAI was similar for both crops. Considering the fact that oil-seed rape was on average 200 cm high in the peak of the season while winter wheat reached maximum of 110 cm LAI in 2015 was very high. The likely explanation involves very favourable conditions for cereals in 2015, and yields above standard.

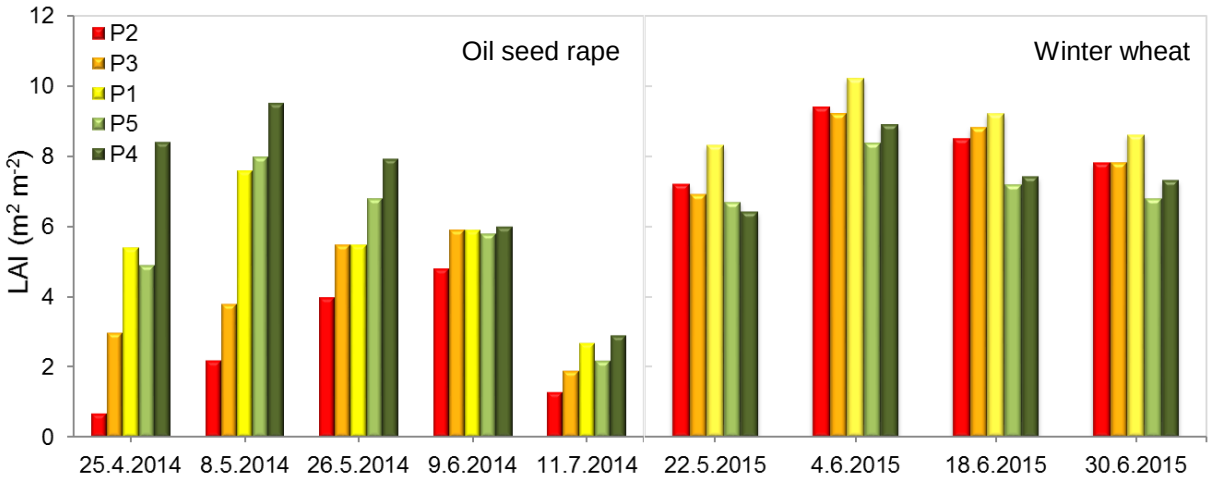

Fig 48 The leaf area index measured by SunScan (Delta T device, UK) in the growing seasons 2014 and 2015 at Polkovice experimental field.

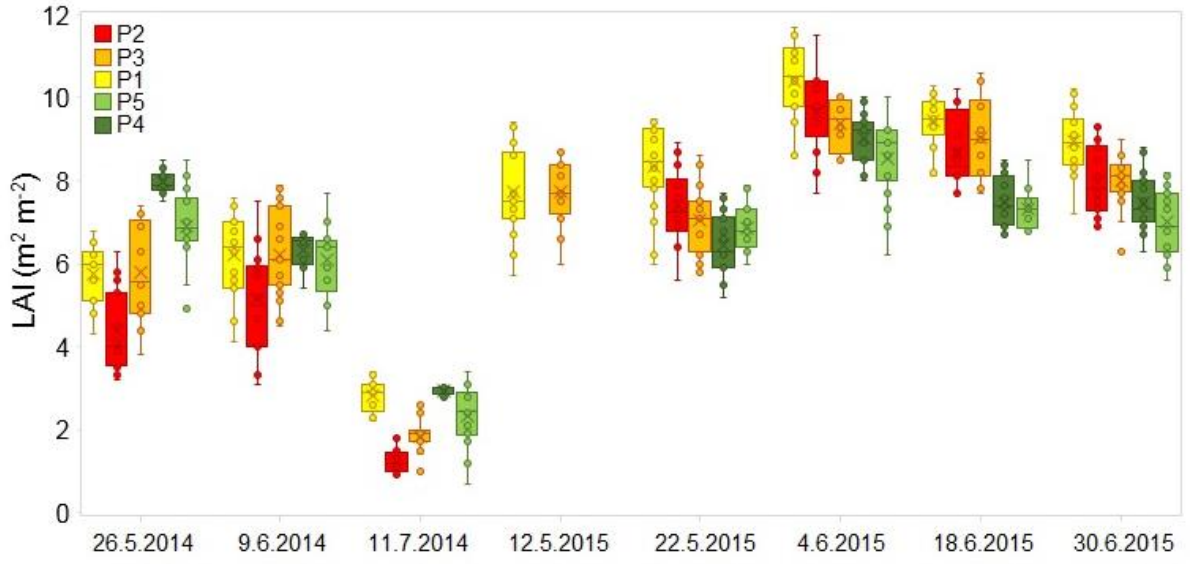

Fig 49 The variability of LAI within five measurement spots in Polkovice in 2014 and 2015.

5.6.2 Soil water content

The results of continuous measurements of soil water content (SWC) by time domain reflectometry (TDR) sensors and also the averages of regular measurements of SWC using PR2 probe are presented in Fig 50. From the first sight it is apparent that the discrepancy between two methods is quite large. Knowing the background of the measurements and the fact that the field conditions in season 2015 were very dry we can argue that soil moisture in 10 cm was low and thus PR2 sensors are more trustworthy. However, TDR measurements realistically reflected rainfall patterns and thus we can claim they describe seasonal course of the SWC correctly although the actual values are overestimated.

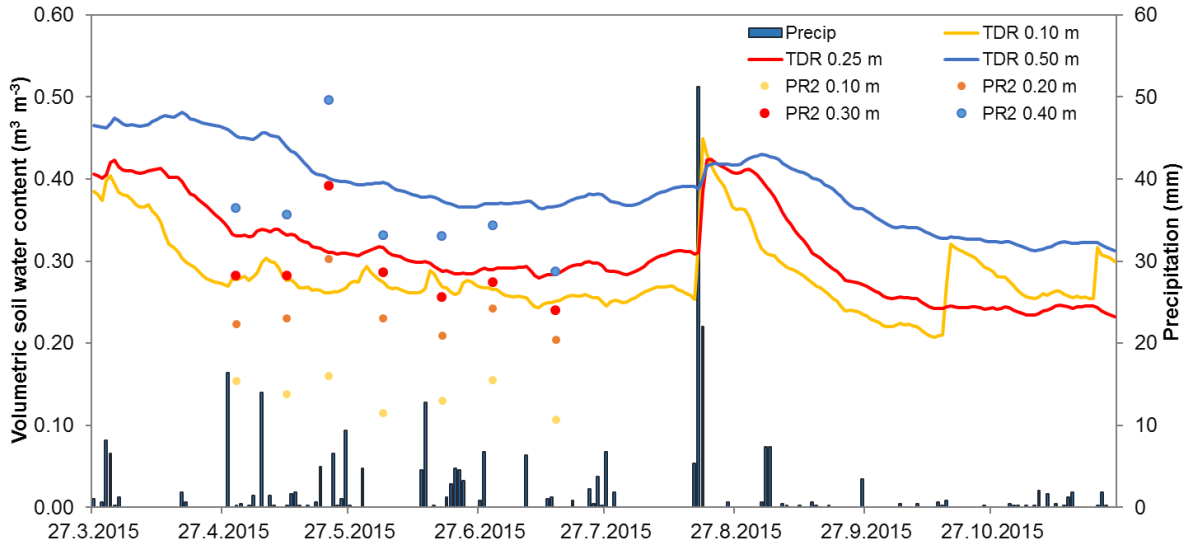

Fig 50 Development of soil water content profile at experimental site in Polkovice in 2015 in the winter wheat field measured periodically by PR2 probe in 12 access tubes across the field (mean value plotted as a point of different colour for different depth). Continuous soil water content measured in profile by 3 TDR sensors.

Detailed results of PR2 measurements are presented in Fig 51. Variability of the measurements at 12 spots is characterized by size of the box, minimum and maximum value for individual measurements is also shown. Different colour of the box plot assigns different depth. Soil moisture near the surface is always lowest (yellow box). The highest variability was observed 22. 5. 2015 and 18. 6. 2015 in all depths. It should be noted that 18. 3. 2015 was the day when access tubes were installed. That is why, measured values of soil water content may be influenced by insufficient coherence between tube and surrounding soil (air bubbles).

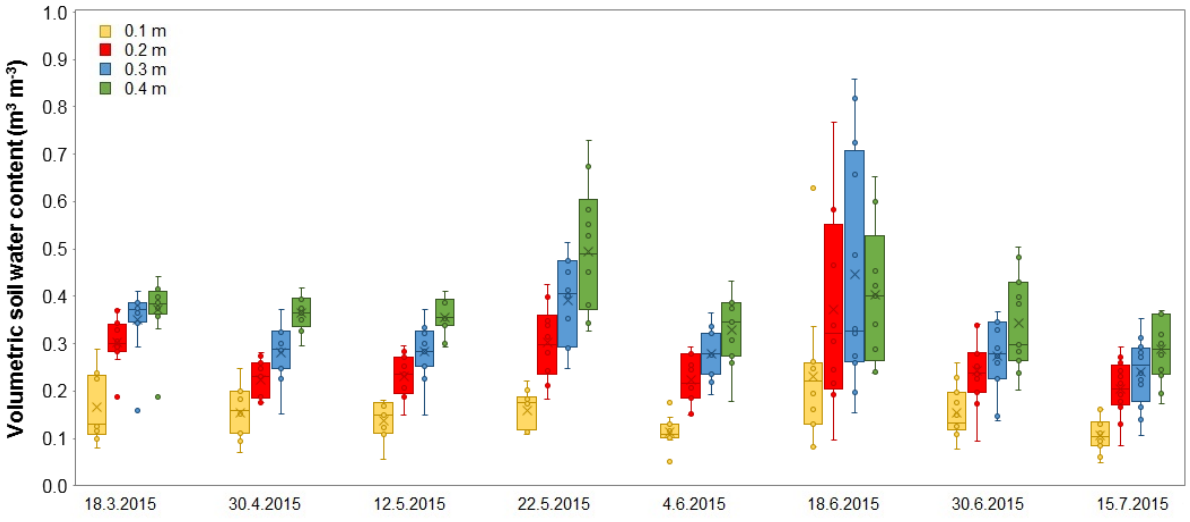

Fig 51 Box plot of the periodical measurements of soil water content measured by PR2 probe in 12 access tubes across the field. Different colours distinguish different measurement depths. Maximum and minimum is showed together with mean value (X - sign) and median (horizontal line).

6 DISCUSSION

6.1 Energy balance closure problem

In our experiment the surface energy balance (EB) disclosure was within generally accepted range 10–30 % underestimation of surface energy fluxes compared to estimates of available energy (Wilson et al., 2002). However, this issue deserves our attention because the energy imbalance has implication for data interpretation and comparison of flux estimates by different methods. The reasons for discrepancies could be summarized based on the results of international study by Wilson et al. (2002). Data from 22 FLUXNET sites all over the world and 50 site-years were used to examine energy balance closure (EBC). The results showed a general lack of closure at most sites, with a mean imbalance in the order of 20 %. The imbalance dominated in all measured vegetation types and in climates ranging from Mediterranean to temperate and arctic. Generally, the causes of incongruity in EBC can be summarized as follows: sampling errors, other energy sinks, instrument biases, low/high pass filtering, and advection (Wilson et al., 2002; Li et al., 2005, Sun et al., 2005).

Firstly, sampling errors are associated with different source areas for individual terms measured (Li et al., 2005). Foken (2008b) explained this issue quite well on the Fig 1 (section 2.7 Energy balance closure). The point is that different scalars (net radiation, soil heat flux or turbulent fluxes) are being recorded at different heights above the surface and thus their footprint is influenced as the size of the underlying surface measured by sensor differs. Moreover, heterogeneity of the surface underlying the sensor plays its role. In our study this could be the case as the net radiation was measured from 3.5 m height, eddy covariance was placed in 2.7 m, SHF was installed 5 cm under the soil surface etc.

Secondly, neglecting other energy sinks and sources is an issue (Li et al., 2005; Foken, 2008b). One of the reasons for EB disclosure can be neglecting several parts of EB equation as described in section 2.7 Energy balance closure. For example, Meyers and Hollinger (2004) found out that although it is assumed that individual neglected parts comprise only up to 5 % of net radiation (*Rn*) individually, together they can contribute up to 15 % of *Rn*. In particular, during their experiment the combination of soil and canopy heat storage and the energy stored during photosynthesis comprised roughly 15 % of the total net radiation for maize and 7 % for soybean during the morning hours from 06:00 to 12:00 h when the canopy was fully developed. When all of the storage terms were considered, the slopes of the 1:1 line between net radiation and the partitioned fluxes (latent, sensible, ground, and storage) increased by 10 % and the scatter about the 1:1 line decreased for both maize and soybean with the R^2 increasing by 0.05.

Lastly, low/high frequency loss of turbulent fluxes and advection of heat and water vapour can be another factor influencing the EBC (Li et al., 2005; Foken 2008b). According to Foken (2008b) an energy transport with large eddies that cannot be measured by EC are the main problem of EB disclosure. The reason for large eddies is seen in heterogeneity of landscape and methods to investigate this issue can be found in literature (Foken, et al., 2006; Sun et al., 2006). However, the

landscape in our experiment was fairly homogeneous with prevailing agricultural land around the study site. The only potential influence causing either turbulence or advection could be adjacent asphalt parking area to the east from our field.

Eddy covariance is a very complex and complicated method and there is not much more space for discussion here. However, Aubinet et al. (2012) published a practical guide to measurement and data analysis where all aspects and potential corrections are explained and discussed citing the up-to-date literature.

6.2 The surface renewal - ramp characteristics

In section 5.3 The surface renewal - ramp characteristics structures typical for surface renewal analysis recorded by fine thermocouples are presented in Fig 30-32. It can be seen in Fig 31a that during the unstable conditions, the shape of ramps is characterized by slow rise of temperature followed by abrupt drop. This can be explained by a parcel of cold air sweeping down into the plant canopy. On the other hand, inverse trend is typical for stable conditions/night time values (Fig 31b) when sudden temperature rise is followed by gradual temperatre decreas. The magnitudes of change are also different comparing stable and unstable conditions. During the day (unstable) an instant change can range between 1–5 °C, whereas at night (stable) it is only around 0. 5–2 °C. Similar results were published by Anandakumar (1999).

The difference in temperature profile during both stability conditions of the atmosphere is also well ilustrated in Fig 32. During the unstable conditions, in the left hand picture (7. 8. 2015 14:30–14:31) all eigth thermocouples of which four are mounted in 1.90 m and four in 3.35 m height above the soil surface show turbulent mixing typical for daytime. Surface is being heated by radiation and the air close to the surface get heated from surface afterwards warmer air reises and mixing is evident from rapid changes in temperature. On the other hand when the atmosphere is stable at night, layers of air do not mix so rapidly and four sensors at each height can be easily distinguished. Four lines in the upper part of the plot are sensors at 3.35 m height above soil surface and the rest of lines represent four sensors in the lower level (1.90 m). The magnitudes of temperature change is slightly higher closer to the ground induced by roughness of the surface.

Due to occasional malfunctions of the system we had only limited time sequence of sensible heat flux data by surface renewal (H_{SR}) to compare with other methods. However, from analysed datased it is quite clear that for situations when H_{SR} underestimated H_{EC} (H derived by the eddy covariance method) the H of the Scale One was closer to H_{EC} than H of the Scale Two. This means, that Shapland´s assumption that the Scale Two is connected to the flux and Scale One correlates with it but it is not associated with the flow itself (Shapland et al., 2012a) is correct, but our empirical observations revealed missing Scale One in particular 30-min values. For this reason, it would be desirable to develop a process to identify Scale Two independently on identification of Scale One and even independently on the existance of Scale One. Moreover, determination of Scale Two based on Scale One can propagate an uncertainity (error propagation) connected to correct assessment of Scale One.

6.3 The sensible heat flux

There are few general aspects influencing the result of our comparison of different approaches to determine sensible heat flux. First of all, different footprint (source area) of individual methods is an issue. This argument is repeated across all the studies dealing with method comparisons (Kleissl, 2008; Pauwels, 2008; Van Kesteren, 2013a). Of course, the argument about different footprints dominate among the case studies aiming to measure heterogeneous surfaces (Beyrich et al., 2002).

In our study site fetch was measured for 16 wind directions and overall layout of the experiment allows us to assume sufficient footprints for all methods. For the fetch values see Tab 8 in section 4.2 Fetch and footprint. Analysis of the wind patterns and the relationship between final sensible heat flux derived by scintillometer and eddy covariance revealed that the wind direction does not play crucial role in their agreement. The values obtained while the wind speed was less than 2 m s^{-1} showed bigger scatter and values corresponding to higher wind speeds (> 5 m s^{-1}) show lower discrepancies when the wind was coming from all directions. This confirms our opinion that the source area of the fluxes for compared methods is the same. Otherwise, stronger winds would bring more scattering to the dataset with different wind directions.

Another general argument influencing the comparative studies is heterogeneity of the measured area. No matter, whether the measurement takes place over the large heterogeneous area (across a valley or agricultural region) or rather homogeneous site (crop field or grassland). In both cases, the inhomogeneity in crop height, soil structure, soil moisture, etc. plays its role and even very local diversity can influence the result. Especially when considering measurement of the soil heat flux by small number of the soil heat flux plates (SHFP) and assuming their average value as SHF for larger areas (Kustas et al., 2000). In our study, we did not correct the soil heat flux for energy storage in the soil above the plates as we did not measure the soil temperature above the SHFP (Pauwels et al., 2008). The heterogeneity of the soil is documented by remotely sensed images (Fig 43–46) and measured values presented in tables of section 5.6 Homogeneity of the site.

Further, soil water content is often mentioned in the literature as a reason for agreement or discrepancy between various methods. For example, Hoedjes et al. (2007) argue that when the experimental area (orchard) became heterogeneous due to irrigation, scatter becomes much larger and correlation between the sensible heat flux derived by EC and LAS worsened. The observations in our case study were in the contrary to their results.

General comparison of methods during the whole measurement season need to be separated into at least two parts: before/after the harvest. Firstly, plant cover - winter wheat was approximately 1 m tall and climatic conditions as described in section 5.1 Environmental conditions. The comparison revealed good agreement between eddy covariance (EC) and scintillometry, preferably boundary layer scintillometer (BLS), while surface layer scintillometer (SLS) was slightly overestimating. However, this overestimation was lower than the one by the Bowen ratio energy balance (BREB) method. The overestimation of the EC by other methods could be partly explained by the general tendency of the EC to underestimate fluxes. However, underestimation by scintillometry (both systems BLS and SLS)

indicates different footprint for different methods. Pauwels et al. (2008) also measured *H* above winter wheat field by the BREB and large aperture scintillometer (LAS) and found that the LAS and BREB estimates of the sensible heat flux are consistent during daytime, but that during nighttime the LAS estimates are approximately 100 W m^{-2} lower than the BREB estimates. Night time values, however, were not within our interest in this study.

The EC, the BREB method and scintillometers do reflect a change in net radiation instantaneously. Moreover, scintillometers show smoother variations than all other method caused by the fact BLS averages larger areas. This phenomenon was recorded by Anandakumar (1999), too. The SR method does not reflect the shadowing effect of the clouds well enough.

Some authors (Hoedjes et al., 2007) explain the discrepancy between different methods by advection. In our study, sufficient fetch, overall flatness of the area, and the fact that majority of the neighboring fields were croplands (except an asphalt parking lot on the east of the experimental site) create favorable conditions, however, some local and occasional incidents of advection might by a case.

The BREB method does provide reliable methods during the day and at night but not at the transition in between (Pauwels et al., 2008). Thus we have decided to examine this phenomenon in detail and conducted an experiment with very fine thermocouples to measure temperature gradient above different agricultural surfaces but also grassland and poplar plantation to study temperature gradients in detail. Preliminary results of this study were published as an article in conference proceedings and can be found in Appendix E.

The differences in *H* obtained by EC and scintillometry result from either inhomogeneity within the field or are the matter of methodological issues. The scintillometers underestimated H_{EC} in the first period, BLS slightly more than SLS. This can be explained due to the similarity of footprints: the SLS footprint is more alike the EC footprint than BLS. We can exclude the within field heterogeneity as the main reason for discrepancy based on the airborne pictures. The methodological issues are more likely the reason and include, for example, different measurement height of BLS (4.22 m) and SLS, EC (2.70 m) and changing height for the BREB method according to movement of AWS arms.

Green et al. (2001) conducted a field experiment over pasture in New Zealand measuring sensible heat flux by scintillometers over the transect of 3.1 km and referring it to the EC measurement. They used infrared and microwave scintillometer. The agreement between the sensible heat flux calculated from the combination of microwave and infrared scintillometers and EC was within 4 % over a measured range 0–300 W m^{-2}, with a residual standard deviation of 45 W m^{-2} and R^2 equal to 67. They commented on the comparison of methods with different spatial resolution (different footprint) by stating that interpretation of such results is complicated and the differences between point and path-averaged measurements could be reflected in the results. However, on truly homogeneous surface they would expect an “on average” agreement between scintillometry and the EC.

6.4 The latent heat flux

Comparison of four methods was technically quite challenging especially in terms of ensuring that all equipment is running at the same time for the whole season. Unfortunately, due to the fact we were using some of the methods for the first time (surface renewal method, surface layer scintillometer) there were unexpected gaps in data for several days owing to, for example, formating of the data storage card in CR1000 datalogger, interuption of SLS signal because of birds sitting on the receiver and so on.

Before commenting on the agreement between different methods it should be reminded, that in case of the boundary layer scintillometer (BLS), surface layer scintilloemter (SLS), and the surface renewal method (SR) the latent heat flux density (*LE*) is determined as a residual term of the energy balance equation (Eq. 23). Consequently, this may accumulate some unavoidable errors (Pauwels et al., 2008). That is why lot of attention should be given to proper measurements of all energy fluxes (Allen et al., 2011a), especially net radiation and soil heat flux (SHF) (Drexler et al., 2004). It is common to measure SHF by several SHF plates, for instance, Suvočarev et al. (2014) used four in their experiment in orchard.

In general, compared methods to determine *LE* within our study agreed quite well. The positive aspect of the eddy covariance (EC) is that it is a direct method which allowes the independent test of accuracy by energy balance closure (Drexler et al., 2004). In presented thesis the whole subsection was dedicated the to this phenomena. The EC method is commonly used worldwide to measure turbulent fluxes and it is considered to be the most accepted method to measure evapotranspiation (Baldocchi et al., 2001; Yu et al., 2006; Allen et al., 2011; Haghighi and Or, 2015; Rosa and Tanny, 2015). That is why, in our study we compared *LE* derived by other methods to *LE* by EC (LE_{EC}) which served as a reference in this case.

The scintillometry tended to overestimate LE_{EC} basically during the whole measured period. Pauwels et al. (2008) showed similar results while comparing LAS and the BREB method. The agreement between the *LE* calculated from the combination of microwave and infrared scintillometers and EC over a pasture in New Zealand was within 12 % over the range 0–450 W m^{-2} (residual standard deviation of 94 W m^{-2}) and an offset of 30 W m^{-2} (Green et al., 2001). Pauwels and Samson (2006) compared the EC with the BREB method over the wet sloping grassland and found good agreement.

The BREB method gave accurate estimates of the *LE* flux, however, as it was mentioned in sections on the Bowen ratio theory and the Bowen ratio energy balance method, close to the sunrise and sunset this method can give large errors. It is result of methodological issues when the Bowen ratio $\beta \approx -1.0$ (Drexler et al., 2004). After correct data filtering this is not an issue anymore.

The BREB vs. EC was investigated by Rana and Katerji (1996) at the field of a sweet sorghum. They measured LE by four different methods: the EC, the BREB, aerodynamic simplified, and floating lysimeter. On a daily scale the LE_{EC} was 102% of Bowen ratio *LE* contrary to our results.

Evaluation of the surface renewal (SR) method to estimate latent heat flux over wheat was performed by Zapata and Martínez-Cobb in 2002. They compared LE_{SR} with lysimetry measurements and found a tendency of the SR method to underestimate lysimetry. The authors explained the discrepancy by difference in source areas and highlighted the need of accurate weighing factor "α" for the SR method. Once determined, this calibration factor is unlikely to change unless there are significant changes in the vegetation canopy (Snyder et al., 1996; Spano et al., 1997, 2000) that is why "α" for a particular canopy can be used regardless of the weather conditions (Drexler et al., 2004). In our case, the sonic anemometer was used for the calibration period. For the future, we are planning to use alternative calculations that would potentially reduce the need of calibration by sonic anemometer (pers. comm. Fischer 2016).

6.5 Boundary layer vs. surface layer scintillometer

The need to measure fluxes (sensible and latent heat) at larger scales (Green et al., 2001, Hoedjes et al., 2007; Kleissl et al., 2008) can be successfully met by the use of scintillometry. The boundary layer scintillometer (BLS) has a great potential for validation of models based on satellite images – surface fluxes at grid scale. The BLS is often used to measure energy fluxes above agricultural land (Anandakumar, 1999; Tang et al., 2011; Liu et al., 2013) but also heterogeneous surfaces (Beyrich et al., 2002; Meijninger et al., 2002a,b; Ezzahar et al., 2007). However, surface layer scintillometer (SLS), sometimes referred to as displaced dual beam or laser scintillometer, is also a useful tool to measure evapotranspiration (Savage, 2009), surface fluxes in general, or momentum and other scalars (Van Kesteren, et al., 2013a,b).

In our study, sensible heat flux densities measured by the BLS and SLS showed very good agreement although we were not measuring at the same height. Therefore, it can be argued that for our conditions – fairly homogeneous flat field with sufficient fetch, and appropriate measurement height, the SLS offers comparable results than BLS. What is more, SLS provides adequate results with less demanding field construction and easier set up. On the top of it SLS offers direct calculation of the friction velocity which is not included in BLS calculation. On the other hand, BLS provides the option of much larger footprint.

6.6 Reference and actual evapotranspiration

There are many approaches of calculating the reference evapotranspiration (ETo). Although this concept is relatively old and actual ET can be sometimes even higher then ETo it is still often used in practical calculations or modelling. In our case actual ET never exceeded ETo pointing out drier conditions or insufficient soil water content. We compared two attitudes: the Priestley-Taylor (PT), and the Penman-Monteith (PM) method. Both methods gave very similar results in total (sum for the measurement season) however, PM was slightly higher. This result corresponds to study of Matejka and Hurtalová (2005) who compared different methods of ETo estimation. The Penman-Monteith fitted better to ET_{EC} during all four measurement periods. Pauwels and Samson (2006) compared the PM

and PT methods for the monthly averages above a wet sloping grassland. Their study showed higher latent heat flux for the PT than PM confirming our results.

The cumulative value of actual ET at our site during the experiment was 58.9 % of the ETo suggesting dry conditions. In other words, Kc of the winter wheat for studied period was 0.59. It should be pointed out that this value corresponds to 3 months of the season only, moreover, from July to September the ET is reduced due to maturity of the crop plus we included also the bare soil after the harvest, which explains relatively low value of Kc. An average seasonal Kc for winter wheat in a semi-arid region of northwest China was 0.92 with min and max values 0.42 and 1.33, respectively (Kang et al., 2003). The average crop coefficient during the whole growth period was 0.93 for winter wheat (Liu et al., 2002) with min and max monthly values 0.43 and 1.42, respectively.

The sum of precipitation reached 57.3 % of measured ET_{EC}. Burba and Verma (2005) found that ET reached 55–61 % of annual precipitation within years 1997–1999 at the wheat site in north-central Oklahoma indicating similar conditions to our experiment.

Two aspects should be mentioned here. Firstly, the eddy covariance method often underestimated ET compared to other methods especially scintillometry. In general, it could be stated that using different method would increase sum of actual ET for the measurement period. Secondly, the SCW is substantial for the magnitude of ET. It was not zero at the beginning of studied period. The SWC present in soil before 1. 7. 2015 was not included in calculations and thus the difference between precipitation and actual ET should be seen just as an informative value.

6.7 Homogeneity of the field

There are various approaches for assessment of the field heterogeneity. In our study we used a combination of remote sensing and periodical field measurements. From the remote sensing data, it is obvious that within field homogeneity was high (Fig 44-45). Similarly, Hoedjes et al. (2007) studied the degree of heterogeneity within the experimental area using thermal infrared imagery. We used thermal image obtained during the plane campaign to get an overall idea about field surface temperature homogeneity and in more detail about the transect of the large aperture scintillometer (Fig 43 and Fig 45). Moreover, we also used the NDVI of the whole field and transect profile (Fig 44 and Fig 46). From these images it is apparent that within field heterogeneity is quite high when comparing contrasting surfaces (green wheat vs. tramlines) otherwise it is homogeneous.

The plane campaign took place during the nice sunny day which is noticeable from the shape of the net radiation curve in Fig 47. Both methods (BLS, BREB) shown very good agreement at the time of overflight. Also the surface temperature measured by the automatic weather station compared to the thermal image was accurate.

6.7.1 Leaf area index

Variability of the LAI was much more pronounced in 2014 when there was oil-seed rape in the field. Based on this variability the measurement spots were chosen and in 2015 the regular reading of LAI and crop height was done at the same spots. However, in 2015 winter wheat was growing

uniformly across the field which is evident from data. The difference between measurement spots was not so evident as in 2014 and moreover the homogeneity was also captured in the airborne pictures during the plane campaign.

6.7.2 Soil water content

Soil moisture is an important factor influencing partitioning of net radiation between sensible and latent heat flux (Hupet and Vanclooster, 2002). Variability of surface soil moisture is high in space and time. Remote sensing is an effective tool for mapping surface moisture content of large areas however, the variability within a pixel-size area stays unrevealed (Famiglietti et al., 1999). This variability must be better understood in order to assess its influence on resulting energy fluxes. Soil moisture variability within an agricultural field was studied by Hupet and Vanclooster (2002) and their results showed that the spatial heterogeneity of the vegetation and subsequently its evapotranspiration has a non-negligible effect on the soil moisture variability for the superficial layers. They indicated a negative correlation between mean soil moisture and the spatial variability, and thus suggested more intensive sampling for the drier conditions. Likewise, Famiglietti et al. (1999) confirmed a clear decrease of relative variability with increasing moisture content. As they explain the observed decrease is largely controlled by increasing mean moisture content rather than decreasing standard deviation, since the range of the observed mean moisture content during their experiment was nearly 6 times greater than the range of the standard deviation. Fischer et al. (2010) conducted an experiment studying soil moisture dynamics within a poplar plantation and they also observed the highest spatial variability of the soil water content during the driest period of the survey.

We used three TDR sensors placed in different depths located in the middle of the experimental field. The TDRs were not calibrated via gravimetric sampling although we did the sampling at the time of their installation. Therefore, the TDR should be perceived as an indicator of the seasonal course of the soil moisture in three depths. At the same time regular reading by PR2 probe was carried out and results are presented in section 5.6.2 Soil water content. The noticeable discrepancy between these two methods could be explained first of all, by heterogeneity of the field. The access tubes for PR2 measurements were located deliberately in the contrasting locations (based on NDVI satellite image of the oil-seed rape field in 2014) and thus final average is influenced by the variability of chosen measurement spots. Secondly, access tubes are prone to errors when not installed properly (air bubble between tube and soil). Due to the fact that our experimental locality is a regular farm we have to install and remove tubes every season which could decrease adhesiveness between soil and tube, N.B. data directly after the installation were not used. Lastly, in our experiment we used maximum of 12 PR2 measurements (access tubes) which may be considered very low number concerning the size of the field (26 ha).

6.8 Implications

This section discusses the differences between methods from the economic perspective, user friendliness, installation and maintenance issues, and the post processing of the measured data.

Information were taken either from the literature especially from the review by Drexler et al. (2004), comparative study carried out by Rana and Katerji (2000), and report on evapotranspiration by Allen et al. (2011), or from own field work experience.

The eddy covariance (EC) method is relatively widely used method (FLUXNET, ChinaFLUX). It is the only direct method to derive latent heat flux density (*LE*) and sensible heat flux density (*H*) individually (Rana and Katerji, 2000). The EC offers the possibility of independent validation through energy balance closure (*LE* can be compared with *Rn–G–H*) (Drexler et al., 2004). However, generally the closure is not often reached and disclosure between 10 and 20 % is not an exception. More detail on EBC is in section 6.1 Energy balance closure problem.

This method requires implementation of expensive and fragile instrumentation (Drexler et al., 2004; Allen et al., 2011) and relatively complicated data postprocessing which includes the series of corrections, e.g. for instrument separation, frequency response, coordinate rotation and to account for the type of hygrometer, sonic temperature correction, and correction for pathlength averaging, sensor separation and high frequency spectral losses (Allen et al., 2011). That is why, EC depends on considerable expertise and personnel who are well-trained in electronics, turbulent theory, and biophysics (Drexler et al., 2004; Allen et al., 2011). However, EC is popular and widely used technique for its relatively easy set up, and the ability to co-measure *H*, *LE* and CO_2 fluxes (Allen et al., 2011).

Scintillometry is suitable for deriving an area averaged fluxes over larger areas, as the path length between transmitter and receiver of scintillometer can reach from hundreds of meters up to several km. For estimates of ET over large areas the large aperture scintillometer has been used with some success in variable environmental conditions since the 1990s (Rambikur-Chávez, 2012). Moreover, the scintillometry has already proven to be a reliable method for determining the spatially averaged flux over heterogeneous surfaces (Meijninger et al., 2002a,b; Beyrich et al., 2006). This is the most significant advantage compared to point measurement techniques, e.g. the EC, the Bowen ratio energy balance (BREB) method, the surface renewal (SR) method. The operation and maintenance are relatively simple (Allen et al., 2011). The type of scintillometer makes a difference (SLS is more difficult to align but does not require towers and has lower energy demand).

There are some methodological issues that can be seen as disadvantage of the scintillometry, e.g. ET is derived as a residual of the energy balance (*Rn−G−H*). That is why, spatially representative *Rn* and *G* are required and any biases in the Rn and G measurements will propagate an error to ET estimate (especially in heterogeneous and sparse vegetation systems). Moreover, scintillometer measurements do require assumptions related to Monin–Obukhov stability functions (Allen et al., 2011) this must be ensured by sufficient fetch and measurement height. Another drawback is that scintillometry derives only a magnitude of *H* and the direction of the flux must be determined by other means (e.g. stability of the atmosphere estimated from temperature gradient). Further, friction velocity has to be measured independently if BLS is lower than free convection layer (SLS is able to determine friction velocity within basic calculations). Moreover, the high cost of equipment and requirement of trained personnel able to perform post-processing and data handling is required.

Savage et al. (2010) compared the EC, SLS and the BREB method to estimate evapotranspiration of grassland. They pointed out a fact that all three methods are practically inappropriate under worsening meteorological conditions, i.e. they are affected by mist, dew, rainfall and other events affecting the complete transmission of either the EC sonic beam or the SLS laser beam. Furthermore, the upper domes of the net radiometer is often covered with droplets of water during such conditions and during rain events, invalidating the *Rn* measurements and therefore invalidating *LE* calculated as a residual from the energy balance or the BREB (Savage et al., 2010).

The biggest advantage of the Bowen ratio energy balance (BREB) technique is its low demand in instrumentation (and thus lower cost) as it is based on the simple measurement of air temperature and vapour pressure at two heights. The result is a gradient-based flux averaged over a medium sized area (footprint) (200–100 000 m^2). This however, requires medium to large fetch which can be seen as a drawback. Moreover, there are some methodological issues. First of all, high precision air temperature and RH sensors are required. The issue with small gradients above some surfaces is well known and different methodologies have been adapted in the past to overcome this problem, for example, periodical change of the sensor positions and so on. Nowadays, commercially available sensors guarantee measurement error up to 0.2 °C and 0.21 % for temperature and relative humidity, respectively. However, an error can be induced, for instance, by applying chemical aerosols to a field crops and thus sensors must be prevented from interference with fertilizers or pesticides during the field experiment. Also the error can change with time and so regular calibration is needed especially for long term experimental campaigns.

Another issue implies incorrect early morning and evening values which often have to be excluded due to failing the data quality check. Method is numerically unstable when *H* is near zero, however, this usually causes only minor problems (Allen et al., 2011a). A strict quality control is necessary to get reliable flux measurements with this method (Guo et al., 2007).

Positive aspect of the BREB method is relatively easy and straightforward post-processing of the data in contrast to scintillometry or the EC method where the processing of the data occurs in some kind of a “black box”. Moreover, the BREB is less demanding on the computer processing capacity and time. On the other hand, software like SRun (Scintec, Rottenburg, Germany) or EddyPro® (LI-COR Inc., Lincoln, NE, USA) are able to process the data in a basic mode, and when the user follows recommended setting, calculation can be done in a “user friendly way” although post processing of the raw eddy covariance data can take 3-4 days if all year is calculated. If the method is aimed for a wider use in agriculture the BREB method is relatively simple and user is able to perform the calculation without extensive expertise. Comparison of error induced by skilled or novice operator were quantified by Allen et al. (2011a) and can be found in Tab 5.

Allen et al. (2011) highlighted also that BREB is a non-destructive, direct sampling of the turbulent boundary layer with no aerodynamic data requirement, and it is able to measure ET over both potential and non-potential surfaces.

On the other hand, accuracy of ET depends substantially on the representativeness and accuracy of *Rn* and *G*, and it relies on the assumption of equal transfer coefficients for *H* and *LE*, therefore, assumes that sources for heat and vapour are horizontally and vertically similar.

The surface renewal method has several advantages, most importantly, it offers a low cost approach for obtaining multiple estimates of ET (Drexler et al., 2004). A drawback is that it must be calibrated against a sonic anemometer to account for unequal heating of air parcels below the temperature sensor height and other potential deviations from the assumptions used in formulating surface renewal theory. Once determined, the calibration factor is unlikely to change unless there are significant changes in the vegetation canopy (Paw U et al., 1995; Snyder et al., 1996; Spano et al., 1997a,b, 2000). The surface renewal method has the potential for wider use in the water balance monitoring network because of its low cost but the determining of the flux bearing scale must be solved first.

When the purpose of our comparison is to improve a network of ground based monitoring system for ET evaluation in agriculture, the price of the measurement plays a role. The goal of this study was not to make a cost-effectiveness study. But in general we can divide the methods according to expenses including the purchase price, maintenance, and repairs. The “cheapest” one is the surface renewal method, where several thermocouples and data logger allows all necessary measurements for sensible heat flux estimates, and additional net radiometer plus ground heat flux plates enable us to measure evapotranspiration. Here it should be noted that initial calibration is usually done by the eddy covariance which increases the cost of the method. Second one would be the BREB method, with more expensive sensors for T/RH measurements. The EC method and scintillometry can be considered as costlier. However, the EC does not require additional sensors as it measures *LE* and *H* directly. To obtain latent heat flux by scintillometry we need sensors to measure other energy balance components. Moreover, if the BLS is in use we also need to measure friction velocity independently (e.g. the EC), while the SLS can compute it itself.

Last but not least, installation, maintenance and operation during the field campaign should be mentioned. The most demanding method in terms of installation is by our experience scintillometry. The BLS needs to be deployed higher above the canopy as the transmitter and receiver need to be several hundred meters apart and must reach blending height. This requires installation of towers or scaffolding but the alignment itself is relatively simpler that alignment of the SLS. On the top of it, laser can be harmful to human eye that is why more caution is necessary with SLS. Point measurements like the EC, the surface renewal or the BREB method are less demanding during the installation and operation.

To sum up, there is no ideal method as there is no ideal field to measure in a real world. All of the listed approaches have their highlights and disadvantages. Having the possibility to work with such variety of systems definitely brings us benefits. Because all individual methods have strengths and weaknesses, it seems prudent to use at least two or more measurement and estimation methods and compare the results (Drexler et al., 2004).

7 CONCLUSIONS

The objective of this thesis was to present the study of evapotranspiration (ET). Several methods to determine ET were considered and theory behind these methods was presented in section 2.4 Theory of measurement techniques. Throughout the years 2013 and 2014 appropriate locations for field experiments were selected followed by installation and data acquisition for the whole season 2015. These data were than analysed and used to assess the methods and relate them. Based on the comparison of four methods during the field experiment in Polkovice (the Czech Republic) on a wheat field under different meteorological conditions we are able to answer the questions asked in the section Objectives of the thesis. Section Conclusions is therefore divided into three parts each of which answers one research question.

(i) Which method is the most suitable for measuring evapotranspiration in our field conditions based on the comparison of the scintillometry, the eddy covariance technique, the Bowen ratio energy balance method, and the surface renewal method during the experimental study carried out in Polkovice agricultural site?

Based on the comparison presented in the Results section of the thesis we can conclude that all methods showed reasonable estimates of the evapotranspiration. Agreement between various methods was the highest during the first and the last period of measurement when precipitation and the soil water content was higher than in other two periods. Therefore, the first general conclusion can be that during wet conditions methods agreed well. This fact highlights the need to find apropriate method for drier periods when we are trying to quantify ET for the purposes of agricultural drought monitoring across the country.

The eddy covariance (EC) technique is widely considered as a standard method to derive ET. In our experiment the EC tended to underestimate other methods probably due to lack of energy balance closure. The Bowen ratio energy balance method reached the best agreeement with the EC method especially during the first measurement period. Later discrepancies were larger due to sensor shifts and inaccurate measurement of the air temperature and relative humidity gradients. Both scintillometers showed very consistent results during entire experiment. The surface renewal method also agreed well with EC during weter periods, however, it needs to be further tested for wider use.

(ii) What are the suggestions for improving the network of ground based measurements for assessment of evapotranspiration in the Czech Republic and Austria? Taking into account installation and operation issues, maintenance requirements, cost, applicability for field measurements, and reliability which methods should be further implemented or avoided in order to increase our effectivity?

We were looking for the method to measure ET which would be: reliable, cheap, labour extensive, easy to maintain, applicable in different conditions, good for long term measurements, and

with large footprint – applicable for validation of remote sensing data. All of the methods, of course, have benefits and drawbacks. There is no one ideal method.

Bearing in mind advantages and disadvantages of all methods we would further recommend to use EC open path at our localities with sufficient footprint because it has proven reliability and lower demand on field work. We would also encourage the experiments with SR method because of the large potential as it is very low-cost method with interesting results. Further, scintillometers has proven to be very good at representing large areas so heterogeneous sites with larger measuring paths should be another logical step to expand our network. Last but not least, the BREB method is traditionally reliable and low-cost method. It is worth to continue with this method because it showed good agreement with the EC however, there is the condition of ensuring more reliable sensors for T and RH gradient measurements.

(iii) What is the influence of the field heterogeneity on the results of energy fluxes and which of the methods represents the area of the potential grid size the best? Which method would be the most suitable for validation of models based on satellite images?

Our experimental field in Polkovice was fairly homogeneous during measurements in 2015. Thus it was very suitable for comparison of different methods. The homogeneity of the field was assessed based on both *in situ* measurements of LAI and soil water content across the field and airborne pictures produced by either satellites (Landsat, Modis) or during the one-day plane campaign. However, even relatively small discrepancies such as field tramlines were emphasized when the field was dry. In such cases, the advantage of scintillometry is generally larger footprint and aggregated value of sensible heat flux for larger area. The recommendation for validation of models based on remote sensing would then be scintillometry. Last note should however be, that practically it is always beneficial to run several methods simultaneously for long term observations in terms of the future possibilities of mutual verification, validation or gap-filling.

REFERENCES

Allen, S.J., 1990. Measurement and estimation of evaporation from soil under sparse barley crops in northern Syria. Agricultural and Forest Meteorology, 49: 291–309.

Allen, R.G., Pereira, L.S., Raes, D. and Smith, M., 1998. FAO Irrigation and Drainage Paper No. 56 Crop evapotranpiration.

Allen, R.G. et al., 2006. A recommendation on standardized surface resistance for hourly calculation of reference ETo by the FAO56 Penman-Monteith method. Agricultural Water Management, 81(1–2): 1–22.

Allen, R.G., Pereira, L.S., Howell, T.A. and Jensen, M.E., 2011a. Evapotranspiration information reporting: I. Factors governing measurement accuracy. Agricultural Water Management, 98(6): 899–920.

Allen, R.G., Pereira, L.S., Howell, T.A. and Jensen, M.E., 2011b. Evapotranspiration information reporting: II. Recommended documentation. Agricultural Water Management, 98(6): 921–929.

Anandakumar, K., 1999. Sensible heat flux over a wheat canopy: optical scintillometer measurements and surface renewal analysis estimations. Agricultural and Forest Meteorology, 96(1–3): 145–156.

Andreas, E.L., 1988. Estimating C over snow and sea ice from meteorological datan 2. Journal of the Optical Society of America, 5(4): 481–495.

Andreas, E.L., 1989. Two-wavelength method of measuring path-averaged turbulent surface heat fluxes. Journal of Atmospheric and Oceanic Technology, 6: 280–292.

Aubinet, M., 2008. Eddy covariance CO2 flux measurements in nocturnal conditions: An analysis of the problem. Ecological Applications, 18(6): 1368–1378.

Aubinet, M., Vesala, T. and Papale, D., 2012. Eddy Covariance - A Practical Guide to Measurement and Data Analysis.

Barr, A.G., King, K.M., Gillespie, T.J., Den Hartog, G. and Neumann, H.H., 1994. A comparison of bowen ratio and eddy correlation sensible and latent heat flux measurements above deciduous forest. Boundary-Layer Meteorology, 71(1): 21–41.

Baldocchi, D.D., 2003. Assessing the eddy covariance technique for evaluating carbon dioxide exchange rates of ecosystems: past, present and future. Global Change Biology, 9: 479–492.

Baldocchi, D., Falge, E., Gu, L. and Olson, R., 2001. FLUXNET: A new tool to study the temporal and spatial variability of ecosystem-scale carbon dioxide, water vapor, and energy flux densities. Bulletin of the American Meteorological Society, 82(11): 2415.

Beeson, R., 2006. Relationship of plant growth and actual evapotranspiration to irrigation frequency based on management allowed deficits for container nursery stock. Journal of the American society for horticultural science, 131(1): 140–148.

Beyrich, F., De Bruin, H.A.R., Meijninger, W.M.L., Schipper, J.W. and Lohse, H., 2002. Results from one-year continuous operation of a large aperture scintillometer over a heterogeneous land surface. Boundary-Layer Meteorology, 105(1): 85–97.

Beyrich, F. and Mengelkamp, H.-T., 2006. Evaporation over a Heterogeneous Land Surface: EVA_GRIPS and the LITFASS-2003 Experiment - An Overview. Boundary-Layer Meteorology, 121(1): 5–32.

Beyrich, F. et al., 2006. Area-averaged surface fluxes over the LITFASS region based on eddy-covariance measurements. Boundary-Layer Meteorology, 121(1): 33–65.

Beyrich, F. et al., 2012. Towards a validation of scintillometer measurements: the LITFASS-2009 experiment. Boundary-Layer Meteorology, 144(1): 83–112.

Bosveld, F.C. and Beljaars, A.C.M., 2001. The impact of sampling rate on eddy-covariance flux estimates. Agricultural and Forest Meteorology, 109(1): 39–45.

Bowen, I.S., 1926. The ratio of heat losses by conduction and by evaporation from any water surface. Physical Reviiew, 27: 779–787.

Brutsaert, W., 1982. Evaporation into the Atmosphere. Theory, History, and Applications; Dordrecht: Holland, D. Reidel Co.

Burba, G., 2013. Eddy covariance method for scientific, industrial, agricultural and regulatory applications: A field book on measuring ecosystem gas exchange and areal emission rates. LI-Cor Biosciences.

Burba, G.G. and Verma, S.B., 2005. Seasonal and interannual variability in evapotranspiration of native tallgrass prairie and cultivated wheat ecosystems. Agricultural and Forest Meteorology, 135(1–4): 190–201.

Burman, R. and Pochop, L.O., 1994. Evaporation, evapotranspiration and climatic data. Elsevier, Amsterdam, 278 pp.

Castellvi, F., 2004. Combining surface renewal analysis and similarity theory: a new approach for estimating sensible heat flux. Water Resources Research, 40(5).

Castellví, F., Snyder, R.L. and Baldocchi, D.D., 2008. Surface energy-balance closure over rangeland grass using the eddy covariance method and surface renewal analysis. Agricultural and Forest Meteorology, 148(6–7): 1147–1160.

Chahal, G.B.S., Sood, A., Jalota, S.K., Choudhury, B.U. and Sharma, P.K., 2007. Yield, evapotranspiration and water productivity of rice (Oryza sativa L.)–wheat (Triticum aestivum L.) system in Punjab (India) as influenced by transplanting date of rice and weather parameters. Agricultural Water Management, 88(1–3): 14–22.

Cooper, P., Gregory, P., Tully, D. and Harris, H., 1987. Improving water use efficiency of annual crops in the rainfed farming systems of West Asia and North Africa. Experimental Agriculture, 23(02): 113–158.

De Bruin, H.A.R., 2002. Renesance of scintillometry. In: A.M. Society (Editor), 15th Conference on Boundary Layer and Turbulence, Wageningen, The Netherlands.

De Bruin, H.A., 2009. Time to think: Reflections of a pre-pensioned scintillometer researcher. Bulletin of the American Meteorological Society, 90(5): ES17–ES26.

De Bruin, H.A.R., Van den Hurk, B. and Kohsiek, W., 1995. The scintillation method tested over a dry vineyard area. Boundary-Layer Meteorology, 76(1–2): 25–40.

Drexler, J.Z., Snyder, R.L., Spano, D., Paw, U. and Tha, K., 2004. A review of models and micrometeorological methods used to estimate wetland evapotranspiration. Hydrological Processes, 18(11): 2071–2101.

Dutta, B., Smith, W.N., Grant, B.B., Pattey, E., Desjardins, R.L., and Li, C., 2016. Model development in DNDC for the prediction of evapotranspiration and water use in temperate field cropping systems. Environmental Modelling & Software, 80: 9–25.

ESA, 2004. Terrestrial and atmospheric components of the water cycle. Released: 10.10.2004. Online: http://www.esa.int/spaceinimages/Images/2004/10/Terrestrial_and_atmospheric_components_of_the_water_cycle.

Ezzahar, J., Chehbouni, A., Hoedjes, J.C.B. and Chehbouni, A., 2007. On the application of scintillometry over heterogeneous grids. Journal of Hydrology, 334(3–4): 493–501.

Famiglietti, J. et al., 1999. Ground- based investigation of soil moisture variability within remote sensing footprints during the Southern Great Plains 1997 (SGP97) Hydrology Experiment. Water Resources Research, 35(6): 1839–1851.

Finnigan, J., 2008. An introduction to flux measurements in difficult conditions. Ecological Applications, 18(6): 1340–1350.

Fischer, M., 2012. Water balance of short rotation coppice., Ph.D. Thesis, Mendel University, Brno, Czech Republic, 261 pp.

Fischer, M., Trnka, M., Kucera, J. and Zalud, Z., 2010. Soil water availability in a short rotation poplar coppice (Populus nigra× P. maximowiczii) in Czech-Moravian Highlands. Folia Oecologica, 37(1): 23.

Foken, T., 2006. 50 Years of the Monin–Obukhov Similarity Theory. Boundary-Layer Meteorology, 119(3): 431–447.

Foken, T., Wimmer, F., Mauder, M., Thomas, C. and Liebethal, C., 2006. Some aspects of the energy balance closure problem. Atmospheric Chemistry and Physics, 6(12): 4395–4402.

Foken, T., 2008a. Micrometeorology. Springer-Verlag Berlin Heidelberg, Berlin, Germany, 306 pp.

Foken, T., 2008b. The energy balance closure problem: An overview. Ecological Applications, 18(6): 1351–1367.

Foken, T., Göockede, M., Mauder, M., Mahrt, L., Amiro, B., and Munger, W., 2004. Post-field data quality control, Handbook of micrometeorology. Springer, pp. 181–208.

Garratt, J.R., 1992. The atmospheric boundary layer. Cambridge University Press, Cambridge, UK, 316 pp.

Green, A.E., Astill, M.S., McAneney, K.J. and Nieveen, J.P., 2001. Path-averaged surface fluxes determined from infrared and microwave scintillometers. Agricultural and Forest Meteorology, 109(3): 233–247.

Guo, X. et al., 2007. Quality control and flux gap filling strategy for Bowen ratio method: revisiting the Priestley–Taylor evaporation model. Environmental Fluid Mechanics, 7(5): 421–437.

Haghighi, E. and Or, D., 2015. Linking evaporative fluxes from bare soil across surface viscous sublayer with the Monin–Obukhov atmospheric flux-profile estimates. Journal of Hydrology, 525: 684–693.

Hartogensis, O.K., De Bruin, H.A.R. and Van de Wiel, B.J.H., 2002. Displaced-beam small aperture scintillometer test. Part II: CASES-99 stable boundary-layer experiment. Boundary-Layer Meteorology, 105(1): 149–176.

Heilman, J.L. and Brittin, C.L., 1989. Fetch requirements for bowen ratio measurements of latent and sensible heat fluxes. Agricultural and Forest Meteorology, 44(3–4): 261–273.

Heitman, J., Horton, R., Sauer, T., Ren, T. and Xiao, X., 2010. Latent heat in soil heat flux measurements. Agricultural and Forest Meteorology, 150(7): 1147–1153.

Heusinkveld, B., Jacobs, A., Holtslag, A. and Berkowicz, S., 2004. Surface energy balance closure in an arid region: role of soil heat flux. Agricultural and Forest Meteorology, 122(1): 21–37.

Hill, R.J., 1982. Theory of Measuring the Path-Averaged Inner Scale of Turbulence by Spatial-Filtering of Optical Scintillation. Applied Optics, 21(7): 1201–1211.

Hill, R.J. and Lataitis, R.J., 1989. Effect of refractive dispersion on the trichromatic correlation of irradiances for atmospheric scintillation. Applied Optics, 28(19): 4121–4125.

Hoedjes, J., Chehbouni, A., Ezzahar, J., Escadafal, R. and De Bruin, H., 2007. Comparison of large aperture scintillometer and eddy covariance measurements: Can thermal infrared data be used to capture footprint-induced differences? Journal of Hydrometeorology, 8(2): 144–159.

Hupet, F. and Vanclooster, M., 2002. Intraseasonal dynamics of soil moisture variability within a small agricultural maize cropped field. Journal of Hydrology, 261(1): 86–101.

Irmak, S. and Haman, D.Z., 2003. Evapotranspiration: potential or reference. IFAS Extension, Agricultural and Biological Engineering, 343.

Kaimal, J. and Gaynor, J., 1991. Another look at sonic thermometry. Boundary-Layer Meteorology, 56(4): 401–410.

Kang, S., Gu, B., Du, T. and Zhang, J., 2003. Crop coefficient and ratio of transpiration to evapotranspiration of winter wheat and maize in a semi-humid region. Agricultural Water Management, 59(3): 239–254.

Katul, G., Hsieh, C.-I., Oren, R., Ellsworth, D. and Phillips, N., 1996. Latent and sensible heat flux predictions from a uniform pine forest using surface renewal and flux variance methods. Boundary-Layer Meteorology, 80(3): 249–282.

Kiehl, J.T. and Trenberth, K.E., 1997. Earth's Annual Global Mean Energy Budget. Bulletin of the American Meteorological Society, 78: 197–208.

Kirda, C., 2002. Deficit irrigation scheduling based on plant growth stages showing water stress tolerance. Food and Agricultural Organization of the United Nations, Deficit Irrigation Practices, Water Reports, 22: 102.

Kleissl, J., Hong, S.-H. and Hendrickx, J.M.H., 2008. New Mexico Scintillometer Network in Support of Remote Sensing, Hydrologic and Meteorological Models, AGU Fall Meeting Abstracts, pp. 6.

Kustas, W.P., Prueger, J.H., Hatfield, J.L., Ramalingam, K. and Hipps, L.E., 2000. Variability in soil heat flux from a mesquite dune site. Agricultural and Forest Meteorology, 103(3): 249–264.

Lecina, S., Martínez-Cob, A., Pérez, P., Villalobos, F. and Baselga, J., 2003. Fixed versus variable bulk canopy resistance for reference evapotranspiration estimation using the Penman–Monteith equation under semiarid conditions. Agricultural Water Management, 60(3): 181–198.

Lee, X. and Finnigan, J., 2004. Coordinate systems and flux bias error, Handbook of Micrometeorology. Springer, pp. 33–66.

Lenschow, D.H., Mann, J. and Kristensen, L., 1994. How Long Is Long Enough When Measuring Fluxes and Other Turbulence Statistics. Journal of Atmospheric and Oceanic Technology, 11(3): 661–673.

Li, Z., Yu, G., Wen,, X., Zhang, L.M., Ren, C.Y., and Fu, Y., 2005. Energy balance closure at ChinaFLUX sites. Science in China Series D-Earth Sciences, 48: 51–62.

Liebethal, C., Huwe, B. and Foken, T., 2005. Sensitivity analysis for two ground heat flux calculation approaches. Agricultural and Forest Meteorology, 132(3–4): 253–262.

Liou, Y.-A. and Kar, S.K., 2014. Evapotranspiration estimation with remote sensing and various surface energy balance algorithms—A review. Energies, 7(5): 2821–2849.

Liu, S.M., Xu, Z.W., Wang, W.Z., Jia, Z.Z., Zhu, M.J., Bai, J., and Wang, J.M., 2011. A comparison of eddy-covariance and large aperture scintillometer measurements with respect to the energy balance closure problem. Hydrology and Earth System Sciences, 15(4): 1291–1306.

Liu, S.M., Xu, Z.W., Zhu, Z.L., Jia, Z.Z. and Zhu, M.J., 2013. Measurements of evapotranspiration from eddy-covariance systems and large aperture scintillometers in the Hai River Basin, China. Journal of Hydrology, 487: 24–38.

Lu, J., Sun, G., McNulty, S.G. and Amatya, D.M., 2005. A comparison of six potential evapotranspiration methods for regional use in the southeastern United States JAWRA Journal of the American Water Resources Association, 41(3): 621–633.

Mahrt, L., 2010. Computing turbulent fluxes near the surface: Needed improvements. Agricultural and Forest Meteorology, 150(4): 501–509.

Matejka, F. and Hurtalová, T., 2005. Vzťah medzi potenciálnou a referenčnou evapotranspiráciou. In: T.L. J. Rožnovský (Editor), Evaporace a evapotranspirace, Brno, the Czech Republic.

Mayocchi, C.L. and Bristow, K.L., 1995. Soil surface heat flux: some general questions and comments on measurements. Agricultural and Forest Meteorology, 75(1): 43–50.

McGee, T.D., 1988. Principles and methods of temperature measurement. John Wiley & Sons.

Meijninger, W.M.L., 2003. Surface fluxes over natural landscapes using scintillometry, Ph.D. Thesis, Wageningen University and Research Centrum, Wageningen, The Netherlands, 164 pp.

Meijninger, W.M.L., Green, A.E., Hartogensis, O.K., Kohsiek, W., Hoedjes, J.C.B., Zuurbier, R.M., and De Bruin, H.A.R., 2002a. Determination of area-averaged water vapour fluxes with large aperture and radio wave scintillometers over a heterogeneous surface – flevoland field experiment. Boundary-Layer Meteorology, 105: 63–83.

Meijninger, W.M.L., Hartogensis, O.K., Kohsiek, W., Hoedjes, J.C.B., Zuurbier, R.M., and De Bruin, H. A. R., 2002b. Determination of area-averaged sensible heat fluxes with a large aperture scintillometer over a heterogeneous surface – Flevoland field expriment. Boundary-Layer Meteorology, 105: 37–62.

Meijninger, W., Beyrich, F., Lüdi, A., Kohsiek, W. and Bruin, H.D., 2006. Scintillometer-based turbulent fluxes of sensible and latent heat over a heterogeneous land surface–a contribution to LITFASS-2003. Boundary-Layer Meteorology, 121(1): 89–110.

Meyers, T.P. and Hollinger, S.E., 2004. An assessment of storage terms in the surface energy balance of maize and soybean. Agricultural and Forest Meteorology, 125(1–2): 105–115.

Moene, A.F., 2003a. Effects of water vapour on the structure parameter of the refractive index for near-infrared radiation. Boundary-Layer Meteorol., 107(3): 635–653.

Moene, A.F., 2003b. Effects of water vapour on the structure parameter of the refractive index for near-infrared radiation. Boundary-Layer Meteorology, 107(3): 635–653.

Moene, A.F., Meijninger, W.M.L., Hartogensis, O.K., Kohsiek, W. and De Bruin, H.A.R., 2004. A review of the relationships describing the signal of a Large Aperture Scintillometer, Lsg Meteorologie en luchtkwaliteit, Wageningen.

Molden, D. et al., 2010. Improving agricultural water productivity: Between optimism and caution. Agricultural Water Management, 97(4): 528–535.

Monteith, J.L., 1965. Evaporation and environment. Symposia of the Society for Experimental Biology, 19: 205–234.

Moore, C.J., 1986. Frequency response corrections for eddy correlation systems. Boundary-Layer Meteorology, 37(1): 17–35.

Možný, M., Trnka, M., Žalud, Z., Hlavinka, P., Nekovar, J., Potop, V., Virag, M., 2012. Use of a soil moisture network for drought monitoring in the Czech Republic. Theoretical and Applied Climatology, 107(1-2): 99-111.

Novák, V., 2012. Evapotranspiration in the Soil-Plant-Atmosphere System. Springer, Netherlands.

Oke, T., 1987. Boundary layer climates. Methuen, London.

Ortega-Farias, S.O., Cuenca, R.H. and Ek, M., 1996. Daytime variation of sensible heat flux estimated by the bulk aerodynamic method over a grass canopy. Agricultural and Forest Meteorology, 81(1): 131–143.

Pauwels, V.R. and Samson, R., 2006. Comparison of different methods to measure and model actual evapotranspiration rates for a wet sloping grassland. Agricultural Water Management, 82(1): 1–24.

Pauwels, V.R., Timmermans, W., and Loew, A., 2008. Comparison of the estimated water and energy budgets of a large winter wheat field during AgriSAR 2006 by multiple sensors and models. Journal of Hydrology, 349(3): 425–440.

Paw U, K.T., Qui, J., Su, H.-B. and Watanabe, T., 1995. Surface renewal analysis: a new method to obtain scalar fluxes. Agricultural and Forest Meteorology, 74(3): 119–119.

Paw U, K.T., Snyder, R.L., Spano, D., Su, H., Hatfield, J.L., Baker, J.M., 2005. Surface renewal estimates of scalar exchange. Agronomy, 47: 455.

Peacock, C.E. and Hess, T.M., 2004. Estimating evapotranspiration from a reed bed using the Bowen ratio energy balance method. Hydrological Processes, 18(2): 247–260.

Penman, H.L., 1948. Natural evaporation from open water, bare soil and grass, Proceedings of the Royal Society of London A: Mathematical, Physical and Engineering Sciences. The Royal Society, pp. 120–145.

Perez, P.J., Castellvi, F., Ibañez, M. and Rosell, J.I., 1999. Assessment of reliability of Bowen ratio method for partitioning fluxes. Agricultural and Forest Meteorology, 97: 141–150.

Rambikur, E. and Chávez, J.L., 2012. Scintillometry for Evapotranspiration estimation over irrigated alfalfa and dry grassland. Hydrology Days: 109–118.

Rana, G. and Katerji, N., 1996. Evapotranspiration measurement for tall plant canopies: The sweet sorghum case. Theoretical and Applied Climatology, 54(3): 187–200.

Rana, G. and Katerji, N., 2000. Measurement and estimation of actual evapotranspiration in the field under Mediterranean climate: a review. European Journal of Agronomy, 13(2): 125–153.

Rockström, J., Barron, J. and Fox, P., 2003. Water productivity in rain-fed agriculture: challenges and opportunities for smallholder farmers in drought-prone tropical agroecosystems. Water productivity in agriculture: Limits and opportunities for improvement, 85199(669): 8.

Rosa, R. and Tanny, J., 2015. Surface renewal and eddy covariance measurements of sensible and latent heat fluxes of cotton during two growing seasons. Biosystems Engineering, 136: 149–161.

Sauer, T.J. and Horton, R., 2005. Soil heat flux, Micrometeorology in Agricultural Systems. Agronomy Monograph 47: 131–154.

Savage, M.J., 2010. Field evaluation of polymer capacitive humidity sensors for Bowen ratio energy balance flux measurements. Sensors, 10(8): 7748–71.

Scintec, 2013. Scintec boundary layer scintillometer BLS450, BLS900, BLS2000 hardware manual. Scintec AG, Rottenburg, 66 pp.

Shapland, T.M., McElrone, A.J., Snyder, R.L. and Paw U, K.T., 2012a. Structure Function Analysis of Two-Scale Scalar Ramps. Part I: Theory and Modelling. Boundary-Layer Meteorology, 145(1): 5–25.

Shapland, T.M., McElrone, A.J., Snyder, R.L. and Paw U, K.T., 2012b. Structure Function Analysis of Two-Scale Scalar Ramps. Part II: Ramp Characteristics and Surface Renewal Flux Estimation. Boundary-Layer Meteorology, 145(1): 27–44.

Shapland, T.M., Snyder, R.L., Smart, D.R. and Williams, L.E., 2012c. Estimation of actual evapotranspiration in winegrape vineyards located on hillside terrain using surface renewal analysis. Irrigation Science, 30(6): 471–484.

Shapland, T.M., Snyder, R.L., Paw U, K.T. and McElrone, A.J., 2014. Thermocouple frequency response compensation leads to convergence of the surface renewal alpha calibration. Agricultural and Forest Meteorology, 189–190: 36–47.

Simmons, L.J., Wang, J., Sammis, T.W. and Miller, D.R., 2007. An evaluation of two inexpensive energy-balance techniques for measuring water use in flood-irrigated pecans (Carya illinoinensis). Agricultural Water Management, 88(1–3): 181–191.

Smith, M., 2000. The application of climatic data for planning and management of sustainable rainfed and irrigated crop production. Agricultural and Forest Meteorology, 103(1–2): 99–108.

Snyder, R.L., Spano, D. and Pawu, K.T., 1996. Surface renewal analysis for sensible and latent heat flux density. Boundary-Layer Meteorology, 77(3): 249–266.

Solignac, P.A., Brut, A., Selves, J.-L., Béteille, J.-P. and Gastellu-Etchegorry, J.-P., 2012. Attenuating the Absorption Contribution on C_n^2 Estimates with a Large-Aperture Scintillometer. Boundary-layer meteorology, 143(2): 261–283.

Spano, D., Snyder, R. and Duce, P., 1997. Surface renewal analysis for sensible heat flux density using structure functions. Agricultural and Forest Meteorology, 86(3): 259–271.

Spano, D., Snyder, R. and Duce, P., 2000. Estimating sensible and latent heat flux densities from grapevine canopies using surface renewal. Agricultural and Forest Meteorology, 104(3): 171–183.

Stull, R.B., 1988. An introduction to boundary layer meteorology. Kluwer Academic Publishers Dordrecht, The Netherlands, 666 pp.

Sun, X. et al., 2005. Determination of averaging period parameter and its effects analysis for eddy covariance measurements. Science in China, Series D: Earth Sciences, 48(SUPPL.1): 33–41.

Sun, X.-M., Zhu, Z.-L., Wen, X.-F., Yuan, G.-F., and Yu, G.-R., 2006. The impact of averaging period on eddy fluxes observed at ChinaFLUX sites. Agricultural and Forest Meteorology, 137(3): 188–193

Suvočarev, K., Shapland, T.M., Snyder, R.L. and Martínez-Cob, A., 2014. Surface renewal performance to independently estimate sensible and latent heat fluxes in heterogeneous crop surfaces. Journal of Hydrology, 509: 83–93.

Swinbank, W., 1951. The measurement of vertical transfer of heat and water vapor by eddies in the lower atmosphere. Journal of Meteorology, 8(3): 135–145.

Tang, R. et al., 2011. An intercomparison of three remote sensing-based energy balance models using Large Aperture Scintillometer measurements over a wheat–corn production region. Remote Sensing of Environment, 115(12): 3187–3202

Thiermann, V. and Grassl, H., 1992. The measurement of turbulent surface-layer fluxes by use of bichromatic scintillation. Boundary-Layer Meteorol., 58(4): 367–389.

Thom, A.S., 1975. Momentum, mass and heat exchange. In: J.L. Monteith (Editor), Vegetation and the atmosphere. Academic Press, London, UK, pp. 57–109.

Thomas, A., 2000. Spatial and temporal characteristics of potential evapotranspiration trends over China. International Journal of Climatology, 20(4): 381–396.

Thornthwaite, C.W., 1948. An approach toward a rational classification of climate. Geographical Review, 38: 55–94.

Tian, H. et al., 2010. Model estimates of net primary productivity, evapotranspiration, and water use efficiency in the terrestrial ecosystems of the southern United States during 1895–2007. Forest Ecology and Management, 259(7): 1311–1327.

Toumi, J., Er-Raki, S., Ezzahar, J., Khabba, S., Jarlan, L., Chehbouni, A., 2016. Performance assessment of AquaCrop model for estimating evapotranspiration, soil water content and grain yield of winter wheat in Tensift Al Haouz (Morocco): Application to irrigation management. Agricultural Water Management, 163: 219–235.

Twine, T.E. et al., 2000. Correcting eddy-covariance flux underestimates over a grassland. Agricultural and Forest Meteorology, 103(3): 279–300.

Van Atta, C., 1977. Effect of coherent structures on structure functions of temperature in the atmospheric boundary layer. Archiwum Mechaniki Stosowanej, 29(1): 161–171.

Van Kesteren, A.J.H., 2008. Sensible and Latent Heat Fluxes with Optical and Millimetre Wave Scintillometers, Wageningen University & Research Centre (WUR), Wageningen, 99 pp.

Van Kesteren, B., Hartogensis, O.K., Van Dinther, D., Moene, A.F., and De Bruin, H.A.R., 2013a. Measuring H2O and CO2 fluxes at field scales with scintillometry: Part I – Introduction and validation of four methods. Agricultural and Forest Meteorology, 178–179: 75–87.

Van Kesteren, B., Hartogensis, O.K., Van Dinther, D., Moene, A.F., De Bruin, H.A.R., and Holtslag, A.A.W., 2013b. Measuring H2O and CO2 fluxes at field scales with scintillometry: Part II – Validation and application of 1-min flux estimates. Agricultural and Forest Meteorology, 178–179: 88–105.

Van Kesteren, B., Beyrich, F., Hartogensis, O.K., and Van den Kroonenberg, A.C., 2014. The Effect of a New Calibration Procedure on the Measurement Accuracy of Scintec's Displaced-Beam Laser Scintillometer. Boundary-Layer Meteorology, 151(2): 257–271.

Verma, S.B., Rosenberg, N.J. and Blad, B.L., 1978. Turbulent exchange coefficients for sensible heat and water vapor under advective conditions. Journal of Applied Meteorology, 17(3): 330–338.

Verstraeten, W.W., Veroustraete, F. and Feyen, J., 2008. Assessment of evapotranspiration and soil moisture content across different scales of observation. Sensors, 8(1): 70–117.

Vickers, D., Thomas, C. and Law, B.E., 2009. Random and systematic CO2 flux sampling errors for tower measurements over forests in the convective boundary layer. Agricultural and Forest Meteorology, 149(1): 73–83.

Wallace, J.S., Jackson, N.A. and Ong, C.K., 1999. Modelling soil evaporation in an agroforestry system in Kenya. Agricultural and Forest Meteorology, 94(3–4): 189–202.

Wang, T.-i., Ochs, G.R. and Clifford, S.F., 1978. A saturation-resistant optical scintillometer to measure Cn2. Journal of the Optical Society of America, 68(3): 334–338.

Ward, H.C., Evans, J.G., Hartogensis, O.K., Moene, A.F., De Bruin, H.A.R., and Grimmond, C.S.B., 2013. A critical revision of the estimation of the latent heat flux from two-wavelength scintillometry. Quarterly Journal of the Royal Meteorological Society, 139(676): 1912–1922.

Ward, H.C., Evans, J.G., Grimmond, C.S.B. and Bradford, J., 2015a. Infrared and millimetre-wave scintillometry in the suburban environment - Part 1: Structure parameters. Atmospheric Measurement Techniques, 8(3): 1385–1405.

Ward, H., Evans, J.G. and Grimmond, C.S.B., 2015b. Infrared and millimetre-wave scintillometry in the suburban environment–Part 2: Large-area sensible and latent heat fluxes. Atmospheric Measurement Techniques, 8(3): 1407–1424.

Webb, E.K., Pearman, G.I. and Leuning, R., 1980. Correction of Flux Measurements for Density Effects Due to Heat and Water-Vapor Transfer. Quarterly Journal of the Royal Meteorological Society, 106(447): 85–100.

Wild, M. et al., 2013. The global energy balance from a surface perspective. Climate dynamics, 40(11–12): 3107–3134.

Wilson, K. et al., 2002. Energy balance closure at FLUXNET sites. Agricultural and Forest Meteorology, 113(1–4): 223–243.

Yee, M.S. et al., 2015. A comparison of optical and microwave scintillometers with eddy covariance derived surface heat fluxes. Agricultural and Forest Meteorology, 213: 226–239.

Yu, G.-R. Wen, X.-F., Sun, X.-M., Tanner, B.D., Lee, X., and Chen, J.-Y., 2006. Overview of ChinaFLUX and evaluation of its eddy covariance measurement. Agricultural and Forest Meteorology, 137(3): 125–137.

APPENDIXIES:

APPENDIX A: List of symbols and abbreviations

List of symbols

a	albedo
a	slope of a linear regression
A_T	function of temperature
A_q	function of humidity
b	intercept of a linear regression
C_p	heat capacity of air at constant pressure [J kg^{-1} K^{-1}]
C_n^2	structure parameter of refractive index fluctuation [$m^{-2/3}$]
C_q^2	structure parameter of air humidity [$m^{-2/3}$]
C_T^2	structure parameter of air temperature [$m^{-2/3}$]
d	zero plane displacement [m]
D	aperture diameter [m]
$d + s$	ramp duration
e	water vapour pressure
e_s	saturated vapour pressure
ET	evapotranspiration [mm]
ETa	actual evapotranspiration [mm]
ETc	crop evapotranspiration [mm]
ETo	reference evapotranspiration [mm]
F	first Fresnel zone [m]
f_T	similarity function for temperature and
f_ε	similarity function for the dissipation rate of turbulent kinetic energy
F_x	is the flux of quantity x [kg m^{-2} s^{-1}]
G	ground heat flux [W m^{-2}]
h	plant canopy height [m]
H	sensible heat flux [W m^{-2}]
J_1	Bessel function of the first kind
k	von Karman constant [0.41]
k	wave number of electromagnetic radiation
K_c	crop coefficient
$K_{c\ act}$	actual crop coefficient

K_{cb}	basal crop coefficient
K_e	soil water evaporation coefficient
K_H	turbulent transfer coefficient for sensible heat flux [$m^2\ s^{-1}$]
K_{LE}	turbulent transfer coefficient for latent heat flux [$m^2\ s^{-1}$]
k_λ	optical wavenumber
$K_{x,std}$	turbulence transport efficiency of the flux-variance method
L	path length between transmitter and receiver of scintillometer
L_O	Obukhov length [m]
l_0	inner scale length [mm]
l_{out}	outer scale length [mm]
LE	latent heat flux [W m^{-2}]
n	refractive index of air
q_*	turbulent scale of the specific humidity
Q	is the sum of all additional energy sources and sinks
R^2	coefficient of determination
r_l	bulk stomatal resistance of well illuminated leaf [s m^{-1}]
r_a	aerodynamic resistance
r_s	surface resistance
Rn	net radiation [W m^{-2}]
S	heat storage in the layer of air between the soil surface and the level of the measurement instrumentation plus the storage in canopy
T	temperature [K]
T	mean day temperature [°C]
T_*	temperature scale
u	horizontal wind speed [m s^{-1}]
u^*	friction velocity [m s^{-1}]
u_z	wind speed at height z [m s^{-1}]
w	vertical wind velocity component
w'	the turbulent part of the vertical wind speed [m s^{-1}]
x	distance along the path [m]
x'	the turbulent part of scalar quantity x
z	effective height [m]
z_0	roughness length [m]
z_{eff}	effective measurement height [m]
z_h	air humidity measurement height [m]

z_m	wind speed measurement height [m]
z_{oh}	roughness length for heat and vapour transfer [m]
z_{om}	roughness length for momentum transfer [m]

Symbols containing Greek letters

α	correction factor for unequal heating of the air column
β	Bowen ratio
γ	psychrometric constant
∂T	is the air temperature difference [°C]
Δ	slope of the vapour pressure curve [kPa C^{-1}]
κ	turbulent spatial wave number
λ	wavelength [nm]
λ	the latent heat of vaporization [J kg^{-1}]
θ_*,	turbulent scale of temperature
ρ	air density [kg m^{-3}]
σ	Stephan-Boltzman constant
$\sigma^2_{\ln I}$	variance of the logarithmic intensity
ϕ_n	three-dimensional spectrum of refractive index

List of abbreviations

AWS	automatic weather station
BLS	boundary layer scintillometer
BREB	Bowen Ratio/Energy Balance method
CT	Connecticut
DBSLS	dual beam small aperture scintillometer
E	east
EBC	energy balance closure
EC	eddy covariance
EMS Brno	Environmental measurement systems Brno
ET	evapotranspiration
ET_{EC}	evapotranspiration by eddy covariance
ET_{PM}	evapotranspiration according to Penman-Monteith

ET_{PT}	evapotranspiration according to Priestley-Taylor
ESA	European Space Agency
FAO	Food and Agriculture Organization
LAI	leaf area index
LAI_{active}	active leaf area index
LAS	large aperture scintillometer
LW	longwave
MOST	Monin-Obukhov similarity theory
MWS	microwave scintillometer
N	north
NE	northeast
NE	Nebrasca
NW	northwest
PET	potential evapotranspiration
PM	Penman-Monteith
PR2	soil moisture profile probe
RH	relative humidity
RMSE	root mean square error
S	south
SAS	surface layer scintillometer
SE	southeast
SHF	soil heat flux
SHFP	soil heat flux plate
SLS	surface layer scintillometer
SPU	signal processing unit
SR	surface renewal method
SW	shortwave
SWC	soil water content
TDR	time domain reflectometry
UK	United Kingdom
USA	United States of America
UT	Utah
W	West
XLAS	extra-large scintillometer

APPENDIX B: List of tables

APPENDIX C: List of figures

APPENDIX D: Case study – Dual crop coefficient

Analyses of spring barley evapotranspiration rates based on gradient measurements and dual crop coefficient model

Abstract

The yield of agricultural crops depends on water availability to a great extent. According some projections, the likelihood of stress caused by drought is increasing in future climates expected for the Central Europe. Therefore, in order to manage agro-ecosystems properly, it is necessary to know water demand of particular crops as precisely as possible. Evapotranspiration (ET) is the main part of water balance which takes the water from agro-ecosystems away. The ET consists of evaporation from the soil (E) and transpiration (T) through the stomata of plants. In this study, we investigated ET of spring barley 1-ha field (Domanínek, Czech Republic) measured by Bowen ratio/energy balance method during growing period 2013 (May 8 to July 31). Special focus was dedicated to comparison of barley ET with the reference grass ETo calculated according FAO-56 model, i.e. the determination of barley crop coefficient (K_c). This crop coefficient was subsequently separated into soil evaporation (K_e) and transpiration fraction (K_{cb}) by adjusting soil and phenological parameters of dual crop coefficient model to minimize the root mean square error between measured and modelled ET. The resulting K_{cb} of barley was 0.98 during mid-growing period and 0.05 during initial and end periods. According to FAO-56, typical values are 1.10 and 0.15 for $K_{cb\ mid}$ and $K_{cb\ end}$, respectively. Modelled and measured ET show satisfactory agreement with root mean square error equal 0.41 mm. Based on the sums of ET and E for the whole growing season of the spring barley, ET partitioning by FAO-56 dual crop coefficient model resulted in E/ET ratio being 0.24.

Keywords

Evapotranspiration, dual crop coefficient model, Bowen ratio/energy balance method, transpiration, soil evaporation, spring barley

Introduction

Water availability is a limiting factor for plants and thus has a great impact on the yields of agricultural crops. In the changing climate it becomes increasingly important to understand better how particular crops perform in water stress conditions. Moreover, it is of our interest how effectively the crops are able to use the water, since the dry periods become more frequent (Trnka *et al*. 2011, Hlavinka *et al*. 2009). The main part of the water balance that transports the water away from the agro-ecosystems is evapotranspiration (ET). Evapotranspiration comprises two parts: evaporation from the soil (E) and transpiration (T) through the stomata of plants (Kool *et al*. 2014). There is also an interception from the wet vegetation's surface but for the purposes of our study it is considered as part of E. Generally, T is considered as a desirable component of ET as this water loss is compromised by plant productivity. This is because stomata regulate both, water loss and carbon dioxide uptake, and its quantity is often described as the water-use efficiency (Larcher 2003). In contrast, E is accounted as a source of unnecessary water loss, though some positive impacts on plants like a decrease of the

air vapour pressure deficit and air cooling should be considered (Tolk 1995). Exact knowledge of the crop ET is also fundamental for both sustainable agricultural practices and irrigation scheduling. To improve water management practices and ensure high biomass productivity by avoiding stress conditions, ET partitioning is of particular importance. According to Kool *et al*. (2014) in 32 out of 52 examined studies focusing on ET partitioning, E/ET ratio was found higher than 30 %. This confirmed their hypothesis that E often constitutes a large fraction of ET and therefore deserves an independent consideration.

In general, ET can be either measured or modelled. Measurements include methods like eddy covariance, scintillometry, Bowen ratio/energy balance method (BREB), lysimeters, soil water balance measurements, etc. Measurements are necessary however, precise measurements are difficult to be maintained continuously in a wide range of representative conditions. In addition, they are costly, time-consuming and demand experienced persons. On the other hand, models can be used to estimate ET of any place and for any time if the basic input data are available but they need measurements for their calibration and validation. One of the simplest ways to model ET is based on a crop coefficient which is in fact the ratio between an actual and reference ET (Doorenbos and Pruitt 1975, Allen *et al*. 1998). Reference evapotranspiration (ETo) is the evapotranspiration rate from a reference surface, i.e. hypothetical grass crop with specific physiological and aerodynamic characteristics, not short of water and nutrients, and with no symptoms of diseases (Allen *et al*. 1998). The ETo expresses the evaporating power of the atmosphere at a specific location and time and does not consider the crop characteristics and soil factors. The ETo can be computed from weather data because the only factors affecting ETo are climatic parameters (Allen *et al*. 1998). On the other hand, actual evapotranspiration (ET) is the ET of particular crop at particular place and time which takes into account also the plant characteristics and stress caused by non-standard conditions, i.e. pests and diseases, soil fertility, water shortage or water logging etc. (Allen *et al*. 1998).

In this study, we used gradient-measurements-based BREB method (Bowen 1926, Savage 2010) to measure ET. To separate ET semi-empirical approach called FAO (Food and Agriculture Organization) dual crop coefficient model (Allen *et al*. 1998) is employed. Finally, our awareness of how the ET is split into soil evaporation and plant transpiration improves our understanding of the plants´ water use efficiency.

The goals of our study were:

1. To test the FAO-56 dual crop coefficient model against BREB measurements at 1-ha spring barley field in rain fed area of Bohemian-Moravian Highlands.
2. To use the FAO model to separate ET into transpiration and evaporation components.

Materials and methods

In presented study the data recorded during the season 2013 at an experimental field in Bystřice nad Pernštejnem (Czech Republic, 49° 31´ N, 16° 14´ E and altitude 530 m a.s.l.) were used. Experimental field was sown by spring barley (*Hordeum vulgare*) variety Bojos on 18th April 2013. It

was fertilized with 60 kg of N ha^{-1} 17th of May 2013. To gain all necessary data, an automatic weather station with BREB system was placed close to the centre of 1-ha barley field in order to maximize the distance from the field edge downwind with respect to prevailing wind direction. Since 7th of May 2013 until 31st of July air temperature and humidity were recorded at two levels above the canopy using the integrated temperature-humidity sensors EMS33R. At the beginning of the growing season they were 0.2 m and 1.2 m high. As the barley was growing the heights of the sensors were increased in order to keep the lower one always 0.1 m above the plant surface and the upper one just 1 meter above the lower sensor. At the end of the growing period of barley the sensors were in 0.9 m and 1.9 m, respectively. The net radiation (W/m^2) and soil heat flux (W/m^2) were recorded by sensors Schenk 8110 and heat flux plate HFP01. Further, precipitation was measured by rain gauge Met One 380 and wind speed and wind direction by anemometer Met One 034B. All sensors were connected to data logger RailBox V32P6 scanning at 30-s intervals and storing 10 min averages. The data were used to calculate actual evapotranspiration (ET) of the spring barley based on BREB method. Another automatic weather station using compatible sensors was placed on nearby turf grass and used for ETo calculation. Turf grass around the station is cut periodically to maintain the reference grass cover 0.05 m high. The air temperature, air humidity, and wind speed were measured in standard 2 m height. The net radiation and soil heat flux were also recorded.

The BREB method uses the measurements of the air temperature and air humidity gradients, radiation balance and the soil heat flux (Savage *et al.* 2009). In particular, the BREB method is based on the energy balance equation and the theory of turbulent diffusion (K-theory) (Savage 2010). The simplified energy balance equation neglecting the energy used in photosynthesis and energy stored in canopy can be written as follows:

$$R_n = \lambda ET + H + G \quad (1)$$

where R_n is the net radiation flux, H and λET are sensible heat and latent heat fluxes respectively, G is soil heat flux (all in W m^{-2}) (Perez *et al*. 1999).

The Bowen ratio (β) is defined as the ratio of the sensible heat flux to the latent heat flux and can be described as:

$$\beta = H / \lambda ET = \gamma \Delta T / \Delta e \quad (2)$$

where γ is the psychrometric constant (~ 0.066 kPa K^{-1} at the sea level) and ΔT and Δe are the temperature and vapour pressure differences between the two levels above surface (Bowen 1926). This equation results from application of the theory of turbulent diffusion where the exchange coefficients of heat and vapour are assumed to be equal, known as the Bowen ratio similarity principle (Bowen 1926), where the scalars are assumed to be carried by the same eddies if they have identical or very similar source and sink distributions.

Thus, it is possible to calculate the Bowen ratio by measuring air temperature (T in K) and water vapor pressure (e in kPa) at two different levels in the atmosphere. Further it allows us to calculate

λET by combining Eqs. 1 and 2 (the radiation balance and the Bowen ratio) which results in an equation (Guo *et al*. 2007):

$$\lambda ET = (Rn - G)/(1 + \beta) \quad (3)$$

To calculate reference evapotranspiration (ETo) in this study FAO Irrigation and Drainage Paper No. 56 was followed (Allen *et al.* 1998). As the reference, hypothetical surface of grassland has been adopted with standard characteristic for reference crop of 0.12 m high, albedo of 0.23 and not limited by water or nutrient and thus with a fixed surface resistance (r_c) of 50 and 200 s m^{-1} for diurnal and nocturnal periods, respectively (Allen 2003). Using these parameters, ETo was then calculated using the Penman-Monteith combination equation which can be written in the final form (Monteith 1965):

$$\lambda ET = \frac{\Delta(R_n - G) + c_p \rho_a \frac{e_{sat} - e}{r_a}}{\Delta + \gamma\left(1 + \frac{r_c}{r_a}\right)}, \quad (4)$$

where Δ (kPa K^{-1}) is the first derivation of the function e_{sat} versus *T* known as the saturation vapour pressure curve where e_{sat} is saturation vapour pressure (kPa) at the evaporating water surface, and r_a is aerodynamic resistance of reference grass cover with constant height 0.12 m (Allen *et al.* 1998). Vapour pressure (e), air temperature (T) and wind speed were measured in standard 2 m height above reference grass cover. The 30 min measured mean values were used to determine ETo half hourly and subsequently the daily sums of ETo were calculated. Subsequently, barley crop coefficient (*Kc*) was calculated as a ratio between actual evapotranspiration (*ET*) of barley and reference evapotranspiration (*ETo*). It can be expressed as follows:

$$K_c = \frac{ET}{ET_0} \quad (5)$$

Crop coefficient can be either single or dual. The single crop coefficient integrates the effect of both crop transpiration and soil evaporation (Allen *et al*. 1998). On the contrary, dual crop coefficient separates them into two coefficients: a basal crop coefficient (*Kcb*) to describe plant transpiration, and a soil water evaporation coefficient (*Ke*). Single crop coefficient Kc is replaced by:

$$K_c = K_{cb} + K_e \quad (6)$$

The purpose of the calculation should be considered when choosing the appropriate approach. The dual K_c is more complicated and more computationally intensive. It suits better research purposes, real time irrigation scheduling or detailed soil and hydrologic water balance studies while single Kc approach is easier and can be applied for basic irrigation schedules (Allen *et al*. 1998).

In this study we are using dual Kc. The actual crop ET is then calculated as:

$$ET = (K_{cb} + K_e)ETo = K_c ETo \quad (7)$$

In present study, a dual crop coefficient model FAO-56 was used according to Allen *et al.* (1998). The crop coefficients ($K_{cb\ ini,\ mid\ and\ end}$), phenological (length of the initial, development, mid and late season stages), and soil water balance parameters were determined specifically for our site. In

particular, soil water balance parameters consisted of information on the field capacity (Fc), wilting point (Twine et al.), maximum root depth (Root max), readily evaporable water from the superficial soil layer (REW), and average fraction of total available soil water (TAW) that can be depleted from the root zone before onset of reduction in ET (p). The above-mentioned parameters can be seen in Tab. I and were constrained within physical ranges reported in literature or within ±10 % to our own observations and solved iteratively to get the smallest root mean square error (RMSE) between ET measured by BREB and ET estimated by the dual crop coefficient model FAO-56.

During the growing season plant area index (PAI) of spring barley was measured periodically using ceptometer based system SunScan (Delta-T Devices ltd., UK). The PAI is the area of all plant tissue, including stems that intercept light and contribute to the measured value. Leaf Area Index (LAI), on the other hand, is one-sided green leaf area per unit ground surface area (LAI = leaf area / ground area, m^2 / m^2) (Watson 1947). The PAI is preferred to LAI in this study because not only leaves but total above ground biomass was measured. The PAI data were used to determine the fraction of soil exposed to sunlight using Beer-Lambert law (Larcher 2003). The field campaign finished before barley was harvested and so our dataset finishes 31st July 2013.

Results and discussion

The actual evapotranspiration of spring barley (ET) and reference evapotranspiration (ETo) for period between 8th of May 2013 and 31st July 2013 are shown in Fig 1a. During the whole period ET total was 229.4 mm and ETo 300.7 mm. The mean daily ET and ETo were 2.7 mm and 3.5 mm, respectively. Fig 1b shows the course of soil moisture in three depths as a consequence of precipitation during the growing season presented in Fig. 1d. During the 85 days of measurement, rain fell on 30 days which is 35 % of time. The ET that occurred on these days formed 30 % of ET of the growing season. In total 184.8 mm rain fell during the growing season, 36 % of which fell in May (67.2 mm), 51 % in June (94.6 mm) and only 23 mm in July (12 % of total precipitation).

It is obvious from the Fig. 1a that towards the end of the growing period ET of barley is declining. The values of ETo were notably higher than ET. The reason might be that the spring barley plants were experiencing some shortage of water especially in the top soil horizons. The lack of rainfall events in July shown in Fig. 1d supports this assumption. However, there is no evidence on decline of water accessibility shown by K_{cb} in Fig 3. More likely, the diminishing ET at the end of the growing period was caused by natural decrease of ET as the transpiration lessens toward yellow ripeness stage.

Fig 1b displays daily values of single crop coefficient (K_c) divided to three groups according to rainfall. There are different points distinguishing days with rain, days after rain and two or more days after rain. The K_c was calculated as a rate between actual evapotranspiration calculated using BREB approach and reference ETo (Fig 1a). Single crop coefficient integrates crop characteristics and averaged effects of evaporation from the soil (Allen *et al.* 1998). More complicated, dual K_c approach, is needed when we need daily values of K_c for specific fields of crops and for specific years. Then transpiration and evaporation coefficient (K_{cb} + K_e) must be separate.

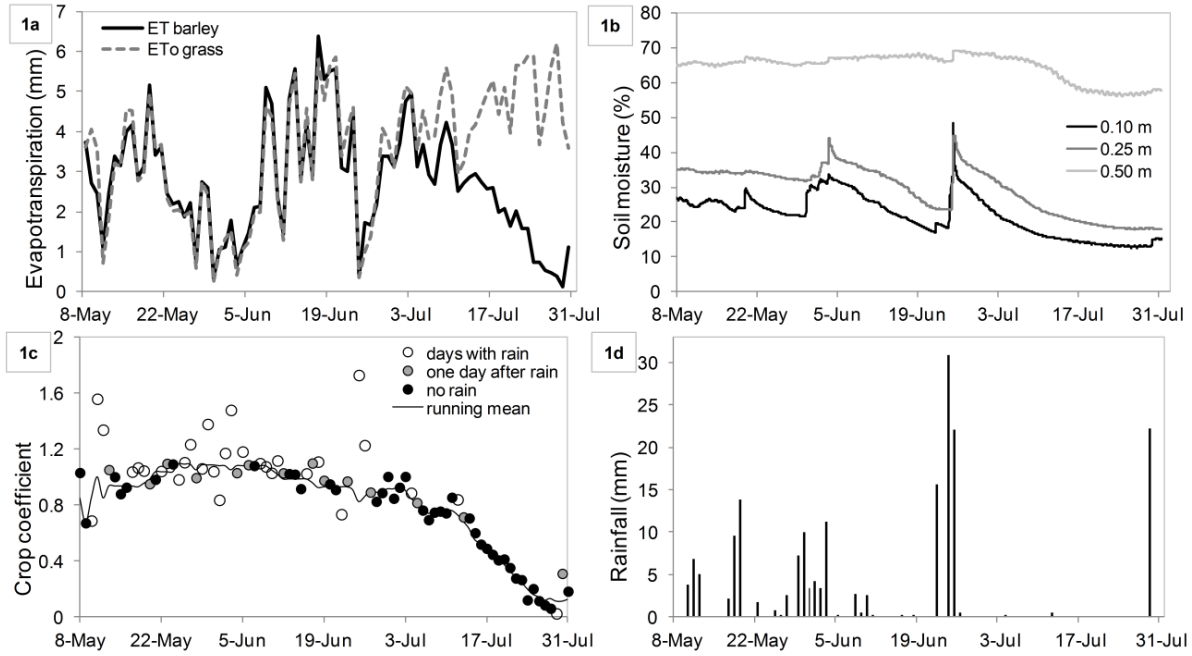

Fig 1a Daily totals of spring barley actual ET measured by BREB and reference ETo in mm in Domanínek during growing period 2013, 1b Soil moisture in Domanínek during growing period of barley in 2013 in three depths, 1c Single crop coefficient (K_c) of barley in growing period 2013 in Domanínek divided according to precipitation to 3 groups and its running mean over 7 days, 1d Precipitation totals during growing period of barley in 2013 in Domanínek

Our results show more scatters from running mean for rainy days. Higher divergence is a consequence of higher actual ET of barley after rain when intercepted water with almost zero surface resistance is evaporating intensively. From the shape of the curve of running mean it is obvious that, at the end of the period, ET of spring barley was much lower than ETo as a consequence of reduced transpiration of barley and dry weather at the end of the season.

For the purposes of this study ET was not only measured but also modelled using FAO-56 dual crop coefficient model. The seasonal course of modelled and measured ET can be seen in Fig 2 indicating very high agreement. The total ET by model equals 226.2 mm which is underestimated only by 3.2 mm compared to BREB method. Fig 3 shows the statistics of the modelled and measured ET as a result of iterative parameterization. The coefficient of determination and the slope of the regression line indicate very good fit between ET modelled by FAO-56 and ET measured using BREB method with RMSE 0.41 mm. The variability in a data set is described by the coefficient of determination R^2 equal 0.92. The parameters and crop coefficient resulting from this RMSE minimizing procedure can be seen in Tab 1.

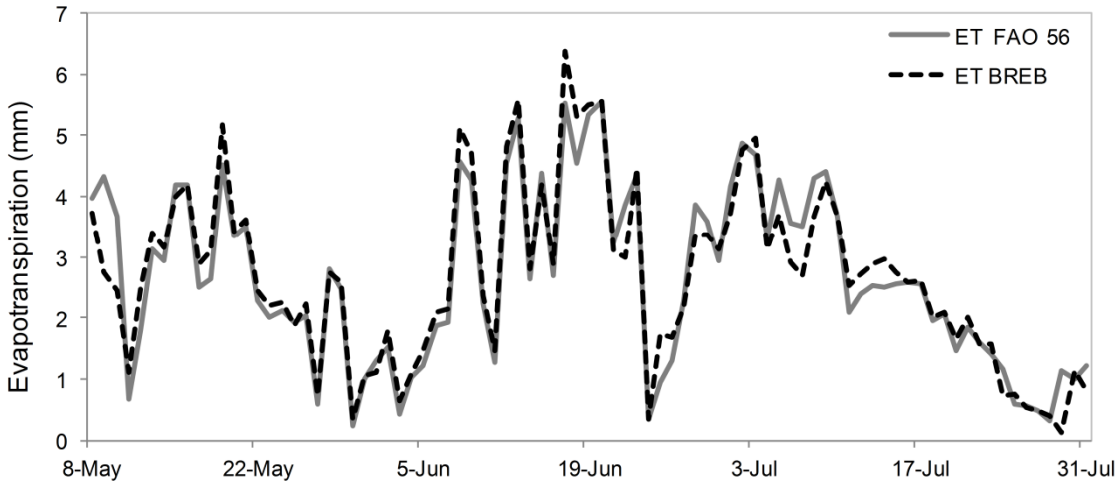

Fig 2 Seasonal course of daily evapotranspiration totals of barley measured by BREB and estimated using the FAO 56 dual crop coefficient model for growing period 2013 in Domanínek.

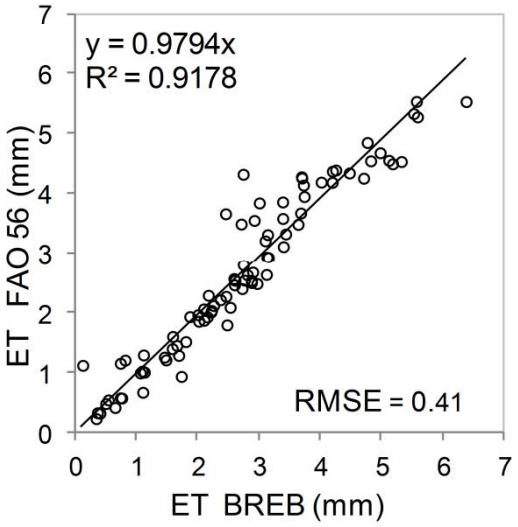

Fig 3 Scatter-plot view describing the relation between actual barley ET measured by BREB and ET modelled using FAO-56 for growing period 2013 in Domanínek with basic descriptive statistics.

Tab 1 Basal K_c and its parameters resulting from the root mean square error minimizing procedure.

Basal Kc		Crop Development Stages (days):		Computed Dates for Stages:		Evaporation parameters	
$K_{cb\ ini}$	0.05	L_{ini}	30.00	J_{Plant}	1	REW	12.81 mm
$K_{cb\ mid}$	0.98	L_{dev}	14.00	J_{Dev}	130	Root max	0.65 m
$K_{cb\ end}$	0.05	L_{mid}	42.66	J_{Mid}	144	Fc	0.36 %
		L_{late}	22.62	J_{Late}	187	Wp	0.16 %
				J_{Harv}	209	p	0.60

The dual crop coefficient can be seen in Fig 4. The basal crop coefficient describes plant transpiration and is associated with conditions of minimum soil evaporation but not water limitation for plants (Allen *et al.* 1998, Paco *et al.* 2012). The soil water evaporation coefficient describes evaporation from the soil surface. It is necessary to mention that in FAO-56, values listed for K_c represent ET under growing conditions with a high level of management and with little or no water or other ET reducing stresses and thus represent what is referred to as potential levels for crop ET (Allen *et al*. 2005). Fig 4 shows both basal crop coefficient (K_{cb}) and soil evaporation coefficient (K_e). The Ke is the difference between the two K_c lines in the picture. Fig. 5 shows PAI of spring barley recorded during the growing period. It can be seen that mid period starts when plant area index is 1.64 and it finishes when PAI is equal 3.97. K_{cb} for initial period is 0.05, K_{cb} mid is 0.98 and K_{cb} end is equal also 0.05. According to FAO-56 (Allen *et al*. 1998), the typical values for spring barley are 1.1 for $K_{cb\ mid}$ and 0.15 for $K_{cb\ ini}$ and $K_{cb\ end}$.

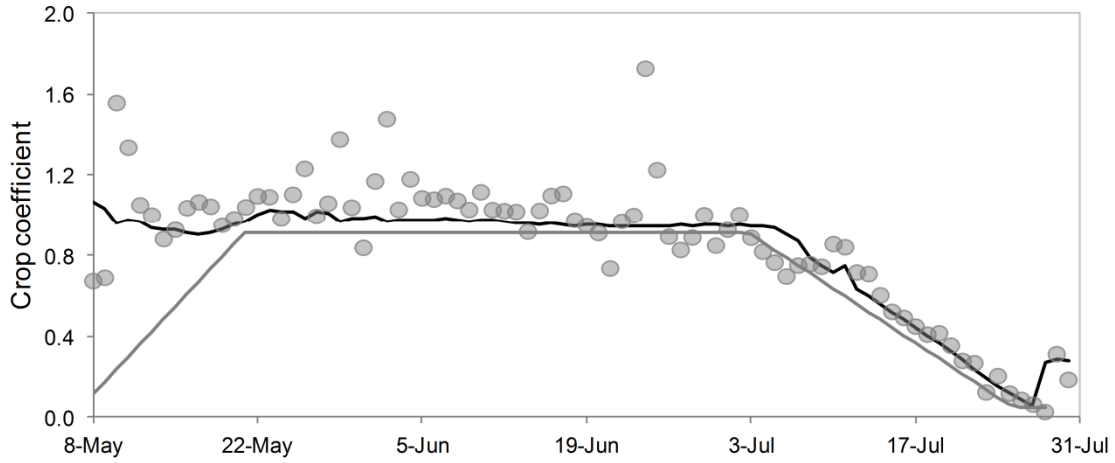

Fig 4 Basal crop coefficient (K_{cb}) (grey line) and soil evaporation coefficient (K_e) (difference between grey and black lines) compared to the actual crop coefficient (grey closed circles) as the ratio between actual ET of barley measured by BREB and reference ETo.

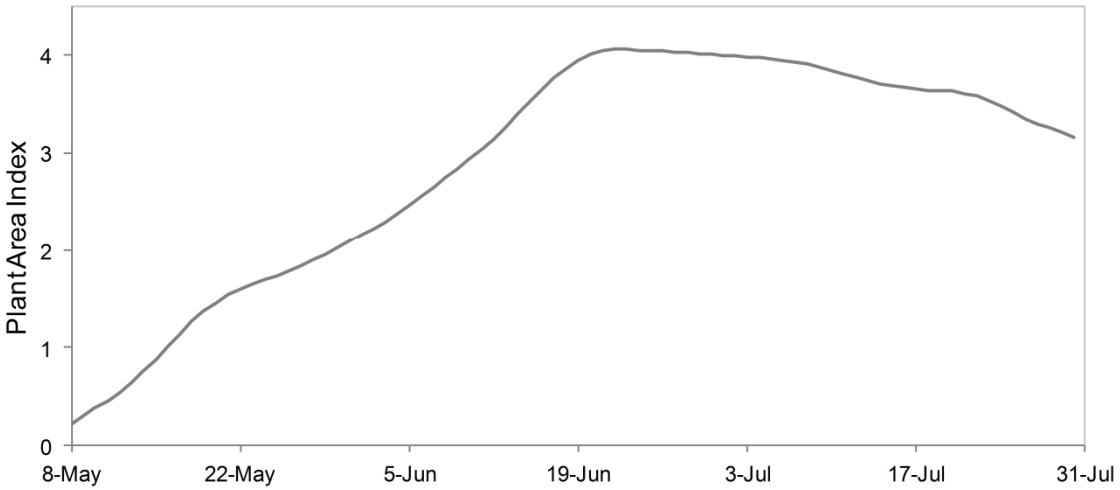

Fig 5 Plant Area Index of spring barley during growing period 2013 in Domanínek.

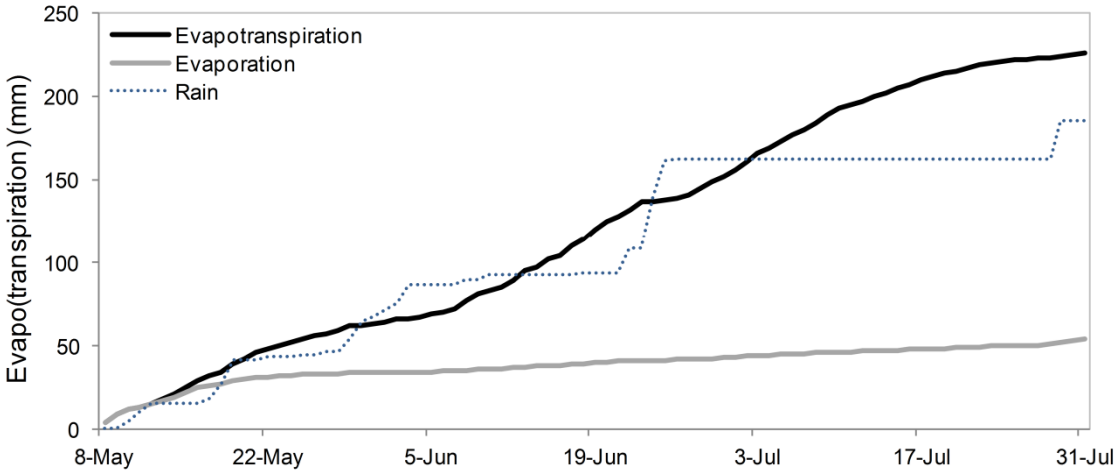

Fig 6 Cumulative evapotranspiration of barley modelled by FAO-56 for growing season 2013 in Domanínek divided to evaporation form soil (grey line) and transpiration (difference between black and grey line), and cumulative precipitation.

As a secondary product of FAO-56 dual crop coefficient model ET was split into evaporation and transpiration. Fig. 6 demonstrates how evapotranspiration is divided between evaporation and transpiration by the FAO-56 model. This fulfils the second objective of presented study. At the beginning of the growth of barley evaporation from the soil in principal equals to ET while toward the end of the growing season evaporation represents about one quarter (24 %) of cumulative ET. The total ET for the whole growing period is 226.2 mm and total E is 53.8 mm. The E/ET ratio for spring barley based on these sums is then 0.24. Compared to literature we can only use one known example of ET partitioning for the same crop. Allen (1990) used different methodology in his study. For estimating E, he used micro-lysimeters and ET was determined by soil water balance measurements using neutron probe. The result E/ET accounted for 0.67–0.77 depending on different fertiliser treatment. Difference in our findings could be explained by the different plant density. In our study spring barley sowing density was 400 seeds per square meter. As a result, we can have more than 900 tillers per square meter. In contrary, in Allen´s (1990) experiment their average final density was 200 tillers per square meter. This means that in our case more soil was covered by plants in higher rate which increased relative role of transpiration. In Allen´s experiment, more soil was uncovered and exposed to radiation, wind and vapour pressure deficit increasing soil evaporation. At the same time, fewer plants present on the site transpired less than in our experiment. Finally, we must take the climatic difference into account. Another study dealing with ET partitioning was conducted on irrigated wheat field in India (Balwinder-Singh *et al.* 2011). Depending on a treatment with or without mulch their E/ET ratio reached values between 0.29 and 0.40. In their experiment daily E was measured using mini-lysimeters, and total seasonal ET was estimated as the missing term in the water balance equation (Balwinder-Singh *et al.* 2011). Two more experiments conducted in China are closer to our results. In particular, Fan *et al.* (2013) came to result of E/ET ratio between 0.30–0.45 for their wheat

experiment depending on tillage system and irrigation treatment. Similarly, Liu *et al.* (2002) found the E/ET ratio to be 0.30 for winter wheat and maize.

Conclusions

In agriculture water is a limiting factor of the yields and in the present changing climate it is important to understand how crops deal with water shortage. Precise information about evapotranspiration is a key as it is the main losing part of the water balance. Measurement of ET on site is not feasible everywhere and that is why modelling plays its significant role. The main aim of this study was to test the FAO-56 dual crop coefficient model against BREB measurements on spring barley field in Bohemian-Moravian Highlands in 2013. Our results show robustness and reliability of the FAO-56 dual K_c model in reproducing daily dynamic of barley ET measured by BREB. Therefore, we used the model to separate ET into transpiration and evaporation components and fulfil the second goal of the study. This attitude narrows down real plant activity and separates it from soil evaporation which is considered to be a non-productive component of evapotranspiration. Our study represents the first application of FAO-56 dual crop coefficient in the Czech Republic. More investigation is needed to find robust and reliable parameters necessary to feed FAO-56 dual K_c model which may potentially provide better ET estimates compared to widely used single crop coefficient models.

Summary

In the present changing climate, it is important to understand how agricultural crops deal with water. Main focus in agro ecosystems is on evapotranspiration as it is the loosing part of water balance. In this study, measured and modelled ET of spring barley was used. Measurement took place in experimental field in Domanínek, Czech Republic in 2013. For modelling ET model FAO-56 dual crop coefficient was applied. The results show very good agreement. Moreover, FAO-56 dual K_c model was used to separate soil evaporation from the evapotranspiration. This is particularly important for deeper understanding of water use efficiency of crops. Only transpiration is considered as a wanted component of ET (it is related to plant productivity) whereas evaporation form the soil is considered as undesired water loss. Our estimation of E/ET ratio was satisfactory. However, for more robust and reliable parameters further investigation is needed.

Acknowledgements

This study was supported by the In-house Grant Agency at FA MENDELU in Brno (IP 10/2013), project InterDrought (no. CZ.1.07/2.3.00/20.0248), and by Czech program KONTAKT II project no. LH12037 “Development of models for assessment of abiotic stresses in selected bioenergy plants”.

References

ALLEN, S. J., 1990: *Measurement and estimation of evaporation from soil under sparse barley crops in Northern Syria*. Agric. For. Meteorol., 49: 291–309.

ALLEN, R. G., 2003: *Crop coefficients. Encyclopaedia of Water Science*, DOI: 10.1081/E-EWS 120010037.

ALLEN, R. G., PEREIRA, L. S., RAES, D., SMITH, M., 1998: *Crop evapotranspiration. In: Guidelines for Computing Crop Water Requirements. FAO Irrigation and Drainage Paper No. 56*, pp. 290.

ALLEN, R. G., PEREIRA, L. S., SMITH, M., RAES, D., WRIGHT, J. L., 2005: *FAO-56 dual crop coefficient method for estimating evaporation from soil and application extensions*. J. Irrig. Drain. Eng., 13: 2–13.

ALLEN, R. G., PRUITT, W. O., WRIGHT, J. L., HOWELL, T. A., VENTURA, F., SNYDER, R., ITENFISU, D., STEDUTOH, P., BERENGENA, J., YRISARRY, J. B., SMITH, M., PEREIRA, L. S., RAES, D., PERRIER, A., ALVES, I., WALTER, I., ELLIOTT, R., 2006: *A recommendation on standardized surface resistance for hourly calculation of reference ETo by the FAO56 Penman-Monteith method*. Agric. Water Manage., 81: 1–22.

BALWINDER-SINGH, EBERBACH, P. L., HUMPHREYS, E., KUKAL, S. S., 2011: *The effect of rice straw mulch on evapotranspiration, transpiration and soil evaporation of irrigated wheat in Punjab, India*. Agric. Water Manage., 98: 1847–1855.

BOWEN, I.S., 1926: *The ratio of heat losses by conduction and evaporation from any water surface*. Phys. Rev., 27: 779–787.

DOORENBOS, J. and PRUITT, W. O., 1975: *Guidelines for predicting crop water requirements, Irrigation and Drainage Paper no. 24.* FAO-ONU, Rome, Italy. 168 pp.

FAN, Z., CHAI, Q., HUANG, G., Yu, A., Huang, P., Yang, C., Tao, Z., Liu, H., 2013: *Yield and water consumption characteristics of wheat/maize intercropping with reduced tillage in an Oasis region*. Eur. J. Agron., 45: 52–58.

FISCHER, M., 2012: *Water balance of short rotation coppice*, Brno: Mendelu Brno, Faculty of Agronomy, Department of Agrosystems and Bioclimatology. Ph.D. thesis, 261 pp.

GUO, X., HONGSHENG, ZHANG, H., KANG, L., DU, J., LI, W., ZHU, Y., 2007: *Quality control and flux gap filling strategy for Bowen ratio method: revisiting the Priestley–Taylor evaporation model.* Environ. Fluid. Mech., 7: 421–437.

HILL, R.J., 1997: *Algorithms for Obtaining Atmospheric Surface-Layer Fluxes from Scintillation Measurements*. J Atmos Ocean Technol 14: 456–467.

HLAVINKA, P., TRNKA, M., SEMERÁDOVÁ, D., DUBROVSKÝ, M., ŽALUD, Z., MOŽNÝ, M., 2009: *Effect of drought on yield variability of key crops in Czech Republic.* Agric. For. Meteorol., 149: 431–442.

KOOL, D., AGAM, N., LAZAROVITCH, N., HEITMAN, J.L., SAUER, T.J., BEN-GAL, A., 2014: *A review of approaches for evapotranspiration partioning*. Agric. For. Meteorol., 184: 56–70.

LARCHER, W., 2003: *Physiological Plant Ecology*, 4th edition. Springer, Berlin, 513 pp.

LIU, CH., ZHANG, X., ZHANG, Y., 2002: *Determination of daily evaporation and evapotranspiration of winter wheat and maize by large-scale weighing lysimeter and micro-lysimeter*. Agric. For. Meteorol., 111: 109–120.

MONTEITH, J., 1965: *Evaporation and environment. 19th Symposia of the Society for Experimental Biology*, University Press, Cambridge, Vol. 19: 205–234.

PACO, T. A., FERREIRA, M. I., ROSA, R. D., PAREDES, P., RODRIGUES, G. C., CONCEIC, N., 2012: *The dual crop coefficient approach using a density factor to simulate the evapotranspiration of a peach orchard: SIMDualKc model versus eddy covariance measurements.* Irrig. Sci., 30:115–126.

SAVAGE, M. J., EVERSON, C. S., METELERKAMP, B. R., 2009: *Bowen ratio evaporation measurement in a remote montane grassland: Data integrity and fluxes*. J. Hydrol., 376: 249–260.

SAVAGE, M. J., 2010: *Field evaluation of polymer capacitive humidity sensors for Bowen ratio energy balance flux measurements.* Sensor, 10: 7748–7771. ISSN 1424–8220.

TOLK, J. A., HOWELL, T. A., STEINER, J. L., KRIEG, D. R., SCHNEIDER, A. D., 1995: *Role of transpiration suppression by evaporation of intercepted water in improving irrigation efficiency.* Irrig. Sci., 16: 89–95.

TRNKA, M., SCHAUMBERGER, A., FORMAYER, H., EITZINGER, J., HLAVINKA, P., SEMERÁDOVÁ, D., DUBROVSKÝ, M., MOŽNÝ, M., THALER, S., ŽALUD, Z., 2011: *Evaluating drought risk for permanent grasslands under present and future climate conditions.* Procedia Environ. Sci., 3: 50–57.

WATSON, D. J., 1947: *Comparative Physiological Studies on the Growth of Field Crops: I. Variation in Net Assimilation Rate and Leaf Area between Species and Varieties, and within and between Years.* Ann. Bot. 11: 41–76.

APPENDIX E: Case study – Temperature gradient measurements

The Bowen Ratio/Energy Balance method and detailed temperature profile measurements to improve data quality control

Pozníková G., Fischer M., Orság M., Trnka M., Žalud, Z.

Abstract

Water plays a key role in the functionality and sustainability of the ecosystems. In the light of the predicted climate change research should be focused on the water cycle and its individual components. The major component of the water balance which drives the water from the ecosystems is represented by the evapotranspiration (ET). One of the standard methods for measuring ET is Bowen Ratio/Energy Balance method (BREB). It is based on the assumption that the water vapour and heat are transported by identical eddies with equal efficiency. When BREB method is used we assume that the profiles of temperature and air humidity are ideally logarithmic or at least consistent. Since the BREB method is usually based on the measurements of temperature and humidity in only two heights, it is difficult to verify that this assumption is fulfilled. The eventual inconsistency of the profiles is more likely for temperature because the sensible heat flux changes its sign more often and the occurrence of negative latent heat flux during positive sensible heat flux is not physically possible. We therefore conducted a field experiment using 4 m high measurement-mast with 20 thermocouples for detailed measurement of air temperature profile above different covers, e.g. grassland, spring barley, poplar plantation. The main goal of our effort was to investigate the basic assumptions of the BREB method, i.e. the temperature profiles consistency under various weather conditions. The main goal of our effort was to investigate the basic assumptions of the BREB method, i.e. the temperature profiles consistency under various weather conditions. To be more specific, we aimed to investigate whether the situation of inflexion point in the temperature profile occurs and when.

Introduction

Water is a key component essential for all ecosystems. In agriculture, evapotranspiration (ET) deserves a special attention as it is the major loosing part of water balance. There are many different methods for deriving ET. One of the basic is called Bowen Ratio/Energy Balance method (Bowen 1926) and it is based on the assumption of logarithmic profiles of temperature and humidity in the surface layer of the atmosphere. It is described by Monin-Obukhov similarity theory (Foken 2006). In our study, we aimed to test this basic assumption with a 4 m tall measuring-mast. The main goal was to find different types of temperature profiles during the day and during the growing season of spring barley (Hordeum vulgare). We wanted to plot a typical nocturnal and diurnal stratification and situation with point of inflexion, so called “kink” (Oke, 1987). This happens when the temperature profile does not change consistently with height but creates an inflexion point which cannot be captured by standard BREB method. In situation when the point of inflexion occurs between the two measuring

sensors of one BREB system it is impossible to estimate the Bowen ratio correctly and calculate ET properly. Using the measurements carried out during the field campaign it Domanínek it was possible to find out when the inflexion point occurs. In the future, the measurement error in calculated fluxes will be quantified for the whole season and subsequently minimised. We will broaden the study to test different cover crops as well.

Materials and methods

The submitted study was conducted on the experimental field situated in Domanínek near Bystřice nad Pernštejnem in an area of the Czech-Moravian Highlands. The data used in this study were recorded during the growing season 2013. During the field experiment a 4 m high measurement-mast with 20 very fine (0.1mm), fast response thermocouples type K was used for detailed measurement of air temperature profile. The thermocouples were connected to the data logger CR1000 by Campbell Scientific coupled with thermoelement multiplexer developed and made by Ing. Wolfgang Laube from BOKU in Vienna. Measurement took place over different covers, e.g. oat, grassland, spring barley, and poplar plantation. Sampling interval was 5s and data were than averaged to 30min values for further processing. In this short paper the period of few days while the measurement took place over the spring barley field was chosen to examine the temperature profiles in detail. Nearby the measurement an automatic weather station was placed to record basic meteorological variables necessary to derive ET by BREB method (Todd et al. 2000, Savage 2010). In particular, the temperature and humidity at two heights above the canopy (0.2 m and 1.0 m) was recorded as well as net radiation (W/m2) and soil heat flux (W/m2). The temperature by thermocouples was measured in 5 s interval and stored as the average every 30 s. These detailed measurements were used to calculate average between two levels of thermocouples and its 30 min averages. Further, correlation coefficient was calculated to describe relationship between the temperature gradients and the height. Different day times were picked to show various temperature profiles and stratification of the lower atmosphere.

Results

Three days at the beginning and three days at the end of July are shown in Fig. 1 to describe green and well-watered barley with high evapotranspiration as well as mature barley with lack of water in soil at the end of growing period. The dashed red line represents the temperature gradient per 1 m height. Taking the vegetation height into account (0.7 m) the gradient was calculated as a difference between the temperature measured by thermocouple in 1.8 m and the temperature in 0.8 m. The gradient reaches the highest positive values at night when the temperature increases with height. On the contrary, the lowest values were measured around the noon on sunny days when the temperature was decreasing with height and near the surface reaches the highest values. The solid grey line shows the course of the correlation coefficient describing the linear relationship between the temperature gradients and the logarithm of the measurement height.

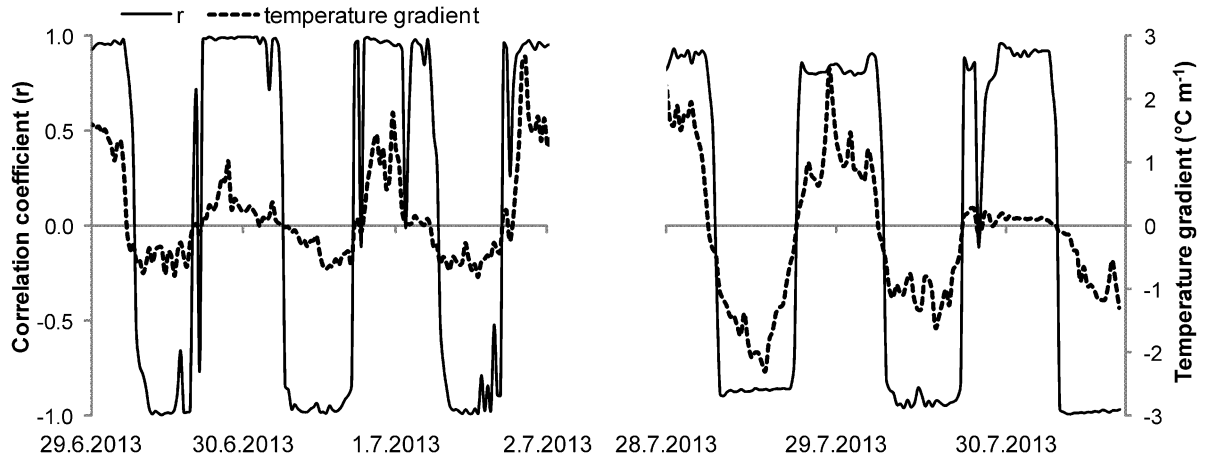

Fig. 1 The correlation coefficient of temperature gradients (differences between two closest thermocouples for 19 different levels above ground) and the temperature gradient (°C m^{-1}) for sample days (29. 6. – 2. 7. 2013 and 28. 7. – 30. 7. 2013) at spring barley field in Domanínek.

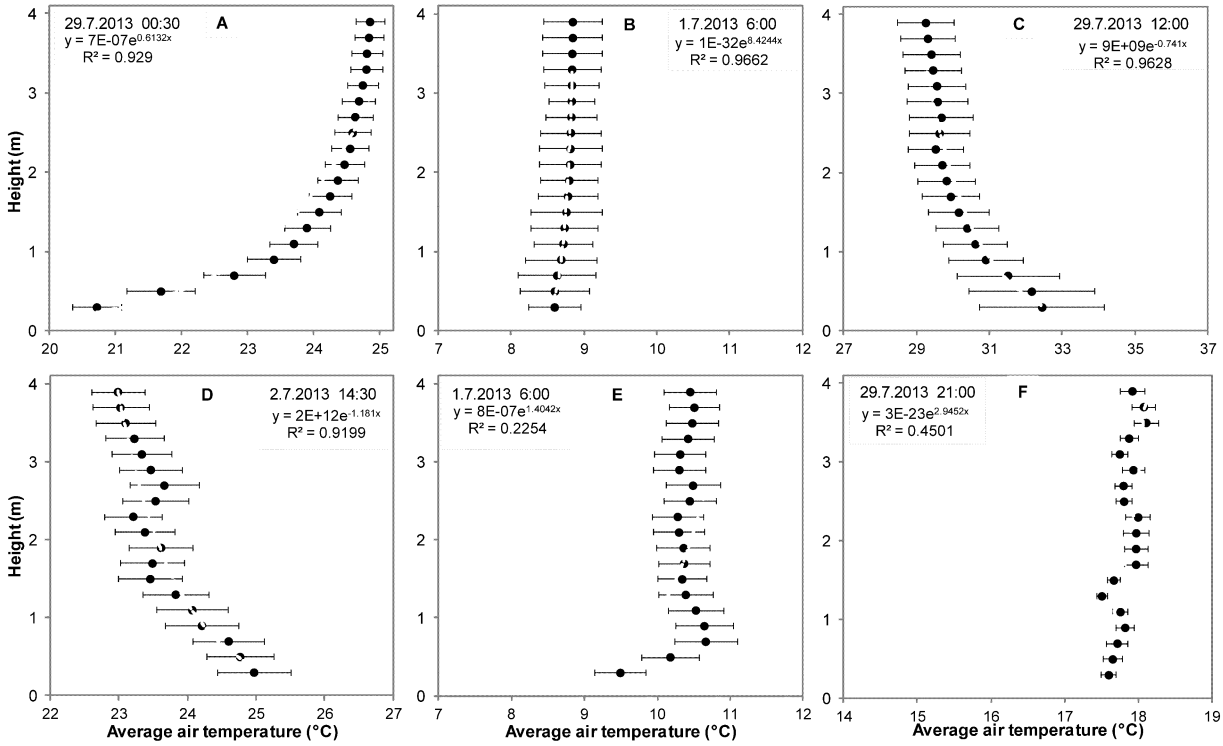

Fig. 2 The temperature gradients during the day. All figures have the same range (5 °C) at x axis to be graphically comparable. The depicted temperature is an average of two levels and the error bars show the standard deviation of the temperature differences between these two levels during 30 min period. A – typical nocturnal conditions with stable stratification, B – near neutral stratification around sunrise C, D – typical diurnal conditions with unstable stratification E – morning situation with inflexion point, F – temperature profile with inflexion point in the evening

The standard deviation of 30 min averages were used for error bars in figures below. Fig. 2A displays the typical nocturnal temperature gradient when the temperature increases with height. On the other hand, figures 2C and 2D show typical diurnal conditions when temperature closer to the surface is higher. Higher turbulent mixing during and more rapid changes in temperature during the day causes high standard deviations (STDs) displayed as error bars. Fig. 2B is an example of neutral stratification near the sunrise. Fig. 2E and 2F were chosen to demonstrate the situation with inflexion point which occurs when the sensible heat flux changes it sign. To have a closer look at the gradients they are zoomed in and displayed in Fig. 3.

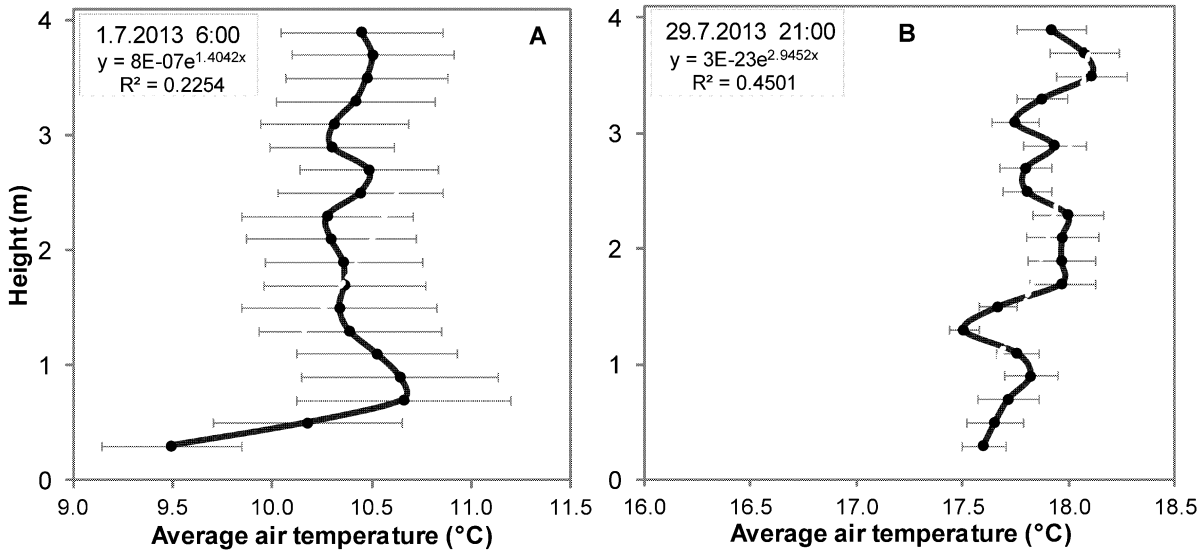

Fig. 3 The zoomed in temperature profiles during the change of day and night with the same range (2.5 °C) at x axis. The typical situation when “kink” occurs in height around 1 m above the surface. A – the standard deviations are high, B – the variability of the data is lover.

Discussion

This short study aimed to use the detailed temperature profile measurements to point out the significance of such measurements in assessing basic assumption of the BREB method. The different climatic conditions were chosen to be compared. For example, 28th July 2013 was the day with a clear sky, net radiation up to 550 $W.m^{-2}$ and the maximum air temperature in 0.9 m exceeded 35.8 °C. Temperature gradient decreases during the day as the land surface is heated by the sun. The gradient that day reached the lowest values (-2.3 °C). For comparison, the 30th July 2013 the maximum temperature measured in 0.9 m was 26.2 °C and the day was cloudy. The temperature gradient reached only half values (-1.3 °C). At night when the temperature rises with height the gradient has positive values. Similarly, the correlation coefficient is close to 1 at night and close to -1 during the day. Soon in the morning and after dusk the “r” value is close to zero and so quality of the data diminishes. These are the situations when the profile of temperature is changing and “kink” occurs. Fig. 3 displays two moments of this kind. Fig. 3A shows the profile at 6:00. The inflexion point was

created between 0.4 m and 1.4 m. The STDs are high which points out the high variability of the averaged data. In this situation we would need extremely accurate sensors (up to +/- 0.1°C) to capture real profile. In our case the sensor bias can influence the result. Fig. 3B captures the situation with “kink” in the evening at 21:00. The STDs are much smaller however; the difference between min and max temperature in all levels is only 0.75 °C.

Correlation coefficient of the profiles is a good indicator of the profile consistency and data quality. Its classification and relating it to the flux errors should be the next effort. Further study will focus on the quantification of error caused by occurrence of the inflexion point in the temperature profiles and comparison of different crop covers.

Acknowledgement

Supported by project "Building up a multidisciplinary scientific team focused on drought" No. CZ.1.07/2.3.00/20.0248, PASED – project supported by Czech program KONTAKT II No. LH12037 “Development of models for assessment of abiotic stresses in selected bioenergy plants” and LD130030 project supporting COST action ES1106. This work was supported by the Ministry of Education, Youth and Sports of CR within the National Sustainability Program I (NPU I), grant number LO1415.

References

Bowen IS (1926) The Ratio of Heat Losses by Conduction and Evaporation from Any Water Surface. In: Physical Review, 27, 779–787.

Foken T (2006) 50 Years of the Monin–Obukhov similarity theory. Boundary-Layer Meteorology 119, 431–447.

Oke TR (1987) Boundary layer climates, 2nd edition. pp. 435, Methuen, London.

Savage MJ (2010) Field evaluation of polymer capacitive humidity sensors for Bowen ratio energy balance flux measurements. Sensors 10, 7748–7771.

Todd RW, Evett SR, Howell TA (2000) The Bowen ratio-energy balance method for estimating latent heat flux of irrigated alfalfa evaluated in a semi-arid, advective environment. Agricultural and Forest Meteorology 103, 335–348.

APPENDIX F: The photodocumentation – ground based measurement network

This appendix contains photos from 13 measurement stations across the Czech Republic and Austria, the position of stations is plotted in Fig 1 followed by the list of stations in Tab 1.

Fig 1 Map of experimental localities for water balance estimation, green labels mark position of sites with scintillometers and/or the eddy covariance systems, white labels mark the Bowen ratio energy balance systems.

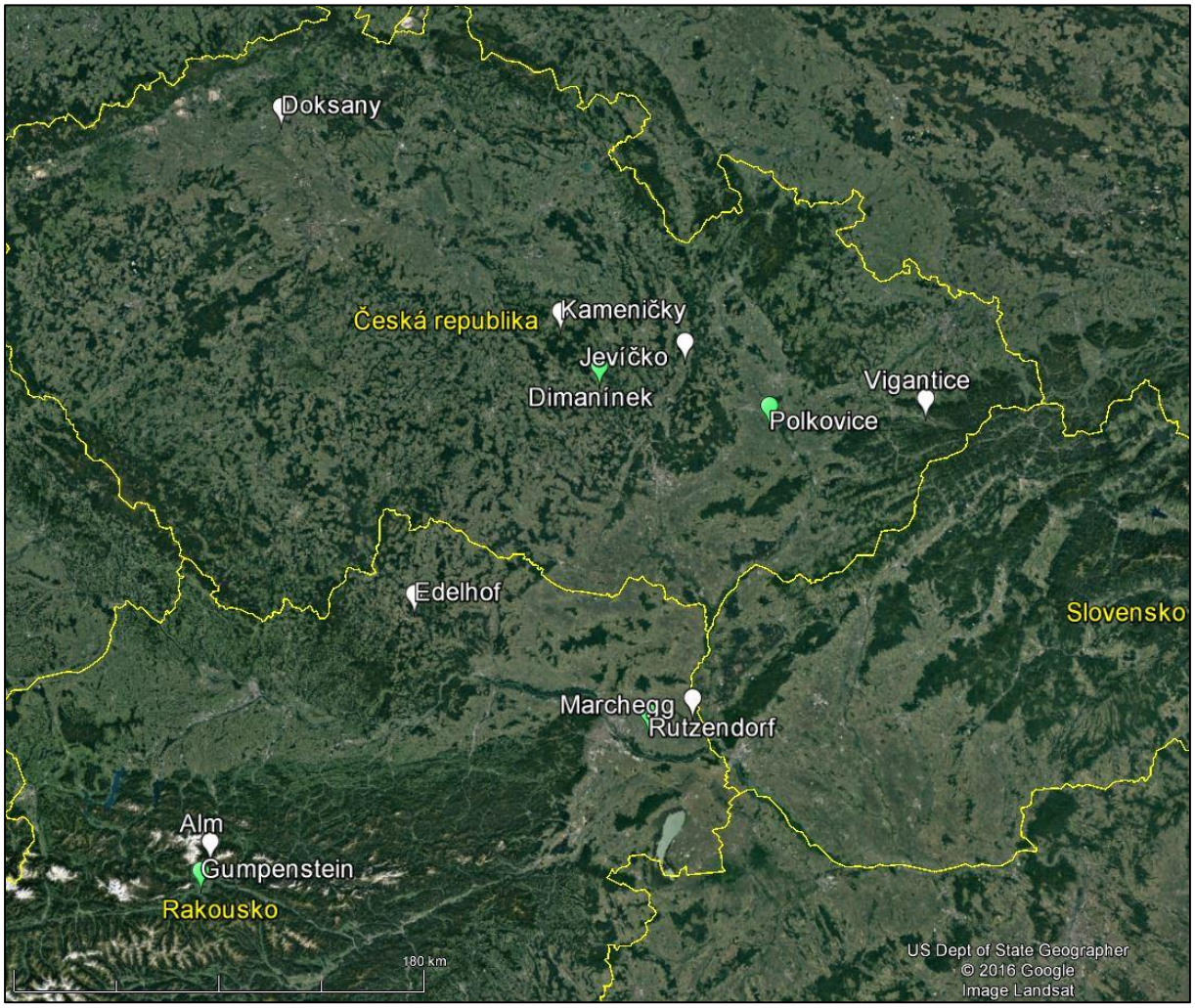

Tab 1 The list of localities within a measurement network for water balance assessment.

Locality	Type of system	First installation	Cover	Elevation m a.s.l.
Doksany	BREB system	6. 5. 2013	Grassland	155
Domanínek	Eddy covariance	28. 9. 2010	Poplar plantation	590
	BREB systems	24. 6. 2008	Agrosystem	
	Scintillometer	? 2016	Grassland	
Jevíčko	BREB system	22. 5. 2014	Grassland	350
Kameničky	BREB system	2. 5. 2013	Grassland	635
Polkovice	Scintillometer	27. 9. 2013	Agrosystem	200
	BREB system	25. 9. 2013		
	Eddy covariance	2. 7. 2015		
Vigantice	BREB system	20. 12. 2014	Grassland	455
Alm	BREB system	22. 7. 2015	Grassland	1802
Edelhof	BREB system	7. 8. 2013	Grassland	400
Gumpenstein	Scintillometer	17. 10. 2013	Experimental	690
	BREB system	17. 10. 2013	locality	
			Grassland	
Marchegg	BREB system	25. 7. 2013	Grassland	150
Rutzendorf	Scintillometer	11. 3. 2014	Agrosystem	150
	BREB system	11. 3. 2014		

Fig 2 Meteorological station in Doksany (left); one of several meteorological stations in Domanínek picture from barley field (right).

Fig 3 The AWS at meadow in Jevíčko (left), experimental site Kameničky (right).

Fig 4 Station in Vigantice (left), the highest measurement site of the network – mountain meadow at locality Alm in Austria (right).

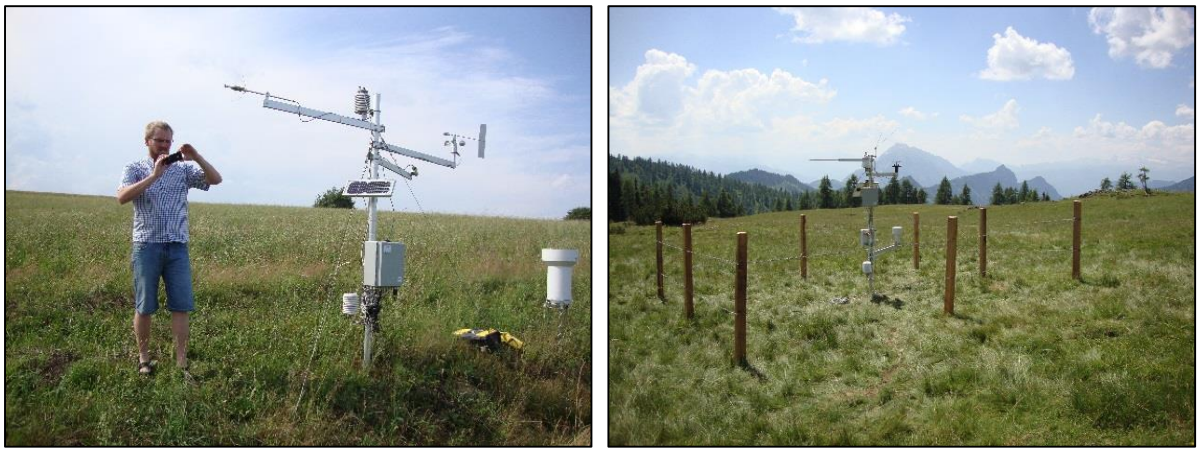

Fig 5 Measurement sites in Austria: Marchegg (left), Edelhof (right).

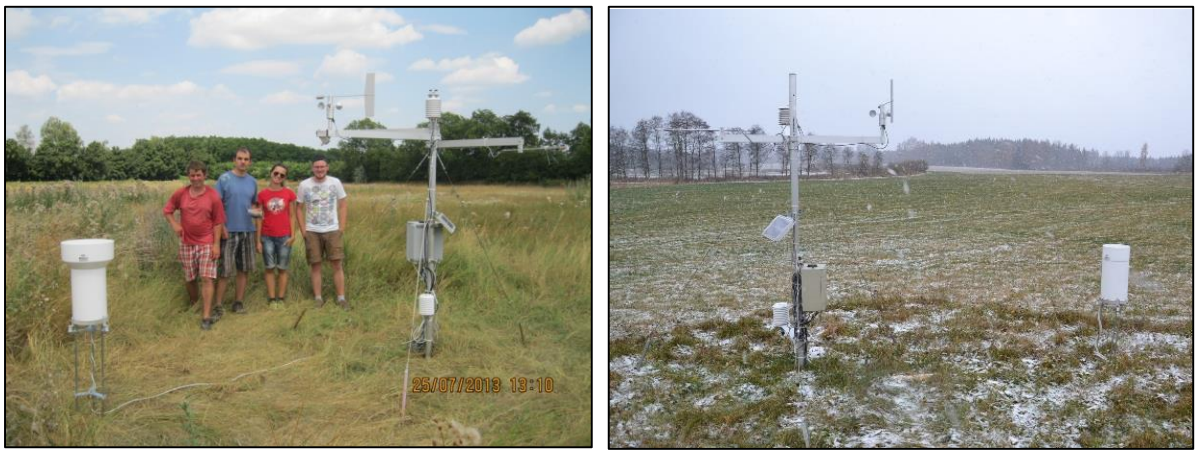

Fig 6 The automatic weather stations at sites with scintillometers in Austria: Rutzendorf (left), Gumpenstein (right).

Fig 7 Rutzendorf BLS900 receiver 8.4.2015 (left), BLS900 transmitter 13.11.2014 (right).

Fig 8 Scintillometer in Gumpenstein transmitter 26.11.2013 (left) receiver 17.10.2013 (right).

ANNOTATION

Evapotranspiration (ET) is an important part of water and energy balance. ET plays inevitable role in agriculture as it is the main water loss part of the water budget and to a great extent it influences agricultural yields, especially in semi-arid and arid regions where transpiration is more dominant component of ET. In general, modelling is a useful tool for assessment of ET but to validate, calibrate and check the performance of any model ground based data are always required.

There are many methods to measure ET directly or indirectly. In presented thesis an overview of the most common methods is given with focus on the methods used in our field experiments. We are running a network of site measurements for water balance assessment in the Czech Republic and Austria. Currently, the eddy covariance (EC) technique, the Bowen ratio energy balance (BREB) method, and the surface renewal (SR) method are used as the examples of point measurements. However, for the purposes of model validation based on satellite data the footprint (source area) of measurement must be ideally of a grid size (min 500x500 m). That is why, scintillometry was applied in our field experiments. This method provides measurement of the area averaged surface fluxes up to several km and thus it said to be valuable for large areas.

Our initial goal was to run four methods at one homogeneous site (Polkovice, the Czech Republic) to test their agreement and reliability in field conditions. Further, we would like to use scintillometers to measure ET for larger footprints above heterogeneous sites. For better understanding of field homogeneity, we took different approaches: the use of satellite images (NDVI, surface temperature), the plane campaign scanning the field, and contrasting the results with ground based measurements of soil water content and leaf area index across the field. The results of this comparison supported our assumption of homogeneous field with small within field variability and large fetch, and the field was always within the footprint of examined methods. Therefore, we could confidently compare the results of four methods claiming that their source areas are similar.

Next aim of presented work was to compare the methods in terms of accuracy, reliability, and user friendliness and to suggest improvements to our measurement network. The BREB method showed to be reliable and agreed well with EC but it was very dependent on accuracy of the combined sensors of air temperature and relative humidity (RH). During the study, our sensors tended to build an inaccuracy and made it impossible to use RH gradients at the end of the season if the sensors. The EC method was the least demanding concerning field work, however, the post processing requires plenty corrections and thus well-educated and skilled personnel. There is also an issue with energy balance closure associated with the EC method. The scintillometry showed good results with slight overestimation of sensible heat flux as compared to the EC. When calculating latent heat (evapotranspiration) it is dependent on precise measurement of other components of energy balance equation, similarly to the SR and BREB methods. Moreover, the boundary layer scintillometer demands larger infrastructure with high power consumption and again an operator witch good micrometeorological background. The surface layer scintillometer, on the other hand, is less demanding concerning infrastructure (tripods instead of towers, lower energy consumption) with the

same results at homogeneous surface. The SR method showed to be promising but some issues with identifying the flux-bearing scales must be solved prior to broader implementation. This is going to be addressed in cooperation with colleagues from North Carolina State university.

Bearing in mind advantages but also drawbacks of all methods we would further recommend to use eddy covariance open path at our localities with sufficient fetch because it has proven reliability and lower demand of field work. Moreover, scintillometers has proven to be good at representing large areas and so, the heterogeneous sites with larger measuring paths should be another logical step to expand our network. The BREB method showed very good agreement with EC at the beginning of season and this traditional method is convenient and low-cost alternative. It is worth continuing with it after ensuring more reliable sensors for air temperature and RH gradient measurements. Last but not least, the SR method showed its potential as a very low-cost method with interesting results however, the issues with determining of the flux bearing scale must be solved before expanding to new localities.